Measurements of Atmospheric Mercury, Dissolved Gaseous Mercury, and Evasional Fluxes in the Amundsen Gulf: The Role of the Sea-Ice Environment

By

Jeffrey Latonas

A Thesis submitted to the Faculty of Graduate Studies of

The University of Manitoba

In partial fulfilment of the requirements of the degree of

MASTER OF SCIENCE

Department of Environment and Geography

University of Manitoba

Winnipeg

Abstract

Mercury (Hg) has been recognized as a contaminant of global concern due to its high toxicity, as well as its ability to mobilize over long distances and biomagnify up through the food chain. The discovery of polar springtime atmospheric mercury depletion events (AMDEs) in the 1990s provides a new mechanism for enhanced atmospheric Hg deposition to the surface environment in the Arctic, yet questions remain on the process leading to AMDEs and the net contribution of AMDEs to Hg loadings to the Arctic marine ecosystem. Here we report the first systematic study of AMDEs over the open ocean conducted in the Amundsen Gulf flaw lead system from February to July 2008. A total of 31 AMDEs were observed which showed clear dependence on local sea ice environment and meteorological conditions. Enhanced concentrations of dissolved gaseous mercury were also measured in both under ice and open water conditions. Our results confirm that the sea ice environment plays a large role in Hg dynamics in the Arctic Ocean.

Acknowledgments

I would first like to thank my supervisors Dr. Feiyue Wang and Dr. Gary Stern for providing me with guidance, financial and intellectual support, and the opportunity to conduct this research. A special thank you is also necessary to Debbie Armstrong for all of her support in the field, her technical expertise, and advice throughout this project. Field support and expertise from Alexandra Steffen, Patrick Lee, and Haley Hung from Environment Canada is also very much appreciated.

I would like to thank my colleagues at the University of Manitoba and beyond for their support, expertise, and friendship throughout this project: John Iacozza, Kerri Warner, Brent Else, Matt Asplin, Dan Leitch, Amanda Chaulk, Alexis Burt, Steeve Gagne, and all members of the IPY-CFL contaminants team. Special thanks go to the Captains and crew of the Canadian Coast Guard Ship Amundsen for their help during this scientific endeavour, and to Andreas Richter at the University of Bremen, who provided GOME satellite images for this study. I would finally like to thank the members my M.Sc. Advisory Committee Drs. Tim Papakyriakou and Mario Tenuta for their time and consideration. Most of the meteorological data used in this thesis were also generously provided by Dr. Tim Papakyriakou. This research would not have been possible without the support from all of you.

This study was also made possible by the financial support from the University of Manitoba, the Circumpolar Flaw Lead System Study, the Canadian Foundation for Innovation, and the Northern Scientific Training Program of the Indian and Northern Affairs Canada.

Dedications

This thesis is dedicated to my parents: Graham and Sylvia Latonas, whose love, support, and encouragement over the years has made this all possible.

Table of Contents

List of Tables

List of Figures

List of Acronyms

AMDE – Atmospheric Mercury Depletion Event
CAMNet – Canadian Atmospheric Mercury Measurement Network
CCGS – Canadian Coast Guard Ship
CFL – Circumpolar Flaw Lead
CVAFS – Cold Vapour Atomic Fluorescence Spectrometry
CH_3Hg^+ – Methyl Mercury
DGM – Dissolved Gaseous Mercury
DMHg – Dimethylmercury
DOC – Dissolved Organic Carbon
EtHg – Ethylmercury
GEM – Gaseous Elemental Mercury
Hg – Mercury
Hg^0 – Elemental Mercury
Hg_p – Particulate Mercury
Hg(II) – Divalent Mercury (Complexed)
Hg^{2+} – Mercuric ion
IPY – International Polar Year
MDL – Method Limit of Detection
MeHg – Monomethylmercury
ODE – Ozone Depletion Event
PAR – Photosynthetically Active Radiation
PFA - Perfluoroalkoxy
PILMS – Portable In-situ Laboratory for Mercury Speciation
POP – Persistent Organic Pollutant
PTFE – Polytetrafluoroethylene (Teflon)
RGM – Reactive Gaseous Mercury
Sc – Schmidt Number
SRB – Sulphate Reducing Bacteria
TAM – Total Atmospheric Mercury
TGM – Total Gaseous Mercury
THg – Total Mercury

Chapter 1: Introduction to Mercury in the Arctic Marine Ecosystem

The Arctic, due to its sparse human populations and minimal industrial activity, was once considered to be one of the last pristine environments on Earth, free of major anthropogenic contaminant influences. In recent years, however, this belief has been shattered by many discoveries leading to the realization that the Arctic is not as pristine as we once thought. The atmosphere is a major pathway in which mercury (Hg), as well as other persistent and toxic chemicals, can be transported to the Arctic environment (Cheng and Schroeder, 2000). In 1995, at a meteorological station located at Alert, Canada (at the most northern tip of Ellesmere Island), very low concentrations of Hg were measured in the troposphere between the spring months of March and June. This was surprising to researchers as elemental Hg (Hg^0) is a species which supposedly has an atmospheric residence time of 6 months to 2 years (Schroeder et al., 1998). The discovery of these atmospheric mercury depletion events (AMDEs) has had a significant influence on the understanding of global geochemical cycling of Hg, and since their discovery AMDEs have sparked intense research on the subject in the Arctic, sub-Arctic, and Antarctic regions.

Mercury, also known as quicksilver or the symbol Hg (from the Latinized Greek word hydrargyrum; "hydr" meaning watery or runny and "argyros" meaning silver), is a naturally occurring element present in the Earth's crust which is released to the environment through both natural and anthropogenic processes. Elemental Hg is in the liquid phase at standard temperature and pressure; however, it has the ability to partition into the gas phase due to a relatively high vapour pressure. The majority

of anthropogenic emissions of Hg originate from the combustion of fossil fuels, particularly in Asian countries such as China, India, and Korea where coal is, and will continue to be, the primary source of energy (Pacyna and Pacyna, 2002). Other emission sources include chlor-alkali plants, mining, medical activities, and consumer products such as fluorescent light bulbs, thermometers, and switches. Natural sources of Hg include forest fires, volcanoes, and emission from soils and oceans. Experimental field data and modeling results suggest that anthropogenic emissions are at least as great as those from natural sources (Mason et al., 1994, Pacyna et al., 2006).

An increase in anthropogenic Hg emissions since the pre-industrial era has been well documented, and it is generally established that global deposition to terrestrial and aquatic ecosystems has increased by a factor of 3 ± 1 (Lindberg et al., 2007). Anthropogenic emissions from both North America and Europe have decreased due to more stringent environmental laws and policies since the 1990s, whereas emissions from Asia and Africa are thought to be increasing (Pacyna et al., 2006). Up until very recently, there has been no discernable net change in the size of the global atmospheric Hg pool in the northern hemisphere in North America and Europe since the mid-1970s (Lindberg et al., 2007). Long term atmospheric trends in gaseous elemental mercury (GEM) measured at Alert Canada have recently begun to show a significant decreasing trend with an estimated slope of approximately 0.0086 ng $m^{-3}y^{-1}$ (Cole and Steffen, 2010). The concentration of total filterable Hg has also shown declines in the Canadian Arctic of approximately 3% per year in the summer and fall, which may be in response to a world-wide calculated reduction rate

of ~3.3% per year by human activities (Li et al., 2009). Despite these declines, the threat of Hg to the Arctic environment is still of great concern.

1.1 Mercury in the Arctic Environment

Mercury's unique chemical properties allow for exceptional behaviour in the environment. Hg is transported into polar environments through a variety of pathways including atmospheric transport, ocean currents, and river inputs. Global atmospheric Hg modeling studies show that the Arctic can act as a sink for Hg, and that the halogen driven oxidation of Hg^0 from AMDEs can accelerate this process (Ariya et al., 2004). Polar Regions present fragile ecosystems and unique conditions which are potentially more sensitive to contaminants than other areas (Macdonald et al., 2005).

Mercury and other semi-volatile contaminants such as persistent organic pollutants (POPs) emitted in southern latitudes are transported northward due to the "grasshopper effect" (Andreas et al., 2002). These pollutants accumulate in the Arctic atmosphere during the winter due to a robust stratification resulting from strong temperature inversions. Once in the Arctic, the atmospheric pollutants are subject to local removal processes which are usually much longer than in temperate regions leading to their concentration in polar environments. Both Hg and POPs are subject to particle scavenging and wet and dry deposition; for Hg, however, this process is mainly photochemically driven.

Mercury is present in 3 major groups of chemical species in the environment: elemental mercury (Hg^0), divalent inorganic mercury [Hg^{2+} and its complexes; Hg(II)] and divalent organically bound mercury such as monomethylmercury

(CH_3Hg^+ and its complexes; or MeHg). Hg^0 in the environment can be oxidized to a more bioavailable Hg(II) species which can then be methylated through a variety of abiotic and biotic processes. The species which causes the greatest threat to humans and the ecosystem is MeHg.

MeHg is a known neurotoxin and readily biomagnifies through both aquatic and terrestrial food chains and thus may have harmful effects on some wildlife species (Sandheinrich and Miller, 2006, Weis, 2009), as well as pose a significant health threat to human populations who consume large quantities of fish and/or marine mammals (Choi and Grandjean, 2008, Salonen et al., 1995, Grandjean et al., 1997). MeHg has the ability to cross the blood brain barrier and thus become neurotoxic as well as act as an immunosuppressant rendering animals and humans more susceptible to disease (Holmes et al., 2009). Elevated MeHg levels are found in many Arctic marine mammals, and in some locations, are above acceptable level in the cord blood of mothers (Wagemann et al., 1995, Lockhart et al., 2005b, Lockhart et al., 2005a). MeHg has been associated with central nervous system effects including a loss of coordination, inability to feed, a reduced responsiveness to stimuli, and starvation (Clarkson and Magos, 2006). The dietary intake of Hg has, at times, exceeded established national guidelines in a number of communities (Johansen et al., 2004), and not surprisingly Hg levels in some Inuit members are higher than those recorded in people living in temperate industrialized regions (Arnold et al., 2003).

Mercury in snow is mainly in the oxidized form (Hg(II)) and can range from a few to hundreds of ng L^{-1} (Lalonde et al., 2002, Lindberg et al., 2002, Ferrari et al., 2005, Douglas et al., 2005). AMDEs have been shown to increase the amount of

Hg(II) in the snow, especially in areas where open water or new ice is present (Lu et al., 2001, Lindberg et al., 2002, Douglas et al., 2005). The fate of Hg deposited by AMDEs to the surface is discussed in Section 1.5 of this chapter. Figure 1-1 shows a general diagram of how Hg behaves once in the Polar environment.

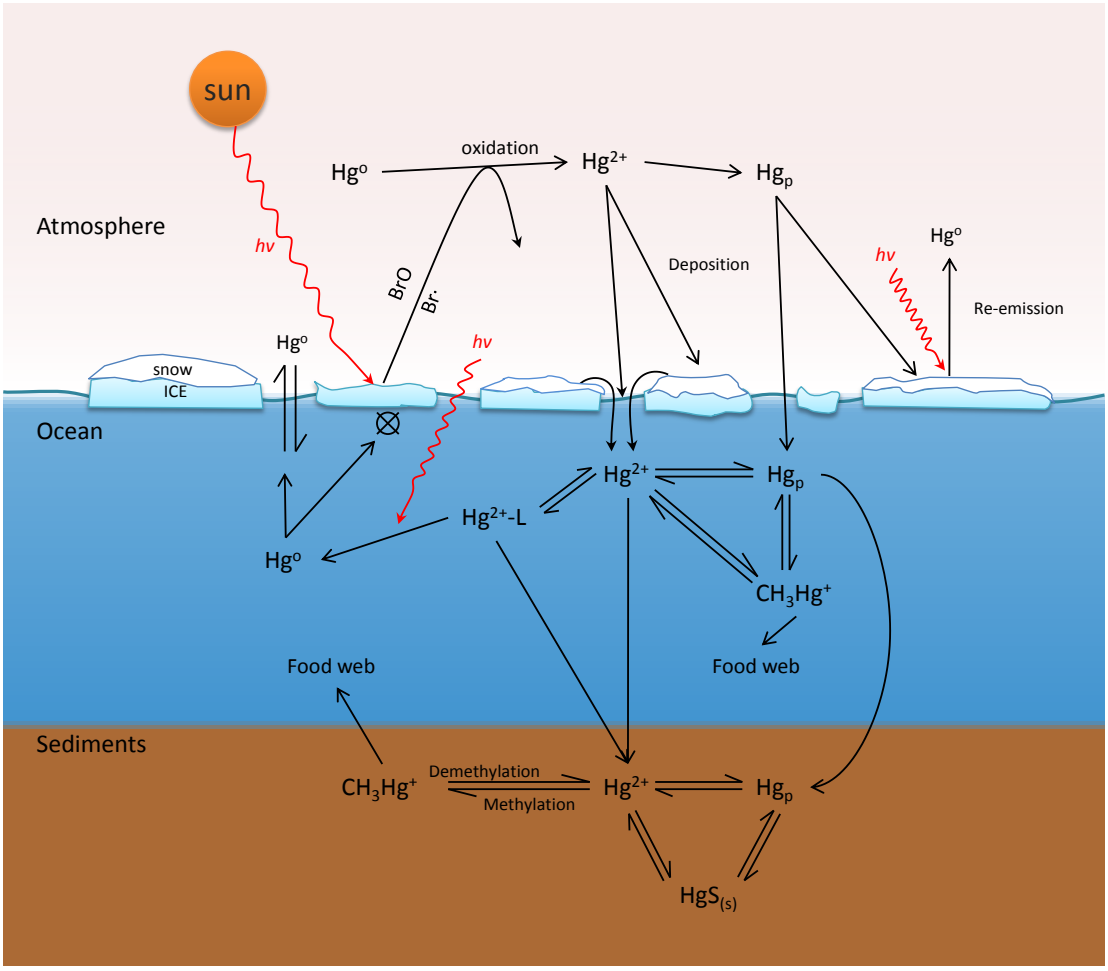

Figure 1-1: Schematic of Hg biogeochemical cycling in Arctic environments, Adapted from Amyot et al., 1997b, Macdonald et al., 2005, Barkay and Poulain, 2007, and Park et al., 2008.

Figure 1-1 shows a general diagram of how Hg behaves in the Arctic environment outlining some of the many different pathways it can take which will be discussed throughout this thesis paper. Atmospheric Hg may be deposited to snow or

ice surfaces where it may re-volatilize to the atmosphere. Hg entering the aquatic system may also re-volatilize to the atmosphere, or become bound to particulates in the water column. The re-volatilization process is mostly photochemically driven, however, there is evidence to suggest a biotic role as well (Section 1.6.2.2). Hg may then become methylated and become incorporated into the food web (Section 1.5.3). The chemical cycling of Hg in the environment is complicated with many processes involved. It is essential that these processes are well understood in order to establish potential impacts to the environment from anthropogenic emissions, as well as to establish potential risk to northern communities.

1.2 Mercury in the Atmosphere

Mercury is characterized by a relatively high vapour pressure (0.227 Pa @ 25°C), thus air currents are the major pathway in which Hg is transported from its emission source to its area of deposition. Hg in the atmosphere is currently characterized by five major components: gaseous elemental mercury (GEM, Hg^0), reactive gaseous mercury (RGM), particulate mercury (Hg_p), total gaseous mercury (TGM), and total atmospheric mercury (TAM). GEM is the dominant form of Hg in the atmosphere (> 90%) and has an average atmospheric residence time of about 1 year (Schroeder and Munthe, 1998). The long residence time allows for thorough mixing and long range transport, even to the far reaches of the Arctic. The average background concentration of GEM at remote sites is generally between 1.5 and 1.7 ng m^{-3} in the northern hemisphere and 1.1 - 1.3 ng m^{-3} in the southern hemisphere (Slemr et al., 2003, Kock et al., 2005, Ebinghaus et al., 2002). The higher levels in

the northern hemisphere are due to the larger land masses and greater levels of industrial activity (Lindberg et al., 2007).

GEM concentrations in the Arctic show strong seasonal variation throughout the year. Lower median concentrations with greater variation are seen in the spring due to AMDEs and higher than mean annual concentrations with decreased variability are observed during the summer (Steffen et al., 2005). It is believed that the higher summer concentrations are due to the re-emission of Hg deposited in snow and ice during the spring, as well as increased temperatures which leads to higher evasion rates from snow, land, and water surfaces. Fall and winter concentrations are typically distributed around the mean annual concentration and show little variation.

RGM is a gas phase oxidized form of Hg consisting of either Hg(II) or Hg(I) species. RGM is readily sorbed onto aerosols present in the air due to its hygroscopic properties forming Hg_p which is Hg(II) or Hg(I) species that are associated with an airborne particle. Hg_p and RGM species are found at much smaller concentrations in the atmosphere except from near emission sources (Pacyna and Pacyna, 2002) or during special atmospheric conditions resulting the rapid oxidation of GEM such as the AMDEs (Lindberg et al., 2002, Lu et al., 2001). RGM is much more reactive than GEM thus traveling only short distances from its source of emission (or formation) before being scavenged by particles in the atmosphere or deposited to the surface. Current technology is not capable of differentiating the Hg species which make up RGM, thus RGM and Hg_p are currently operationally defined. TGM includes all Hg species in the gaseous phase, namely GEM and RGM. TAM is the sum of all Hg

components in the atmosphere including Hg_p and organic mercury species such as dimethylmercury [$(CH_3)_2Hg$, DMHg] and MeHg.

1.3 Atmospheric Mercury Depletion Events

AMDEs were first observed in 1995 (Schroeder et al., 1998) and have since been found to be an annual reoccurring phenomenon (Steffen et al., 2005) throughout the Arctic, sub-Arctic and Antarctic following polar sunrise (Berg et al., 2003, Lindberg et al., 2001, Skov et al., 2004, Ebinghaus et al., 2002). AMDEs are characterized by rapid decreases in GEM concentrations coupled with an increase in Hg_p and RGM in the troposphere, and are restricted vertically to a surface layer usually less than 1km thick (Banic et al., 2003, Tackett et al., 2007). Events can last from a few hours to a few days and have been associated with increased Hg deposition in snow and ice (Lu et al., 2001). Typically, AMDEs have been estimated to contribute between 50 and 325 tons of Hg to the Arctic environment each year (Ariya et al., 2004, Banic et al., 2003). These models, however, did not include an evasional term; recent work has estimated that the net annual atmospheric flux to the Arctic could be as low as 8.4 t y^{-1} (Outridge et al., 2008). Dry deposition associated with AMDEs has been estimated to be as high as 40-50 µg m^{-2} y^{-1} near the Arctic ocean coast (Lindberg et al., 2002), which is considerably higher than inland wet deposition measurements (1.5 ± 0.5 µg m^{-2} y^{-1}) and the mass balance derived dry deposition of 1.2 ± 0.7 µg m^{-2} y^{-1} (Fitzgerald et al., 2004). Several studies have confirmed higher concentrations of Hg in snow over the open ocean and at coastal sites during the spring compared to inland sites (Garbarino et al., 2002, Douglas et al., 2005, Lindberg et al., 2002). This suggests that these depletion events are primarily

taking place over the open ocean, and those locations will see higher Hg fluxes due to AMDEs.

Factors presumed to initiate AMDEs include the presence of sunlight, low temperatures, snow or ice surfaces and the presence of halogen species derived from sea salts (Steffen et al., 2005). AMDEs begin shortly after polar sunrise and an increase in UV-B radiation has been correlated with an increase in Hg in surface snow over the spring. The termination of depletion events in most cases is characterized by the onset of sustained air temperatures above 0°C which also coincides with snow/ice melt (Lu et al., 2001, Lindberg et al., 2002). Following snow melt, GEM concentrations in the air then typically increase due to out-gassing from the surface as the deposited Hg is reduced to its elemental form and evaded back to the atmosphere.

Both RGM and Hg_p are typically measured during AMDEs; however, their concentrations relative to one another can differ from location to location and time of year. In Alert, Canada, Hg_p is the predominant form of Hg(II) observed in the atmosphere during AMDEs; however, a clear shift to RGM dominance was observed later in the spring (Kirk et al., 2006, Cobbett et al., 2007). RGM is the dominant species observed at Barrow, Alaska during AMDEs where concentrations as high as 900 ng m^{-3} have been reported (Lindberg et al., 2001, Lindberg et al., 2002). The distribution of Hg_p and RGM among different sites, especially between coastal and marine sites, is still a topic requiring further research. Some studies suggest that it is an indication of the age of the air mass (Lindberg et al., 2002, Steffen et al., 2003a) where others suggest it is an indicator of local events compared to transported events (Gauchard et al., 2005). UV radiation has also been thought to contribute to the

Hg(II) distribution as during high levels of UV, the Hg_p aerosol could be rapidly decomposed leaving RGM as the dominant species (Sprovieri et al., 2005).

It has been noticed that the sum of individually measured components (GEM, RGM, and Hg_p) does not equal that of the measured TAM during most studies, including this one. It is thought that this is due to the inaccuracy of the measured RGM and Hg_p concentrations due to a lack of a standard calibration method for these components, or the lack of a knowledge associated with the % recovery of the instruments. This is an area which requires more study in order to establish where this "missing Hg" is from the mass balance.

1.4 AMDE Chemistry

1.4.1 Ozone Depletion

Arctic tropospheric Hg depletion has been found to be strongly correlated with tropospheric ozone (O_3) depletion which is a well-known phenomenon discovered in the late 1980s (Oltmans, 1981, Oltmans and Komhyr, 1986, Bottenheim et al., 1986). Ozone depletion events (ODEs) are characterized by having O_3 mixing ratios below 10 ppbv which occur regularly in the atmospheric boundary layer following polar sunrise (Tarasick and Bottenheim, 2002). The correlation coefficient (R^2) between GEM and ozone following polar sunrise is typically around 0.8 (Steffen et al., 2007) which suggests that the atmospheric chemistry driving AMDEs and ODEs are interlinked. The leading hypothesis, based on kinetic experiments and mechanistic data, suggests that the chain is initiated through the photolysis of O_3 by gas phase bromine compounds (Impey et al., 1999, Impey et al., 1997), although some evidence

suggests chlorine reactions may also contribute. Ozone depletion catalyzed by bromine reactions are suggested as follows (Foster et al., 2001):

(1) $Br\cdot + O_3 \rightarrow BrO + O_2$
(2) $BrO + HO_2 \rightarrow HOBr + O_2$
(3) $HOBr + hv \rightarrow OH + Br\cdot$
(4) $BrO + BrO \rightarrow 2Br\cdot + O_2$ (or $Br_2 + O_2$)
(5) $Br_2 + hv \rightarrow 2Br\cdot$

The removal of bromine from the catalytic reaction chain occurs through reactions with organic species such as formaldehyde which are present in polar spring at high Arctic sites (Sumner and Shepson, 1999). The bromine then becomes temporarily sequestered in aerosol, surface snow, and ice. Some bromine may be recycled to the atmosphere through the uptake of gaseous HOBr on snow followed by its reaction with $Br\cdot$ (reaction 6) which can sustain the ozone destruction process (McConnell et al., 1992).

(6) $HOBr + H^+ + Br\cdot \rightarrow Br_2 + H_2O$

The highest levels of BrO are observed in Arctic regions over sea ice following polar sunrise (Ridley et al., 2003, Zeng et al., 2003) and bromine has been shown to very effectively destroy ozone in two interlinked catalytic reactions producing BrO (reaction 1) and HOBr.

1.4.2 Mercury Depletion

Due to the undeniable relationship between ozone depletion and Hg depletion, it is hypothesized that the halogen driven mechanisms responsible for ozone depletion are similar to those driving Hg depletion (Lu et al., 2001, Lindberg et al., 2002). Based on observed high BrO concentrations in the polar troposphere after polar

sunrise specifically during AMDEs (Van Roozendael et al., 2002), it has been assumed that bromine radicals are largely responsible for GEM oxidation (Lu et al., 2001). Kinetic models have also show that out of all halogens that may contribute to GEM oxidation, Br atoms and BrO are the most effective (Ariya et al., 2004). The bromine radicals destroy ozone to form BrO (reaction 1), and both BrO and Br· can react with GEM to form oxidized Hg species. It is hypothesized that Hg^0 is oxidized by one or more of the following pathways (Lindberg et al., 2002, Simpson et al., 2007):

(7) $2Br\cdot + Hg^0 \rightarrow HgBr_2$
(8) $Br\cdot + Hg^0 \rightarrow HgBr$
(9) $BrO + Hg^0 \rightarrow HgO + Br\cdot$
(10) $BrO + Hg^0 \rightarrow HgOBr$
(11) $BrO + Hg^0 \rightarrow HgBr + O\cdot$

Increases in BrO have been observed with a decrease in GEM (Steffen et al., 2003b); this coupled with the trends in ozone suggest that bromine is a key factor controlling AMDEs. Coincidently, high BrO concentrations have also been confirmed by imagery from the GOME satellite in areas of high AMDE occurrences (Lindberg et al., 2002, Wangberg et al., 2003, Skov et al., 2004, Ariya et al., 2004). The existence of stable Hg(I) and Hg(II) products (HgBr, HgOBr, HgBrO, HgO) were confirmed in the gas phase, on reactor wall deposits and on suspended aerosols in one study on BrO initiated oxidation of GEM, further implicating BrO in AMDEs (Raofie and Ariya, 2004). Existing kinetic studies suggest that the Br· reaction pathway (reactions (7) & (8) with GEM is more important than BrO (Goodsite et al., 2004, Raofie and Ariya, 2003) which has also been confirmed with modeling studies (Ariya et al., 2004, Skov et al., 2004). Although bromine is the most viable oxidant as

determined through theoretical mechanisms and calculations as well as empirical evidence, the physical presence of Hg-Br compounds have not been directly measured during AMDEs or from deposited Hg.

1.4.3 Sources of Bromine

The main source of bromine over the open ocean outside Polar Regions has been found to be from sea salt aerosols generated by breaking waves on the ocean surface (Sander et al., 2003, Amato et al., 2007). In the Arctic, the main source is thought to be from emission from snow and sea ice surfaces, although the mechanisms are still not well understood (Kaleschke et al., 2004b). Other sources are hypothesized to include bubble bursting from the sea surface microlayer and organic Br emitted from marine algae (Lindberg et al., 2002). Flaw lead areas are considered as primary sources of BrO due to the presence of open water and re-freezing leads during the spring. Halogen chemistry affecting AMDEs has been shown to be most active within the first 100 to 200m from snow/ice/water surface (Tackett et al., 2007) and AMDEs have been recorded within 2m from the snow surface suggesting frozen surfaces play a key role in AMDE chemistry. Studies at different elevations have also shown that AMDEs at lower altitudes have a higher variability in comparison to those at higher elevations (Sommar et al., 2007).

1.4.4 Frost Flowers

Recently the role of frost flowers (Figure 1-2) has been suggested in the production of this "bromine explosion" following polar sunrise (Rankin and Wolff, 2002). It has been estimated that at least 60% of the total sea salt arriving at Halley (Antarctica) is from brine and frost flowers on the sea ice surface rather than from sea

spray sourced from open water (Rankin and Wolff, 2003). Frost flowers are vapour-deposited ice crystals which form as a normal part of ice formation in cold atmospheres at the ice-atmosphere interface. They are commonly found on newly frozen leads (linear breaks in sea ice cover) or polynyas (breaks between the mobile pack ice and land fast ice). The formation of frost flowers takes place in several major steps (Martin et al., 1996). First, the thermomolecular pressure gradient transports the brine from within the pores of newly formed ice to the surface where it accumulates as a liquid or slushy layer (Wettlaufer and Worster, 1995). Once above the ice the brine evaporates into the colder air which creates a 1-3 cm boundary layer of supersaturated air above the surface. This supersaturated layer promotes the growth of ice crystals from the surface. The slushy layer below the crystals continues to grow in thickness (2-4 cm) where its surface tension effects draw up the surface brine onto the frost crystals, yielding their large observed salinities (Rankin and Wolff, 2002). Frost flowers typically last for a few days before they are either covered by drifting snow or dispersed by strong winds (Perovich and Richtermenge, 1994).

Figure 1-2: Photograph of frost flowers developing near an open lead in the Amundsen Gulf in February. Photo by Jeffrey Latonas

Recently frost flowers have been shown to be a dominant source of sea salt aerosols in Antarctica due to the depleted sulphate to chloride ratios which is typical of aerosols produced by frost flowers (Rankin et al., 2002). It is also proposed that they are a source of reactive bromine to the polar troposphere (Kaleschke et al., 2004a, Jones et al., 2006). Frost flowers typically have increased salinity of up to 3 times higher than seawater due to their brine wicking characteristics (Rankin and Wolff, 2002); however, the bromide enrichment factors measured are within error of seawater composition suggesting the direct losses of bromide from frost flowers (Alvarez-Aviles et al., 2008). Another characteristic implying that frost flowers are a potential source of bromine and aerosols to the troposphere is their large surface area which may provide a chemically reactive surface for atmospheric exchange (Rankin and Wolff, 2002). Troposphere chemistry in areas which are subjected to increased

ice movement, such as the Amundsen Gulf, will likely be strongly influenced by the potential effects of frost flowers. The greater degree of surface roughness characteristic of frost flowers increases their backscatter coefficient over that of snow and ice thus making it possible to identify out crops remotely via satellite (Nghiem et al., 1997). These increases in radar backscatter makes areas of new ice (areas of potential frost flowers) appear brighter on radar derived imagery.

Elevated concentrations of Hg(II) have been found on frost flowers collected near open leads with four hour old frost flower crystals showing double that of the expected AMDE deposition to snow (Douglas et al., 2005), and older frost flowers showing concentrations as high as 185 ± 32 ng L^{-1}. This may be due to the fact that frost flowers grow from the vapour phase, in which their large surface areas (300 to 590 g cm^{-3}) increase their Hg scavenging properties (Legagneux et al., 2002). The elevated concentrations may also be a result of the frost flower itself acting as a reaction surface along with increased bromine concentrations (Rankin and Wolff, 2002).

1.5 Fate of Deposited Mercury

The fate of AMDE-deposited Hg is still under debate in the scientific community as it is not known how much Hg is deposited by AMDEs versus how much is re-emitted to the atmosphere following the event. Several studies have shown an increase in Hg concentrations in snow during and after AMDE events (Steffen et al., 2002, Lu et al., 2001, Lindberg et al., 2002) whereas some studies have shown no significant increase in snow concentrations (Ferrari et al., 2005). This suggests that Hg deposition to the surface is not uniform across the Polar Regions and

that the location of origin of the AMDEs is likely to be subjected to increased deposition over areas in which the depleted air masses are transported. As stated earlier, sea ice is necessary for the release of reactive halogens, thus deposition tends to occur over the frozen ocean or at coastal sites (Garbarino et al., 2002) and not more than 200 km inland (Lu et al., 2001, Douglas and Sturm, 2004).

Hg can be deposited by either wet or dry deposition. Wet deposition includes precipitation events such as snow or rain where dry deposition refers to particle settling. Dry deposition of Hg in the Arctic is mainly attributed to RGM and Hg_p produced during AMDEs. It has also been found that increased Hg deposition occurs during snow fall events suggesting that in-cloud oxidation of GEM is an important deposition process for Hg(II) (Ferrari et al., 2008). Hg(II) species are much more water soluble than Hg^0 due to their significantly lower Henry's law coefficients. They can also be readily assimilated by polar ecosystems giving rise to potential toxic effects to the biota. The deposition surface will play a large role in the fate of the deposited Hg; a general diagram can be seen in Figure 1-1.

1.5.1 Mercury in the Snow Pack

Both Hg^0 and Hg(II) are found in the snow pack; however, Hg^0 only contributes approximately 1% of the total Hg (Bottenheim and Chan, 2006). Concentrations reported during the Arctic winter are between <1 ng L^{-1} and 5 ng L^{-1} (Ferrari et al., 2005, Steffen et al., 2002); however, following polar sunrise during AMDEs these levels range between 20 and 100 ng L^{-1} (Lu et al., 2001, Lindberg et al., 2002, Steffen et al., 2002, Lalonde et al., 2002). Once deposited, there are two main pathways the Hg(II) may take: (1) In the presence of sunlight, it may be

photoreduced back into the atmosphere (Lalonde et al., 2002) or (2) It can become incorporated into melt water and released to the marine environment (Lindberg et al., 2002) leading to an influx of biologically available Hg at snowmelt - a pathway in which it can become incorporated into the ecosystem (Dommergue et al., 2003). MeHg has also been reported in the snowpack in the high Canadian Arctic with values ranging between 0.02 ng L^{-1} and 0.28 ng L^{-1} (Brooks et al., 2006, Kirk et al., 2006). It is hypothesized that the origin of this organic Hg is from volatilization from seawater upwelling and not from formation in the snow (Kirk et al., 2006, Constant et al., 2007).

Diurnal cycling in Hg concentrations also show that both oxidation and reduction processes occur at the snow surface leading to Hg deposition and GEM reemission (Ferrari et al., 2008). Snow packs offer a larger surface area with a high degree of air space, thus exchange with the atmosphere within the snowpack can occur. Solar radiation has been shown to penetrate the first few cm of the snow pack (Arnold et al., 2003), thus photoreduction of Hg(II) is possible in the upper layer of the pack. It has been estimated that up to 80% of Hg deposited during a depletion event is reemitted back to the atmosphere within days following the event (Ferrari et al., 2008). GEM flux to the atmosphere from the snow pack has been found to be correlated strongly with solar irradiation with maximum flux occurring mid-day (Ferrari et al., 2008), thus the Arctic snowpack can also be viewed as a source of GEM to the atmosphere. A warming snowpack close to melting has been shown to emit more GEM than when temperatures are lower (Dommergue et al., 2003). Warming snow temperatures leads to a metamorphism of the snow; increasing the water layer around snow grains, which leads to augmenting GEM production and

emission from the snow (Ferrari et al., 2005). Thus the fraction of Hg(II) remaining in the snow tends to decrease as the spring progresses, possibly due to the changing snow characteristics.

Alternatively, it has been shown that bacteria in the Arctic snowpack can interact strongly with Hg(II) (Banic et al., 2005). An increase in snow temperature allows for an increased growth of bacteria which increases the potential of the remaining Hg(II) species to become incorporated into biota and flushed into the marine ecosystem. It has also been shown that increased liquid layers around snow crystal grains during snow melt can aid in the binding of Hg(II) species to particle surfaces (Landis et al., 2002). This process may also be influenced by the interaction of micro-organisms within the water layer which can form strong complexes with metals (Ariya et al., 2002) potentially leading to Hg being flushed into the ocean where it may become incorporated into the food web.

The potential impact of AMDEs to the ecosystem will depend largely on location and meteorological conditions. The amount of Hg that is deposited during the spring and the amount which becomes re-emitted to the atmosphere or incorporated into spring runoff will vary widely from site to site and year to year. Different distributions of Hg species have been observed at different sites under varying meteorological conditions (Lindberg et al., 2001, Temme et al., 2003, Steffen et al., 2003a). Although the exact species involved with AMDEs are not fully understood, it is conceivable that different species have different tendencies to enter the biosphere. More research is required to help establish the potential influx of Hg into the ecosystem attributed to AMDEs as well as the ability for deposited Hg to

undergo methylation in order to fully understand the potential damage that AMDEs may have on Arctic environments.

1.5.2 Mercury in Arctic Waters

Deposited Hg can enter the aquatic system by either direct deposit to open water (potentially through open leads) or through melt water at snow and ice melt in the spring. The ocean hosts a vulnerable ecosystem thus understanding processes occurring and assessing the potential impacts of AMDEs is important. Hg(II) entering the water can be reduced by either abiotic or biotic processes back to Hg^0, known as dissolved gaseous mercury (DGM), which may either become trapped by the ice cap leading to supersaturated conditions, or evade to the atmosphere through open leads or the open ocean during the summer (Section 1.6). Hg^{2+} will bind readily with various ligands in the water column, or become methylated and enter the food chain. MeHg and DMHg have been reported in polar oceans with the highest concentrations occurring in deep water samples (Brooks et al., 2006) which suggest the role of sediments and anoxic environment in the methylation process.

1.5.3 Mercury Methylation in Polar Environments

MeHg is the most toxic form of Hg and has the highest environmental relevance due to its biomagnification along the food chain leading to humans; however the processes involved in the transformation in the Arctic are poorly understood. Sulphate reducing bacteria (SRB) are considered the main Hg methylators in aquatic temperate ecosystems; however, low levels of SRB have been found in Arctic environments suggesting other mechanisms may be involved (Loseto et al., 2004b). A peak in MeHg concentration in drainage basins and runoff

immediately following snowmelt was reported which suggests that MeHg is either produced in the snow or has been deposited from the atmosphere (Loseto et al., 2004a).

MeHg concentrations as high as 280 ng m^{-3} have been reported in high Arctic snow (St. Louis et al., 2005), and it is proposed that the source may be the photochemical breakdown of DMHg evaded from the ocean. MeHg can also be produced by irradiation in the presence of organic matter in the surface of temperate lakes (Carpi and Lindberg, 1998), thus 24 hour daylight coupled with organic carbon may contribute to MeHg production in Polar environments. It has also been suggested that MeHg production in aerosols and snow is a result of high levels of total Hg (THg) combined with high levels of heterotrophic bacteria (Constant et al., 2007). MeHg may also be formed in the atmosphere through a reaction with Hg(II) and unknown methylating agents, potentially acetate or similar molecules (Hammerschmidt et al., 2007). With high levels of bioavailable Hg(II) following AMDEs and these alternate pathways of methylation, there is the potential for AMDEs to have a significant negative impact on the Arctic environment. Further study is required to determine which of these processes is/are the most significant, and to which extent the AMDE deposited Hg(II) is methylated in the ecosystem.

MeHg is known to degrade readily in fresh waters, however the degradation rates in marine waters is slower for reasons which are unclear (Whalin et al., 2007). It has recently been found that the rates of degradation in marine waters is regulated by which MeHg biding ligands are present; MeHg bound to sulphur-containing ligands have been found to degrade more readily than MeHg-chloride complexes (Zhang and

Hsu-Kim, 2010). It is thus important to consider the water composition and MeHg speciation when determining potential ecosystem impact.

1.6 Dissolved Gaseous Mercury

DGM is a central species in the geochemical Hg cycle, as its formation and potential evasion to the atmosphere may reduce the ionic Hg concentration in the water body, and thus reduce the potential for methylation and incorporation into the food web; the substrate hypothesis (Fitzgerald et al., 1991). DGM can exchange readily with the atmosphere, and thus it represents a critical species by linking two environmental compartments. Understanding its behaviour in the environment is essential to understanding the global geochemical Hg cycle, which will undoubtedly help in determining potential ecosystem impact of this trace element. The following sections of this chapter will review the behaviour of DGM in the environment with a central focus on the Arctic marine environment. They will also discuss the methods used for both sampling and determining DGM concentrations in natural waters, as well as the methods used in calculating potential air-sea Hg flux rates.

1.6.1 DGM in Natural Waters

As previously mentioned, Hg in natural waters occurs in several main chemical species: elemental Hg (Hg^0), dissolved inorganic (Hg(II)), and organic Hg (mainly in the form of MeHg and DMHg and some ethylmercury (EtHg)). Dissolved inorganic Hg(II) is not found as its free ion Hg^{2+}, but rather complexed in a variety of species such as hydroxides, chlorides, and sulphides (Morel et al., 1998). DGM represents a group of volatile Hg species in which under certain circumstances can easily evade to the atmosphere. DGM consists of approximately 2-3% of the total Hg

in marine and freshwaters (Mason et al., 2001), and exists mainly (90 - 95%) as Hg^0 and to a lesser extent as DMHg (Vandal et al., 1991, Mason et al., 2001). Since the bulk of DGM is composed of Hg^0, this study will focus solely on the formation and evasion of Hg^0, hereby referred to solely as DGM.

Several studies have found that DGM evasion can be a substantial portion of the water body Hg mass budget, in fact evasional fluxes of Hg^0 from remote lakes can represent from 7% (Vandal et al., 1991) up to 95% (Xiao et al., 1991) of the estimated atmospheric Hg deposition to the water body. As mentioned earlier, this evasion may, in turn, decrease the amount of Hg available for methylation thereby reducing the potential toxic impact to the aquatic system and the surrounding communities. Oceanic evasion also constitutes one of the most important natural sources of Hg^0 to the atmosphere, and represents a crucial link in the geochemical cycle of Hg (Nriagu and Pacyna, 1988). The Oceans may play a very important role in the long-range transport of Hg through a multiple hop mechanism as atmospheric Hg is deposited, and re-emitted to the atmosphere (Schroeder and Munthe, 1998).

Studies have shown that the reduction of Hg(II) to Hg^0 in natural waters can be driven by both abiotic and biotic processes (Amyot et al., 1994, Krabbenhoft et al., 1998, Mason et al., 1994, Siciliano et al., 2002). Depending on conditions observed in the lake or water body in question, one process may be significantly more important than the other. Several studies have suggested that abiotic photochemical reduction of Hg(II) species is largely responsible for DGM production (Amyot et al., 1997b, Lalonde et al., 2004, Amyot et al., 1994, Xiao et al., 1995). The mechanisms involved will be discussed in Section 1.6.2.1. Biological formation has also been

suggested as a significant mechanism in which Hg(II) species can be reduced to DGM (Siciliano et al., 2002), and will be discussed in section 1.6.2.2.

Typically higher DGM concentrations are noted at the air-water interface (Poulain et al., 2004); however, it is occasionally observed at deeper depths of lakes where photochemical reactions are unlikely to play a major role (Vandal et al., 1991, Mason et al., 1995). A typical DGM profile shows the highest DGM concentrations occur in the epilimnion. A sharp decrease is observed in the metalimnion followed by a slight increase in the denser bottom layer (Amyot et al., 1994). At times, a peak in DGM has been recorded in the metalimnion, specifically at the depth of maximum chlorophyll concentration (Poulain et al., 2004). A study in a Canadian boreal lake has indicated that DGM production is mainly photo-mediated at the surface, whereas at depth, DGM production is linked to the presence of algae and metalimnetic phytoplankton blooms (Poulain et al., 2004). Increased levels of DGM found at the sediment-water interface have been suggested to be primarily due to chemical reactions involving humic substances in anoxic environments (Allard and Arsenie, 1991), or microbial activities (Poulain et al., 2004).

1.6.2 Formation of DGM in Natural Waters

1.6.2.1 Abiotic Formation

Both laboratory and field experiments have shown that abiotic photochemical reduction is one of the main routes of formation of DGM in natural waters (Amyot et al., 1994, Amyot et al., 1997b, Rolfhus and Fitzgerald, 2004). DGM has been found to vary seasonally with increased production in the spring and summer months (Park et al., 2008). Several temporal studies have shown that highest DGM production rates

occur during the month of July when solar radiation is at its highest (Amyot et al., 1997b, Rolfhus and Fitzgerald, 2004). DGM production in surface waters also yields a diurnal pattern which is characterized by an increase in concentration in the morning, peak values at the time of maximum solar radiation, and a decline thereafter (Garcia et al., 2005). Some studies have found that shorter wavelengths (290-360 nm) are more effective at reducing Hg(II) than longer ones (400 – 600 nm) suggesting that radiation in the UV range is most effective in the DGM formation process, most likely due to the increased activity of the photons (Costa and Liss, 2000). The basic reaction for abiotic Hg reduction in the water column is:

$$\text{Hg(II)} + h\nu \rightarrow Hg^0 \quad \textbf{Equation 1}$$

Where: *hv* represents incident solar radiation and Hg(II) represents all divalent Hg species which are available for reduction. Not all Hg(II) species, however, are in an easily reducible form (Strode et al., 2007), and it has been suggested that reducible Hg in fresh water lakes only accounts for approximately 40% of the total Hg (O'Driscoll et al., 2006).

Several studies have been conducted by incubating natural waters in clear and dark bottles and monitoring subsequent DGM production over time. It was found that samples incubated in the clear bottles yielded DGM concentrations 2.4 to 8.9 times higher than those measured in the corresponding dark bottles providing further evidence that DGM production is greatly dependent on the presence of natural light (Amyot et al., 1994, Amyot et al., 1997b). Spiking samples with inorganic Hg(II) prior to in situ incubation was found to greatly increase DGM production rates (Amyot et al., 1994). This suggests that the presence of photoreducible Hg(II)

complexes in the sample bottles is a limiting factor in the DGM production. Hg(II) concentration has also been found to affect DGM concentrations in natural settings (Fantozzi et al., 2007); in fact, the concentration of DGM has been found to be directly proportional to the rate of Hg(II) loading in mesocosm studies (Poulain et al., 2006). This suggests that water bodies which have higher Hg concentrations due to either contamination or natural Hg loadings will likely exhibit greater DGM concentrations, provided that Hg is in an easily reducible complex. DGM levels at the water surface have also been found to be slightly lower than the main bulk of the epilimnion; this may be due to rapid evasion of Hg^0 from the upper layer to the atmosphere (Amyot et al., 1994).

A mesocosm study in a northern temperate lake found that DGM in the surface water increased rapidly after spiking the enclosures with an Hg(II) solution. The maximum DGM photoproduction (1 ng L^{-1} h^{-1}) occurred 3 days after the initial spike, suggesting rapid evasion to the atmosphere following a sudden increase in reducible Hg(II) species to a water body (Amyot et al., 2004). The increase in flux to the atmosphere was also coupled with a decrease in THg in the enclosure over time. DGM production has also been found to increase significantly after a rainfall suggesting that rain can act as a source for reducible Hg substrates (Lindberg et al., 2000). These studies suggest that a large portion of deposited Hg(II) can rapidly be reduced and re-emitted to the atmosphere.

Abiotic reduction of Hg(II) to Hg^0 (DGM) in water can also be initiated by humic substances (Alberts et al., 1974, Allard and Arsenie, 1991). It has been hypothesized that Hg(II) must be complexed with dissolved organic matter (DOM) in

order for Hg(II) photoreduction to take place (Allard and Arsenie, 1991); the reduction then takes place via electron transfer from the organic ligand to Hg(II). This could account for as much as 10 - 70% of Hg released from contaminated streams (Turner et al., 1989). Amyot et al. (1997a) found that DGM production in a northern temperate lake was lower in August than in June and July due to photobleaching of dissolved organic carbon (DOC). THg in the water was still elevated suggesting that the pool of photoreducible Hg was substantial; however, reduced DGM production was observed. Photobleaching of DOC is thought, therefore, to result in a decrease in organic radicals that may be involved in photoredox processes (Amyot et al., 2004). Costa and Liss (1999) also demonstrated that DGM production rates in seawater are greatly enhanced by the addition of chromophoric DOC. This suggests that DOC (or humic substances) can not only act as a screen for incoming light, but also as a source for reactive species involved with Hg transformations. Lakes or water bodies with low DOC may thus be more susceptible to Hg contamination due to the reduced ability to mobilize significant quantities of Hg to the atmosphere.

Photoinduced reduction of Hg in ocean samples has been found to follow pseudofirst order kinetics (Equation 2) with rate constants (k_r) in the range of 0.15 to 0.93 h^{-1} (Qureshi et al., 2010). These values are similar to fresh water rate constants of 0.32 to 0.65 h^{-1} for UV-B radiation and 0.28 to 0.65 h^{-1} for UV-A radiation (O'Driscoll et al., 2006). In Ocean surface samples, it was found that the presence of microbes and colloids did not influence the Hg reduction kinetics as pseudofirst order rate constants are in the order of 10^{-4} h^{-1} (Strode et al., 2007). These results indicate that abiotic reduction dominates biotic reduction of Hg near the surface of the ocean.

$$Hg(II) \rightarrow DGM; \quad k_r \qquad \textbf{Equation 2}$$

Some oxidation in the dark has been found to be carried out by the hydroxyl radical from photochemically produced hydrogen peroxide (Amyot et al., 1997a, Zhang and Lindberg, 2001); however, prior exposure to sunlight is necessary. Fe(III) induced photochemical production of DGM has also been suggested as a mechanism as it has been found that freshwater spiked with Fe(III) yielded significantly larger amounts of DGM (Zhang and Lindberg, 2001). It is suggested that the Hg(II) is reduced by photochemically produced Fe(III)-organic free radicals.

Laboratory experiments have also shown that Hg^0 oxidation is stimulated by chloride ions in a dose and time dependent manner, suggesting that DGM production in seawater may be more rapid than in freshwater (Yamamoto, 1996). Studies involving natural seawater have confirmed Yamamoto's findings that the presence of chloride promotes Hg oxidation in seawater over freshwater (Amyot et al., 1997a). It was also found that DGM was oxidized to Hg(II) in the dark in the presence of chloride which may be an important mechanism in the depletion of the Hg pool. Filtered seawater samples yielded approximately 45% less DGM than unfiltered samples suggesting that filtration may be removing a readily exchangeable or photolabile particulate Hg pool or a biotic component (e.g., bacteria and algae) that can reduce Hg(II). This suggests that photoinduced DGM production is a result of more than one mechanism.

1.6.2.2 Biotic Formation

Both laboratory and incubation experiments with natural seawater have suggested that the biologically mediated reduction of Hg(II) contributes to DGM

production. In several studies, DGM production has been found to occur without the presence of light (Fantozzi et al., 2009, Rolfhus and Fitzgerald, 2004) and in deeper waters where photochemical reactions are unlikely to play a significant role (Vandal et al., 1991, Amyot et al., 1997a). These results imply the existence of a biological pathway for reducing Hg(II). The production of DGM in the absence of light was originally hypothesized to be the result of Hg resistant bacteria associated with deep marine sediments to produce Hg^0 which is transported to the surface by upwelling zones (Kim and Fitzgerald, 1988). Several other studies have strengthened the biological role and extended it to not only bacteria, but phytoplankton (diatoms) as well (Rolfhus and Fitzgerald, 2004, Lanzillotta et al., 2004).

Eukaryotic microorganisms have been found to have the ability to reduce Hg(II) as DGM formation was found to decrease as a function of the inhibition of photosynthesis in cultures of the green algae *Chlorella* (Kelly et al., 2007). It has also been found that the high DGM concentrations are sometimes observed at depth along with the highest values of chlorophyll-a, or during algal blooms, suggesting that phytoplankton may produce DGM (Vandal et al., 1991, Poulain et al., 2004). DGM concentrations in the metalimnion were found to be strongly correlated to phytoplankton biomass. Concentrations decreased below the method detection limit when the phytoplankton biomass decreased by 75%, then rose when biomass increased (Poulain et al., 2004). Like other metals, it is hypothesized that algae and diatoms are able to reduce Hg(II) externally by cell surface enzymatic processes (Jones et al., 1987). DGM production has been found to occur in the dark for up to 2 hours after UV irradiance has stopped in solutions containing the marine diatom *Chaetoceros* (Lanzillotta et al., 2004). It is suggested that photo-activation of the

organic matter released by the cells is responsible for the observed DGM production in the dark; thus Hg(II) reduction can also be linked to light-dependant biological processes.

The primary Hg detoxifying mechanism used by Hg resistant bacteria is the reduction of mercuric ion to volatile Hg^0 (Steffan et al., 1988), and recently microbial reduction has been proposed as a more significant mechanism for the reduction of Hg in remote lakes (Siciliano et al., 2002). Bacteria have been found to play a significant role in dark conditions with a DGM production rate of about 2-4% of that produced under light conditions (Fantozzi et al., 2007). In areas where Hg contamination is present, it is hypothesized that bacterial reduction may even be more important than photochemically driven processes (Barkay et al., 1989). Studies of Hg(II) reduction by prokaryotic microorganisms at high Hg(II) concentrations have demonstrated that some bacteria can reduce Hg(II) using a plasmid encoded enzymatic pathway, the mer gene (Barkay et al., 1991, Barkay, 2001). The mechanisms by which Hg(II) is reduced to DGM in instances of low light is still poorly understood and further studies are needed.

Increased concentrations of DGM have been noted at the sediment-water interface, and it is suggested that bacterially mediated Hg(II) reduction is largely responsible (Kim and Fitzgerald, 1988). Very little is known about DGM production in the anoxic zones of the hypolimnion, and it is suspected that it is the result of chemical reactions involving humic substances, or an unidentified bacterial pathway (Poulain et al., 2004). Biologically formed compounds (Xiao et al., 1995) and cell metabolites (Lanzillotta et al., 2004) have been found to play a role in DGM

formation (abiotic reduction requiring sunlight, Section 1.6.2). In-situ methods of measurement are currently not able to assess the relative contributions of biotic Hg(II) reduction to the total reduction or to determine the ratio between the two formation processes. Many pathways, both abiotic and biotic, have been suggested to contribute to DGM formation; however, the dominant mechanism responsible in natural systems remains highly uncertain. Abiotic and biotic mechanisms are most likely inter-connected and work in a synergistic way, and more study is required on the ability to define DGM production pathways.

1.6.3 Environmental Factors Affecting DGM

When considering DGM concentrations in natural systems, it is important to look at the surrounding environment at the time of sampling. DGM production rates can vary on a daily, monthly, and seasonal basis. Micrometeorological parameters are known to play an important role in controlling the dynamics of DGM production and evasion; for example, warmer waters will lower the solubility of Hg^0 increasing the amount evaded to the atmosphere and thus reducing the concentrations present in the sample. Wind induced turbulence can also destabilize the boundary layer at the air-water interface thus reducing transfer resistance and increasing the overall flux of DGM to the atmosphere (Section 1.7). The incidence of solar radiation will also affect the rate in which DGM is formed (Section 1.6.2), thus the geographical location, cloud cover, and time of year will also have a role in production rates.

The physical environment is also important to consider as during the winter months, the Arctic Ocean and most temperate lakes will freeze. During this time, light is still able to penetrate the ice cover (depending on the amount of snow cover);

however, produced DGM will be unable to completely evade to the atmosphere which may lead to supersaturation in water, and increased concentrations in the water column. Factors such as turbidity may also influence production as it may decrease light penetration; however, it may also give rise to an increase in the amount of DOC present in the water.

1.6.4 DGM in the Arctic

There are many pathways proposed for the formation of DGM; however, the mechanisms which may be the most relevant in Arctic systems are highly uncertain. DGM in the Arctic will behave differently than in more southern temperate regions due to lower temperatures, and elongated periods of daylight and darkness. The permanent and intermittent ice cover will also affect evasion of DGM to the atmosphere and thus affect Hg^0 flux patterns.

Photochemical production of DGM will be likely favoured over biological ones in the colder Arctic waters. Surface water temperatures during the summer are low, generally ranging between 3 and 6°C, resulting in reduced primary production and thus the reduced importance of the biologically mediated DGM production pathway. Due to periods of 24 hour sunlight in the summer, the abiotic processes may be enhanced, as it has been shown that increases in sunlight radiation also increase DGM production (Section 1.6.2). In the high Arctic, however, there is a lower sun angle and UV-B levels are only one quarter what they are in temperate regions. During the dark period, DGM production may be mediated more by biological activity, either in the sediments or in the water column.

Enhanced DGM concentrations have been recorded in the Arctic Ocean in several studies (Andersson et al., 2008b, St. Louis et al., 2007). It was also found that DGM levels increased with proximity to the pole with values approximately 10 times higher than observed in the North Atlantic (Andersson et al., 2008b). However, average DGM measurements conducted near Ellesmere Island in Northern Canada were reported to be as high as 128.4 ng m^{-3}, inferring that the ice free Arctic marine waters may actually act as a source of Hg^0 to the atmosphere (St. Louis et al., 2007). More work is needed to determine whether the Arctic Ocean is acting either as a sink or a source of Hg.

1.6.5 Determining DGM Concentrations

There are a number of different methods used in determining the concentration of DGM in samples and all of them follow the principle that DGM is volatile, and will partition readily to the surrounding air. One significant weakness in the measurement of DGM is the absence in the literature of a standardized methodology. This would be extremely helpful when it comes to comparing data between studies, as well as in determining long term changes or trends.

Major factors need to be considered when determining DGM concentrations including sampling methods, sample volumes, purging times, flow rates of purging gas, and storage/handling of water samples. Some studies have shown that collected water samples are not stable even over short time periods due to the volatility of DGM (Lindberg et al., 2000, Rolfhus and Fitzgerald, 2004), while other studies suggest that there is no loss of DGM in samples stored for up to 2 days (Rolfhus and Fitzgerald, 2004). As DGM is very sensitive to its surrounding environmental

conditions (temperature, solar radiation, etc.), it makes sense, however, to analyze the samples as soon as possible following collection. Typical sampling volumes range from 500 ml to 20 L depending on the type of vessel used, and purging times can range from 15 min to 60 min depending on the sample volume, method, and desired recovery.

Before sampling for DGM it is important to consider the cleanliness of the environment in which the analysis is to be performed. Since typical levels of DGM in natural waters are in the pg L^{-1} range, a clean lab of class 1000 or lower with Hg scrubbing air filters is ideal to avoid potential contamination of the sample by the analytical technique itself. Due to the sensitivity of DGM to solar radiation, it is best if analysis is performed in the dark or low light conditions (Lindberg et al., 2000, Lanzillotta and Ferrara, 2001). Sample collection and transport is also critical, and measures should be taken to avoid contamination at all steps. The use of clean sampling protocol is recommended such as "clean hands dirty hands" described by Fitzgerald (1999). Care must also be taken to avoid exposure to air or extreme changes in temperature prior to analysis. Sample turbulence should be avoided at time of collection and minimized during transport.

There are 2 main techniques of DGM measurement currently in use: 1) purge and trap, and 2) air/water equilibration. Of these two methods, there are also both manual and automatic variations. Purge and trap is the most widely used method which involves bubbling an inert, Hg free carrier gas (e.g., Ar) through the water sample, then capturing the extracted Hg^0 (DGM) on a gold cartridge for analysis (Poissant et al., 2000, Poulain et al., 2004, Amyot et al., 1994). The equilibration

method involves a much larger vessel, in which air above the surface is allowed to reach equilibrium with the sample below, and the DGM value is calculated based on Henry's law (Kuss and Schneider, 2007, Andersson et al., 2008a). The Hg^0 detection method is very well established using cold vapour atomic fluorescence spectrometry (CVAFS), and is typically performed by a commercially available instrument such as a Tekran 2500. Normally the analysis is done in-situ due to the nature of DGM; however, some studies have been conducted where the DGM is immediately purged onto a gold trap, which can then be easily transported and analyzed at a later date (Narukawa et al., 2006).

An automated approach is useful in that it simplifies the process for the operator, and allows for a higher sample through put (Gårdfeldt et al., 2002). An automated system, however, will only work if a constant supply of sample is available, thus it is especially suited for sampling from research ships or labs with a continuous source to a sample such as a portable clean room. For most applications, the manual method is preferred. The manual setup used in this study can be seen in Figure 3-1, and a description of both manual and automatic systems can be found in Gardfeldt et al. (2002). Many methods use generated Hg free air instead of Ar as a carrier gas (O'Driscoll et al., 2003, Poissant et al., 2000) and some use N_2 (Narukawa et al., 2006). The major difference between automatic and manual measurement is that the automated system must have a vessel (sparger/impinger) designed with in- and out-flows in which the sample can flow continuously. The detector unit must also be capable of running continuously and sampling at a regular time interval determined by the operator.

The air/water equilibrium method involves isolating air and water in a large vessel, and allowing for equilibrium to be obtained (approx. 1 h). Once complete, air from the vessel is analyzed using CVAFS and the DGM is calculated using Henry's law and the following equation:

$$DGM = \frac{Hg^0_{eq}}{K_H} \quad \textbf{Equation 3}$$

Where Hg^0_{eq} is the amount of Hg^0 contained in air at equilibrium, and K_H is the temperature corrected Henry's Law Constant. A detailed description for this setup can be found in Kuss et al. (2007). The equilibrium system has also been adapted to an automatic system and a description can be found in Andersson et al. (2008a). Although all of these systems are based on the same principles, they can yield different results due to variations in the methodologies such as sample volume, purge times, flow rates, etc.

1.7 Air-Sea Exchange of Mercury

For biogeochemical cycles, air-water gas exchange is an important link between the atmosphere and the oceans as it governs the transport between the dissolved state in the water and the gaseous phase in the atmosphere. Gas transfer at water surfaces is becoming increasingly important in understanding the various pathways of chemicals and is a critical factor in understanding their cycling in the environment. Atmospheric deposition is the main source of Hg to the ocean, and conversely, the ocean reemits Hg to the atmosphere as a result of supersaturation of DGM in the ocean with respect to air (Schroeder and Munthe, 1998).

The global flux of Hg^0 to the atmosphere has been estimated to balance that of total wet and dry deposition to the oceans, 2608 t y^{-1}, approximately 40% of total annual emission to the atmosphere (Mason and Sheu, 2002). Another estimate suggests that global evasional Hg^0 flux to the atmosphere could be as high as 2828 t y^{-1} (Strode et al., 2007). Open ocean fluxes have been found to range from 19.7 ng m^{-2} d^{-1} in the North Pacific in May (Laurier et al., 2003), to 1970 ng m^{-2} d^{-1} in the equatorial and South Atlantic in May and June (Lamborg et al., 1999). This large variation is due to temperature variation, local wind speeds, local Hg(II) concentrations, and biological activity.

Estimating air-sea fluxes is a complex science, as the air and water surfaces are usually turbulent in motion and the interface between them is disturbed by waves and other factors (Section 1.7.2). Over the past 3 decades many theories and methods have been developed for estimating Hg^0 flux across the air-sea interface. The following section will describe current models used in determining fluxes from measured environmental parameters, including various methods for determining the transfer velocity (k_w) across the air-water interface. The methods described in Section 1.7.1 apply to most gasses, and here will be used to calculate air-sea Hg^0 flux rates.

1.7.1 Air-water Exchange Theory

As a gas dissolved in the surface layer, DGM will equilibrate with the atmosphere and establish a net flux; the direction of which will depend on the saturation state with respect to its concentration in the air. Much work has been done on determining the relationship between gas transfer and wind speed and several methods are in existence for determining flux values of gases based on the

concentration differences between air and water and a kinetic term often referred to as a transfer velocity (k_w) (Wanninkhof et al., 1985, Liss and Merlivat, 1986, Liss et al., 2004, Wanninkhof, 1992, Loux, 2006, Poissant et al., 2000). The k_w is frequently parameterized solely in terms of wind speed, although the actual process is also affected by other physical processes which will be elucidated in Sections 1.7.2 and 1.7.3.

The basic mathematical theory for determining flux is well established and is based on the stagnant film model (Whitman, 1923), also known as the two-layer model. In Figure 1-3 below, Z in the diagram depicts the air-sea interface, and both the atmospheric and ocean turbulent regions are further away where Hg is assumed to be well mixed within each compartment. This model is based on the assumption that there is no turbulence at the boundary layer resulting in two stable stagnant films of finite thickness, one on the air side and the other on the ocean side. The transfer of Hg or other gasses through these stagnant layers is governed by molecular diffusion, consequently, the concentration and partial pressures of the gas changes linearly in the film until the saturation level at the interface is reached. Since molecular transfer occurs much more slowly than turbulent transfer, the exchange across the film is considered the rate determining step.

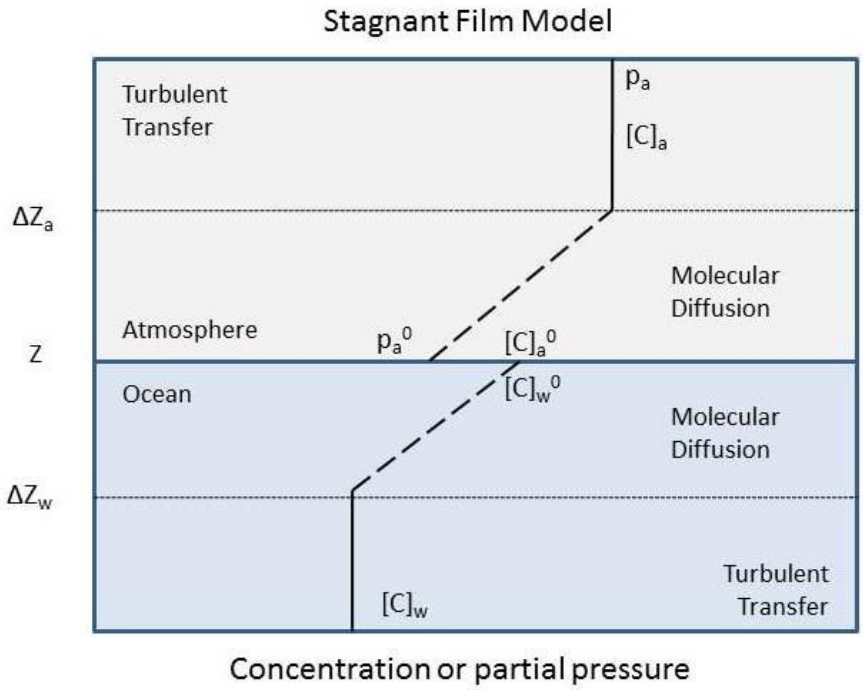

Figure 1-3: Diagram showing the stagnant film (two-layer) model theory, Z represents the air/sea interface, ΔZ represents boundary layer thicknesses, [C] represents concentrations, ρ represents partial pressures.

The gas flux (typically mol m^{-2} s^{-1}) on both the air and water films can be estimated by the concentration difference across the layers of distance Z as follows:

$$F_a = -D_a \frac{[C]_a - [C]_a^0}{\Delta Z_a} \quad \textbf{Equation 4}$$

Where F_a is the gas exchange flux in the atmospheric stagnant film (mol m^{-2} s^{-1}), D_a is the diffusivity (Section 1.7.3) of the gas across the film, $[C]_a$ is the concentration of the gas in the atmosphere and $[C]_a^0$ is the concentration of the gas at the interface between the two mediums. Partial pressure can also be used in the estimation as follows:

$$pV = nRT \quad \textbf{Equation 5}$$

Where n is the number of moles, R is the gas constant (R = 8.314 J K^{-1} mol^{-1}**)**, T is the temperature in Kelvin, p is pressure (Pa) and V is volume (m^{-3}). [C] Can be determined using partial pressure as follows:

$$[C] = \frac{n}{V} \quad \textbf{Equation 6}$$

$$[C] = \frac{P}{RT} \quad \textbf{Equation 7}$$

Substituting Equation 7 into Equation 4 gives the following equation for gas flux on the atmospheric side:

$$F_a = -\frac{D_a}{RT\Delta Z_a}(p_a - p_a^0) \quad \textbf{Equation 8}$$

The gas exchange flux on the water side can be calculated similarly as below:

$$F_w = -D_w \frac{[C]_w^0 - [C]_w}{\Delta Z_w} \quad \textbf{Equation 9}$$

Where $[C]_w^0$ is the concentration of the gas at the interface and $[C]_w$ is the concentration of the dissolved gas in the upper layer of the water. It is important to know that at the interface $[C]_w^0$ and $[C]_a^0$ are equal; they are separated in the diagram simply to denote separation between the two compartments. It is not possible to determine the concentration of gas $[C]_w^0$ at the interface directly, thus it must be calculated. Since there are no other sources or sinks into each of the films we can assume that according to Henry's law and Equation 7:

$$[C]_w^0 = \frac{p_a^0}{K_H} = \frac{RT[C]_a^0}{K_H} \quad \textbf{Equation 10}$$

Where p_a^0 is the partial pressure of the gas at the interface and K_H is the Henry's law constant which is a dimensionless constant expressing the ratio between the concentration of gas in the air phase to the concentration of gas in the water phase at equilibrium ($K_H = [C]_a/[C]_w$). The theoretical Henry's Law Constant (H = atm m^3 mol^{-1}) should be corrected for temperature and pressure as the equilibrium rate will be affected by both of these parameters. In an infinitely diluted aqueous system:

$$K_H = 0.987 H M_w / p_T \quad \textbf{Equation 11}$$

Where M_w is the molecular mass of H_2O (0.018 kg mol^{-1}), and p_T is the density of water which is temperature dependent. K_H can be corrected for temperature as follows (Clever et al., 1985):

$$lnH = 55.7339 - 95.4036/(T/100) - 16.0477 \ln(T/100) \quad \textbf{Equation 12}$$

This can be further simplified to:

$$K_H = \frac{0.01777}{p_T} e^{129.6363 - 9540.36/T - 16.0477 lnT} \quad \textbf{Equation 13}$$

Since the Hg data collected was from seawater, it is also necessary to correct the Henry's law constant for salinity. This under the assumption that the seawater is equivalent to an electrolyte solution of 0.7 mol L^{-1} (Sanemasa et al., 1981):

$$K'_H = 1.136 K_H \quad \textbf{Equation 14}$$

We can assume that $F_a = F_w$ because the overall amount of gas traveling through the two layers from the water to the air must be equal since the side with the

lowest transfer velocity (k) will limit the overall exchange. Transfer velocity is a term that is introduced to encompass both the diffusivity (D) and the depth of the boundary layer (ΔZ). Diffusivity is a function of temperature and has been determined experimentally for many gases. Z is the depth of each film and is affected by turbulence intensity; as turbulence increases, the films erode leading to more rapid gas transfer. The determination of the transfer velocity is where many models begin to diverge as there are many different factors that can affect this process.

$$k_a = \frac{D_a}{\Delta Z_a} \quad \textbf{Equation 15}$$

$$k_w = \frac{D_w}{\Delta Z_w} \quad \textbf{Equation 16}$$

By combining Equation 4 and Equation **9**, under the assumption of $F_a = F_w$, and introducing the transfer velocities through air and water (see more in Section 1.7.3), we can solve the equation to determine the concentration at the interface as follows:

$$[C]_w^0 = \frac{k_a[C]_a + k_w[C]_w}{k_a + k_w RT/K_H} \quad \textbf{Equation 17}$$

Substituting Equation 17 into Equation 4 and isolating the values for k_a and k_w we arrive at the following equation:

$$F = F_a = F_w = -\frac{k_a k_w}{k_a + RTk_w/K_H}(RT[C]_a/K_H - [C]_w) \quad \textbf{Equation 18}$$

For Hg, as well as many other geochemically important gases, the K_H value is known to be quite large (~ 729 Pa $m^{-3}mol^{-1}$ for Hg), thus $k_a \gg RTk_w/K_H$ signifying

that the flux is limited on the water side. Because of this we can remove k_a from the equation, and assume the overall flux is controlled on the water side, and equal to:

$$F \approx -k_w(RT[C]_a/K_H - [C]_w) \quad \textbf{Equation 19}$$

Substituting in the corrected values for K_H from Equation 13, we arrive at the following flux model:

$$F \approx -k_w\left(\frac{RT}{\frac{0.01777}{p_T}e^{129.6363-9540.36/T-16.0477lnT}}[C]_a - [C]_w\right) \quad \textbf{Equation 20}$$

The above model is useful for fresh water fluxes. In seawater, the K_H must be further corrected by using the K'_H value from Equation 14.

1.7.2 Factors Affecting Gas Exchange

Gas transfer is thought to be regulated mainly by turbulence at the air-water interface (Jahne et al., 1987); however, this is not solely linked to wind speed. Thus, it is likely that relationships based on wind speed alone to predict the gas transfer velocities will be flawed (Wanninkhof, 1992). Methods such as the backscatter of microwave radiation from water surfaces may be a more accurate predictor of gas transfer as it is more directly related to the observed surface turbulence, and may be better suited for prediction of air-sea exchange. That being said, wind tunnel experiments have shown that wind speed is one of the major factors influencing gas transfer rates (Wanninkhof and Bliven, 1991) and so, in the current study we use this relationship to calculate our Hg^0 flux estimates. There is currently an estimated

uncertainty of about a factor of 2 when using wind speed parameterization (Liss et al., 2004).

The transfer velocity quantifies the kinetics of air-sea gas exchange and is controlled by a variety of factors: wave height and slope, wind fetch, sea state, bubble field, and degree of white capping. These factors can all affect the degree of turbulence in the stagnant film model (Liss et al., 2004). Due to the fact that these factors are largely wind driven they are often amalgamated together in terms of wind speed (u). The transfer rates can also be affected by chemical reactions of the gas in seawater, which may be significant for gases with rapid aqueous phase chemistry. Surfactants are also suggested to play a potential role in the transfer rate, however their role is less well established (Frew, 1997). For our purposes we will not look at chemical reactions within the water column or the role of surfactants as there is a large degree of uncertainty associated with these parameters.

Studies conducted in wind-wave tanks have indicated that fetch has an influence on gas transfer (Jahne et al., 1989). Wave fields over the open ocean have the ability to grow over distances of hundreds of kilometers (Hasselman, 1975) suggesting that the turbulence over the ocean at a certain wind speed is larger than the turbulence over a smaller lake or bay with a smaller fetch and equal wind speeds. There is also evidence of fetch dependence at low wind speeds based on work performed using the gas tracer sulphur hexafluoride (SF_6) on lakes with differing surface areas (Wanninkhof et al., 1985, Wanninkhof et al., 1987, Wanninkhof et al., 1990, Upstill-Goddard et al., 1990). Pyramid Lake, the largest lake in the studies, had the highest average gas transfer velocity and exhibited the strongest dependence on

wind speed (Wanninkhof et al., 1991). Wind speed variance can also play a significant role on the gas transfer velocity. It has been found that gas transfer velocities measured over long time periods with variable winds are higher than if they are measured instantaneously or under steady wind conditions (Olsen et al., 2005). These differences can most likely be attributed to the wave pattern produced on the surface. Lake water temperature differences may also give rise to discrepancies among the results. Gas transfer and wind speeds can also be biased by the placement of the wind meters during experiments.

1.7.3 Estimating the Transfer Velocity (k_w)

There are two main ways in which k_w has been investigated: in the laboratory using primarily wind tunnel experiments, and field measurements. From these several models have been developed to calculate k_w. As denoted in Section 1.7.1, we are only focused on the transfer velocity through the water side of the film. Thus, Equation 16 is used as the basis to calculate k_w. As mentioned, D_w is dependent on temperature, and ΔZ_w is dependent on the wind speed and viscosity of the water; also a function of temperature. The following methods for determining k_w are all based on two major parameters: wind speed corrected to 10 m above the surface (u_{10}), and the Schmidt number (Sc). The wind speed can be corrected to 10 m using Equation 21 (Schwarzenbach et al., 1993), or by the National Oceanic and Atmospheric Administration Coupled Ocean-Atmosphere Response Experiment routine (NOAA COARE) as described in Fairall et al., 2003.

$$u_{10} = \frac{10.4 u_z}{\ln(z) + 8.1} \quad \textbf{Equation 21}$$

Where u_z is the measured wind speed at height z (m).

The Schmidt number is used in most methods for determining k_w as it incorporates the kinematic viscosity of the water and the diffusion coefficient into the equation for k_w. The Sc number can be broken down as:

$$Sc = \frac{v}{D} = \frac{n}{\rho D} \quad \textbf{Equation 22}$$

Where v is the kinematic viscosity ($cm^2\ s^{-1}$), n is the dynamic viscosity of water (Pa s), and ρ is the density of water ($g\ cm^{-3}$) (a table for the determination of the dynamic viscosity and density in water can be found in Appendix B). For a smooth liquid interface, k_w is proportional to $Sc^{-2/3}$ (Deacon, 1977). For an interface with waves, most models predict that k_w is proportional to $Sc^{-1/2}$ (Coantic, 1986). One can use Sc to calculate the k_w for any gas by relating it to a known value (600 for CO_2 in freshwater and 660 for seawater) as long as the Sc for the gas in question is known (Jahne et al., 1987, Wanninkhof, 1992). D can be estimated for varying temperatures using the Wilke-Chang relationship as follows:

$$D = D_{298.15} \times \frac{T}{298.15} \times \frac{n_{298.15}}{n_T} \quad \textbf{Equation 23}$$

The diffusivity for Hg^0 in water at 25°C has been estimated at 7.23×10^{-6} $cm^2\ s^{-1}$ (Loux, 2004), and $n_{298.15} = 8.907 \times 10^{-4}$ Pa s, which can be used to estimate the Sc for Hg based on Equation 22.

1.7.3.1 Wanninkhof (1992)

Wanninkhof (1992) looks at the relationship between wind speed and gas transfer over the ocean as well as the possibility of chemical enhancement of CO_2

exchange at low wind speeds in the determination of CO_2 flux. The effect of wind speed is illustrated through a quadratic dependence of gas exchange on wind speed which is fit through gas transfer velocities determined by natural ^{14}C disequilibrium and the bomb ^{14}C inventory methods. From previous experimentally determined results for CO_2 gas exchange values, the following equation was derived:

$$k = 0.39u_{av}^2 \quad \textbf{Equation 24}$$

Where u_{av} is the long term averaged wind speed during the experiment and 0.39 represents the proportionality constant (denoted *a*) for gas transfer. By including the Sc for Hg we get:

$$k_{av} = 0.39u_{av}^2\left(Sc_{Hg}/660\right)^{-0.5} \quad \textbf{Equation 25}$$

Where k_{av} represents the long term transfer velocity, Sc_{Hg} represents the calculated Schmidt number for Hg, and 660 represents the Sc of CO_2 in seawater at 20°C. Using long term average winds speeds yields a value for a = 0.31, experimental results yield 0.32, thus for steady winds, the relationship between gas transfer and wind speed is determined as:

$$k = 0.31u_{10}^2\left(Sc_{Hg}/660\right)^{-0.5} \quad \textbf{Equation 26}$$

Equation 26 can then be used to deduce gas transfer velocities for Hg at steady winds from spot measurements made by ship board anemometers.

1.7.3.2 Liss and Merlivat (1986)

Liss and Merlivat (1986) use a synthesis of results from various experiments, wind tunnel and field, to propose 3 separate equations for determining k_w based on

different wind speed regimes. The smooth surface regime includes wind speeds (corrected to 10 m) up to 3.6 m s^{-1} where the water is generally smooth or with only a few waves. In this regime it was found that the k_w value is proportional to $Sc^{-2/3}$. The resulting equation for $u_{10} < 3.6$ m s^{-1} is:

$$k_w = 0.17u_{10}(Sc_{Hg}/660)^{-0.67} \quad \textbf{Equation 27}$$

The rough surface regime is where the water surface is wave covered but is not rough enough for wave breaking to be common. The rough surface regime has been estimated to commence at 3.6 m s^{-1} and go to approximately 13 m s^{-1}. As previously discussed, the presence of waves can increase the slope of k_w *vs.* wind speed as it increases the area available for gas transfer and destabilizes the film layers. Studies have shown that in this regime the k_w is proportional to $Sc^{-1/2}$ for higher wind speeds, the resulting equation for $3.6 > u_{10} > 13$ m s^{-1} is:

$$k_w = 2.8u_{10} - 9.6(Sc_{Hg}/660)^{-0.5} \quad \textbf{Equation 28}$$

The breaking wave or bubble regime begins at wind speeds above 13 m s^{-1} where bubbles from breaking waves act to enhance gas transfer by increasing the surface area available for exchange even further. The enhancement of gas transfer associated with wave breaking can cause a significant increase in slope of the transfer velocity vs. wind speed plot (Merlivat and Memery, 1983), the resulting equation for $u_{10} > 13$ m s^{-1}:

$$k_w = 5.9u_{10} - 49.3(Sc_{Hg}/660)^{-0.5} \quad \textbf{Equation 29}$$

1.7.3.3 Wanninkhof (1985) as per Poissant et al. (2000)

Poissant et al. (2000) presents a dataset including Hg^0 fluxes over the water surface of the upper St. Laurence River and Lake Ontario using the two layer model described above. The method for calculating k_w was adapted from the publication by Wanninkhof et al. (1985), and several additional corrections were introduced. First, the Sc for CO_2 was temperature corrected as follows:

$$Sc(CO_2) = 0.11T^2 - 6.16T' + 644.7 \quad \textbf{Equation 30}$$

Temperature-corrected kinematic viscosity of water and Hg diffusivity in water was calculated as follows:

$$v = 0.017^{(-0.025T')} \quad \textbf{Equation 31}$$

Finally, Henry's law constant was corrected for temperature using:

$$H' = 0.0074T' + 0.1551 \quad \textbf{Equation 32}$$

These values are incorporated into the k_w equation determined from Wanninkhof (1985) and are based on experiments with the tracer SF_6 on a natural lake as well as the flux equations described in the above sections:

$$k_w = 0.45u_{10}^{1.64}(Sc_{Hg}/Sc_{C02})^{-0.5} \quad \textbf{Equation 33}$$

1.7.3.4 Cole and Caraco (1998) as per Loux (2004)

Loux (2004) also looked at air-water exchange parameters specific to Hg, adapting the k_w equation from Cole and Caraco (1998) which is based on experiments using SF_6 as a tracer on a small, soft water low wind lake (Cole and Caraco, 1998). He uses the coefficient values for *a* determined experimentally, followed by the

assumption that k_w is proportional to $Sc^{-2/3}$ at low wind speeds (u_{10} < 3.6 m s^{-1}) and $Sc^{-1/2}$ at moderate wind speeds (u_{10} > 3.6 m s^{-1}). The resulting equation is:

$$k_w = 2.07 + 0.215u_{10}^{1.17}(Sc_{Hg}/660)^n \quad \textbf{Equation 34}$$

Where *n* is -0.67 or -0.5 depending on the wind speed regimes.

1.7.3.5 Nightingale et al. (2000)

Nightingale et al. (2000) developed the following method for evaluating k_w based on multiple dual tracer experiments in marine settings. The k_w equation is the result of the best fit line to the total dataset used in the experiments covering a wide range of wind speeds. This accounted for up to 80% of the total variance:

$$k_w = (0.22u_{10}^2 + 0.333u_{10})(Sc_{Hg}/660)^{-0.5} \quad \textbf{Equation 35}$$

This method was found to produce results mid-way between those produced by Liss and Merlivat 1986 and Wanninkhof 1992.

1.7.4 Air-Sea Exchange Synthesis

All methods described above aim to estimate the flux of various gases across the air/sea interface; however, some are better suited for the conditions observed in the Arctic. There are two main assumptions which are required to apply the stagnant film model in flux calculations which are: a) Hg does not undergo any reaction within the film layers, and b) the concentrations at the boundaries are kept constant long enough that the concentration profile reaches a steady state (Schwarzenbach et al., 1993).

Conditions in the Amundsen Gulf were significantly different compared to the studies used to derive these equations, thus their applicability may be limited.

Temperatures differed greatly from the original studies which were all performed in more temperate regions. Water in the open leads and under ice can approach -2°C and air temperatures were quite often in the -20°C range. These differences may have implications in the applicability of the Henry's law constants and the k_w calculations. Cold water is also known to hold more gas than warmer water thus the solubility of Hg^0 itself will be higher. More study is required to determine whether or not these methods are suitable for Arctic applications.

Due to the previously discussed nature of DGM, variation in the sample location, time, and method of sample collection may yield large differences in results. Conditions at the time of DGM measurement, i.e. ice conditions, air temperature, water temperature, pressure, and wind speed were recorded. Equations geared more towards instantaneous flux values were used over long term averaged ones due to the dynamic conditions observed. Measurements for GEM and DGM can be introduced into Equation 20 to give the general equation to be used in Hg^0 flux calculations:

$$F \approx -k_w \left(\frac{RT}{\frac{0.01777}{p_T} e^{129.6363 - 9540.36/T - 16.0477 ln T}} [GEM] - [DGM] \right) \quad \textbf{Equation 36}$$

Calculating Hg^0 flux across the water surface using the stagnant film model is convenient but not necessarily accurate. Given the various uncertainties in the designed models combined with the uncertainty towards the applicability of the models to Arctic environments, this area should remain a productive area of research in the future given the ever increasing concern for Hg contamination in the North. The model for determining flux above represents a synthesis of available methods and

has proven to be fairly reliable when compared with experimental data. Much of the variability comes from the implementation of the system dependent k_w coefficient. More research is required into the Hg specific parameters such as the specific Sc values and aqueous Hg^0 diffusivities.

1.8 The Role of Sea Ice and the Circumpolar Flaw Lead System

The Circumpolar Flaw Lead (CFL) system is an area in which open leads and polynyas reoccur annually due to natural oceanic processes. Leads are stretches of open water formed by ice movement caused by either wind or ocean currents. Polynyas are formed from either warm water upwelling (sensible heat polynya), or wind or ocean currents driving mobile pack ice away from fixed boundaries such as land fast ice, ice bridges, or coastlines (latent heat polynyas). Flaw lead areas are among the most dynamic and productive regions in Arctic environments thus they provide a unique site for studying the potential effects of climate change. The Amundsen Gulf in Canada's western Arctic is an area or reoccurring flaw leads and is the center for the international circumpolar flaw lead system study funded as part of the 4^{th} International Polar Year (2007 – 2008).

As previously mentioned the sea ice environment plays an essential role in AMDEs however the chemistry and mechanisms are not yet fully understood. The dynamic ice shifting characteristic of the CFL system may greatly contribute to AMDEs in that the continual opening and refreezing of leads has been suggested as a source for halogen species required for AMDEs. Halogen concentrations in snow on sea ice have been found to be elevated (Simpson et al., 2005, Simpson et al., 2007)

which may lead to enhanced AMDE chemistry near sea ice. As mentioned previously, newly formed ice is also ideal for frost flower formation which is considered a main contributor to the bromine explosion seen during Arctic spring (Alvarez-Aviles et al., 2008, Kaleschke et al., 2004a, Rankin and Wolff, 2002). High densities of BrO have been confirmed over marginal ice zones by the GOME satellite throughout the Arctic and Antarctic (Ridley et al., 2003, Zeng et al., 2003) and ODEs have been reported to have originated from these areas (Bottenheim and Chan, 2006). Due to these factors it is hypothesized that GEM may be converted to oxidized forms at an increased rate in or around CFL systems. The CFL system thus provides a unique setting for the study of AMDEs and the processes which control them.

The open leads provide a direct link between the warmer ocean water and the colder air above. The large temperature difference between the open water and air creates a supersaturated environment for water vapour near the open leads. This leads to convective plumes, dark clouds of vapour rising from open water areas, being common in flaw lead environments (Douglas et al., 2005). This water vapour saturated environment leads to the formation of diamond dust (ice crystal precipitation) and surface hoar, the faceted feather structure ice crystals forming on nearby snow and ice surfaces (Berg et al., 2001, Andreas et al., 2002). Surface hoar samples collected near leads have been found to have Hg concentrations as high as 820 ng L^{-1} (Douglas et al., 2008) which is much higher than the typical snow values following AMDEs of 80 -100 ng L^{-1} (Lu et al., 2001). This suggests that the convective plumes formed from open water either enhance the transfer of halogens to the atmosphere, or that they promote the deposition of RGM through increased scavenging though the formation of ice crystals (Douglas et al., 2005). Hg

concentrations in diamond dust was later confirmed to be as high as 1370 ng L^{-1} which further implicates its role in Hg scavenging and deposition near flaw leads (Douglas et al., 2008).

Leads may also provide a path in which Hg can be directly deposited to the marine ecosystem by exposing open water and bypassing the ice barrier where there is the potential for re-emission. Since Hg(II) is highly soluble in water, this may lead to increased Hg contamination in these biologically active CFL system areas. Recent and accelerating changes in climate and sea ice cover in Polar Regions are likely to play a significant role in Arctic Hg cycling. CFL system areas may be the most highly impacted environments by these changes, and thus must be studied first to assess the potential impact to the Arctic system as a whole.

1.9 Objectives and Thesis Organisation

The overall goal of the Hg component of the CFL system study is to determine the net contribution of AMDE-deposited Hg to Arctic marine ecosystems, and identify whether AMDEs are a significant contributing factor to increased Hg levels observed in the North. This goal requires the collaboration of several research projects including atmospheric, hydrospheric, biospheric, and cryospheric components. The main objectives of this research component is to (1); determine the contribution of the dynamic sea-ice environment of the CFL system to AMDEs (2); determine if AMDEs over the ocean surface behave differently from those measured at coastal sites, and (3); determine DGM concentrations in the Gulf, which will be used in determining the direction and rate of flux between the ocean/atmosphere interface. Secondary objectives will look to establish the role of temperature, wind

speed, and wind direction on AMDEs, as well as to determine the role of AMDE duration on minimum GEM values. As mentioned earlier, AMDEs have been extensively studied and documented; however most research has taken place from land based or coastal research stations. This is the first study carried out over the ocean surface near a flaw lead system for an entire AMDE season.

This thesis is organised in 4 chapters. Chapter 1 (this chapter) provides a thorough literature review on topics relevant to this study. Chapter 2 reports the atmospheric component of this study and identifies the occurrences and characteristics of AMDEs observed over the Amundsen Gulf throughout the entire AMDE season of 2008. The roles of meteorological and sea ice conditions on AMDEs are discussed, and a comparison is made between this ocean-based study to previous coastal-based studies.

Chapter 3 reports the DGM and flux component of this study, and highlights differences observed in the Amundsen Gulf over those reported from other areas. A comparison between several flux calculation techniques is also discussed.

Chapter 4 summarizes the major findings from this study, and discusses the need and direction of future research. The sources of error and potential improvements to both components of this study are also discussed.

Chapter 2: The Role of the Circumpolar Flaw Lead System on Atmospheric Mercury Depletion

In this chapter, results from the first component of this research project are presented and discussed: atmospheric measurements of Hg species in the Amundsen Gulf. This study encompasses the first atmospheric Hg speciation dataset produced directly over the ocean for an entire AMDE season, thus, the findings complement earlier studies that were conducted along polar coastal regions. This study will investigate 3 major atmospheric Hg species in relation to several additional parameters including the sea ice environment, and meteorological conditions.

2.1 Hypothesis

Due to the dynamic nature of the CFL system and its potential to provide a source of catalytic reactive halogen radicals, it is hypothesized that AMDEs observed in the Beaufort Sea will be highly variable due to the effects of the local sea ice and meteorological conditions. We expect to see increased AMDEs at sites with large amounts of new ice, and/or in the presence of open leads. Air masses moving in from locations where AMDEs are occurring (e.g. with open water or new ice) are expected to contribute to low GEM values at the receiving sites and vice versa.

2.2 Experimental

2.2.1 Study Area

Atmospheric Hg measurements took place during the IPY-CFL project from mid-January to mid-July 2008 on board the CCGS Amundsen. Most of the period

was spent in the Amundsen Gulf (approx. 71º 00´N, 124º 00´W), approximately 10 to 20 nautical miles south of Banks Island in the Canadian Arctic. The Amundsen Gulf is an area where leads and polynyas commonly reoccur thus making it a suitable environment to study the effects that the flaw lead system may have on AMDEs. The constantly shifting ice in the gulf, allowing the formation of open leads, keeps the ice in the area relatively young making it possible for the ship to remain mobile over the winter months. This resulted in a dynamic dataset covering a large portion of the Amundsen Gulf during the AMDE season as well as the CFL project. Figure 2-1 portrays all the stations studied during the CFL expedition. Drift stations refer to stations where the ship was wedged into a suitable ice floe and left to drift with the natural movement of the ice. When the ship drifted to far from the desired study area, it would relocate to a new floe. This method of sampling was used largely to conserve fuel during the winter months. The fast ice stations were stations in which the ship would make its way into coastal fast ice, and stay there for the desired amount of time. Fast ice stations were located mostly in Franklin and Darnley bay during the spring season.

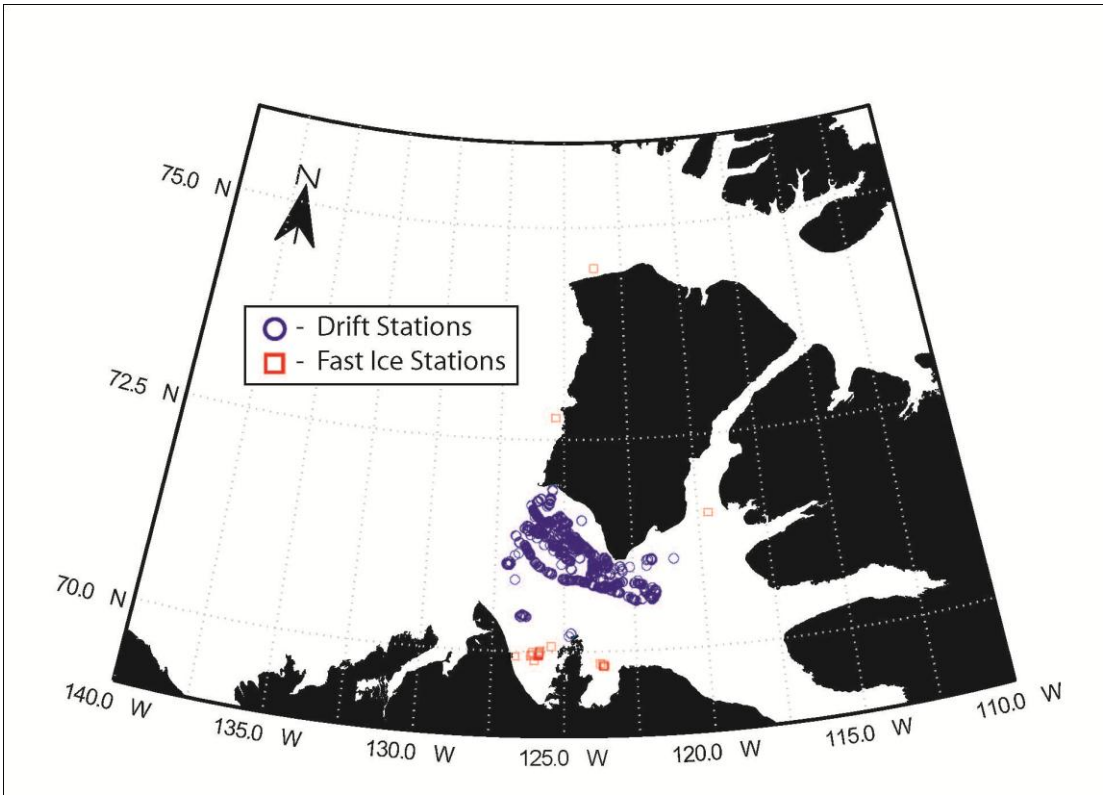

Figure 2-1: Sampling stations visited in the Amundsen Gulf during the 2008 CFL system study, drift stations are represented in blue (circle), and fast ice stations are represented in red (Square).

2.2.2 Methods

Measurements of atmospheric Hg began on January 20, 2008 and continued until July 11, 2008. Among the measured parameters were GEM, TAM, TGM, Hg_p, and RGM. The Hg instruments were installed in a container lab located on the starboard side of the ship's bow (Figure 2-2) with the air inlet located adjacent to the container near the edge of the ship approximately 5 m from the ocean surface (Figure 2-3). The instruments included 3 Tekran 2537A/B units (University of Manitoba, and Environment Canada), a Tekran 1130/1135 speciation unit (University of Manitoba), and a Tekran Model 1105 Arctic pyrolyzer (Environment Canada). GEM, RGM and Hg_p samples were taken from an intake located at the base of the 1130/1135 system

(Figure 2-3) located towards the edge of the ship above the pyrolyzer. TGM as well as TAM samples were taken from an alternate glass mushroom inlet located on top of the pyrolyzer unit below and slightly adjacent to the other inlet. The samples from all instruments were then transported through heated Teflon lines into a nearby temperature regulated container lab where the Hg analyzers were housed (Figure 2-2).

Figure 2-2: Tekran 2537 (top) and Tekran 1130 pump unit (bottom) housed inside foredeck container lab adjacent to sample inlet (inside instruments). Photo by Jeffrey Latonas

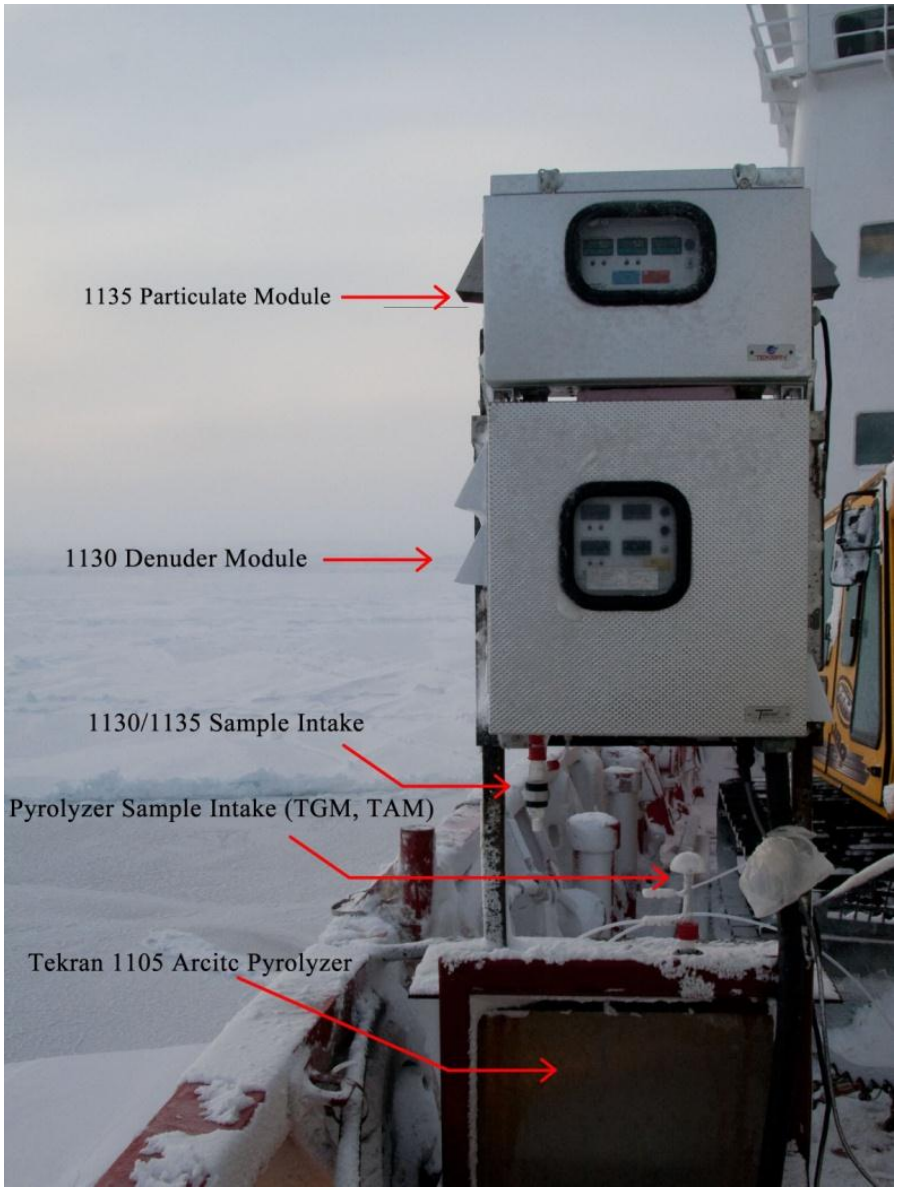

Figure 2-3: The Tekran model 1130/1135 Hg speciation system (top) with Arctic pyrolyzer (bottom) mounted on the port side of the ship off the bow of the CCGS Amundsen (outside instruments). Photo by Jeffrey Latonas

The quantification of all Hg species was done by Tekran 2537s. During the GEM measurement phase, the instrument samples air and traps Hg^0 onto a cartridge containing an ultra-pure gold adsorbent. The amalgamated Hg is then thermally desorbed at a temperature greater than 500°C releasing the Hg^0 from the trap which is carried by ultra-high purity argon to an atomic fluorescence detector (AFS, $\lambda = 253.7$

nm). During the desorption phase of RGM and Hg_p, any Hg(II) present in the sample would be thermally reduced to Hg^0 and detected by AFS as described above. A dual cartridge design allows alternate sampling and desorption cycles providing a greater sample resolution of 1 every 5 minutes. Results are automatically calculated based on sample volume, detector response, and instrument calibration to the final output concentration displayed in ng m^{-3}. The method limit of detection (MDL) is approximately 0.1 ng m^{-3} of Hg^0.

TAM was measured by passing the sample through a glass pyrolyzer (Tekran 1105) which heats the sample to 900ºC converting all Hg species to Hg^0, which is subsequently measured by AFS on a separate Tekran 2537. TGM was measured by a third 2537 unit using the same method; however, the air sample bypasses the Tekran 1105 unit and the sample is measured at ambient temperature. Both of these instruments were owned and operated by Environment Canada, thus the data will be interpreted by them with the possibility of a collaboration paper in the future. This chapter will only consider data collected from the 1130/1135 speciation system, namely GEM, Hg_p and RGM that were collected from the University of Manitoba instruments.

RGM, Hg_p and GEM were measured using a Tekran 1130-1135-2537B automated speciation system (Figure 2-3). This system allows for the continuous measurement of RGM and Hg_p every 3 hours while monitoring GEM during Hg_p and RGM loading periods. The load time for RGM and Hg_p is 2 hours, much longer than for GEM and TGM due to the lower concentrations present in the atmosphere. The 1130 denuder module (Figure 2-3) is designed to trap Hg(II) species onto a KCl

coated denuder. The incoming sample from the intake is split by a pointed glass airstream splitter, and the thinly spread air moves over the KCl coated tube which retains RGM allowing GEM and Hg_p to pass by unaffected. The sample airstream then converges and moves into the 1135 particulate module (Figure 2-3: top), which traps Hg_p on a filter allowing GEM species to pass through. During the RGM and Hg_p loading period GEM is sampled at 5 min intervals with a 5L sample size. After the loading period is complete, the denuder and particulate filter are thermally desorbed in sequence with the introduction of Hg free air (zero air) from the 1130 pump unit, and subsequently analyzed on the Tekran 2537 analyzer. Each RGM and Hg_p desorption cycle takes approximately 1 hour to complete resulting in an RGM and Hg_p sample resolution of 1 every 3 hours.

2.2.2.1 Maintenance

During the CFL study, all instruments were monitored closely and checked several times a day following standard operating procedures developed under the Canadian Atmospheric Mercury Measurement Network (CAMNet). Daily check sheets were completed in order to monitor the state of the instruments and quality of the data. The routine instrument checks included such things as date and time settings, pump flow rates, baseline voltage, baseline voltage deviation, temperature conditions, filter conditions, soda lime condition, lamp voltage, and previous calibration results. The data output were also watched closely for potential contamination or unexpected values. As part of the daily maintenance procedures, percent differences between A and B cartridges within the 2537s were calculated to determine if there were any significant deviations between them. If any of these

parameters were changing significantly, the daily checks allowed us to capture developing problems before the quality of the data was impacted.

The outdoor instruments (Tekran 1130/1135) were also checked daily for salt build-up around the inlet as well as inside the sample lines. The conditions of the inlet heating boot as well as the internal heaters were also checked for proper operation and settings. A freshly coated denuder as well as a new particulate filter was installed every two weeks as part of the standard operating procedures. Upon replacement, several desorb cycles were initiated to assure that any Hg on the glassware was burned off prior to taking measurements. A log of all maintenance operations performed to the instruments during the study was kept to aid in the data cleaning steps.

2.2.2.2 Instrument Calibration

The 2537 has an internal Hg permeation source and performs an automatic calibration daily. This involves the injection of a known amount of Hg^0 from the internal source into the instrument, which is then used to calibrate the results until the next calibration cycle (set for 24 hours). Manual calibrations were performed monthly in order to confirm the permeation rate of the 2537s internal Hg source. This was done by injecting a known volume of Hg saturated air from the temperature controlled Tekran model 2505 calibration unit. If the results from the manual injections were within 5% of the expected output from the instrument, the automatic calibrations could be taken as true. If the values were not as expected, the permeation rate in the 2537 software was updated to reflect the internal sources true Hg emission rate.

The state of the calibration on all 2537s was checked daily to identify if any variation in the internal permeation source was developing. Area counts for the auto calibration were compared with previous calibrations to determine if there was significant deviation in the response of the instrument. The state of the zero air was also determined here as a zero is performed on the instrument prior to Hg injection. If the response was decreasing, the appropriate measure was taken in order to optimize the instruments performance.

Calibration is only available for Hg^0, currently there is no method for calibrating the 1130/1135 system due to the nature of RGM and Hg_p. As a result, the recovery of RGM and Hg_p from the sample is unknown and results from the 1130/1135 cannot be taken to represent true atmospheric values. The system can, however, identify the presence or RGM and Hg_p species as well as any temporal trends in the atmosphere.

2.2.3 Data Interpretation

2.2.3.1 Data Cleaning

The dataset was cleaned and interpreted following protocols developed by Environment Canada (Ms. Sandy Steffen). All data were cleaned to remove any results that were suspected to be non-representative of true values such as: values obtained during maintenance operations, when line contamination was suspected, or instrument parameters were not correct. The daily check sheets were reviewed in depth to determine if there were any changes in the instrument conditions over time that would lead to results not representing true values. Both cartridges were averaged to minimize variation resulting from which cartridge was used in the instrument;

results were then further averaged depending on the required sample resolution. During the desorb cycle from the 1130/1135 system, several results are produced for both RGM and Hg_p which must then be compiled to produce a final result, this was completed and checked for every desorb cycle during the study.

Based on the logs and daily check sheets, any data produced when the instrument's operating parameters were questionable were removed from the dataset. Any data where the environmental conditions were questionable, (i.e., motorized equipment operating near the inlet or ship refuelling) was removed from the dataset as well. Due to the intensive quality assurance and control procedures applied during this study, potential problems were identified and corrected while onboard the ship which resulted in very little data having to be removed from the dataset (less than 10%).

2.2.3.2 AMDE Identification

In order to compare between episodes, all AMDE periods in the dataset were identified based on the same criteria. The beginning of an AMDE was marked when the GEM values begin to drop significantly from a steady state or gradual increase/decline. Most literature studies use a GEM threshold of 1.0 ng m^{-3} to classify an AMDE event (Steffen et al., 2005, Aspmo et al., 2005, Steffen et al., 2002) which has also been shown as a good approximation based on statistical significance (Cole and Steffen, 2010). This threshold, however, is subjective as a depletion event can still occur if the background GEM is high and if the duration of the event is not long enough for GEM to fall below 1.0 ng m^{-3}. Whatever the case, the event must be associated with a corresponding increase in Hg_p and/or RGM to confirm the oxidation of GEM. Each recorded AMDE is compared in terms of duration, minimum GEM

value, maximum values for Hg_p and RGM, average values for all components, and ship position. Key AMDE episodes identified are also compared with meteorological conditions (e.g., temperature, wind speed, wind direction), and sea ice conditions (e.g., sea ice coverage, presence of open leads, type of sea ice) where data are available.

2.2.3.3 Supplementary Data

Meteorological and positional data retrieved from the automatic voluntary observation ship system (AVOS) is the largest and most complete dataset available for the duration of the study (temperature, humidity, pressure, wind speed, wind direction). These data were used for long term monitoring of temperature and ship position (latitude/longitude). A meteorological observation tower was installed on the bow of the ship (Dr. T. Papakyriakou; University of Manitoba) approximately 14m above the ocean surface which produced more accurate results for wind speed and direction since the design of ship commonly leads to corrupted data from AVOS sensors. The wind data were collected using an RM young marine model anemometer, and were further corrected for ship's speed and heading to remove data which may be corrupted by the position and movement of the ship relative to the wind. The dataset was then averaged hourly and matched to the identified periods of AMDEs. Temperature data were also taken from the tower and used when available. Only events which match with complete sets of meteorological data were chosen for further analysis.

2.2.3.4 Satellite Imagery

Satellite images for key AMDE episodes were obtained from the Canadian Ice Service (CIS) to evaluate ice conditions around the ship. The images were processed and geo-rectified, allowing the position of the ship to be located. From these images we can see areas where new leads have formed as well as areas where frost flowers are prevalent. Knowing the direction of the wind during AMDEs helped identify whether or not BrO from the open leads can be linked to observed events. GOME satellite maps for BrO were provided by the Institute of Environmental Physics in Bremen (http://www.iup.physik.uni-bremen.de/gomenrt), which were used to identify when the bromine explosions began, and when BrO levels are highest near our study site.

2.3 Results

Two-hour average GEM values within the study period (January to July) ranged from as high as 4.27 ng m^{-3} during the out gassing phase in early May, to as low as 0.019 ng m^{-3} during strong AMDE events. During AMDE events, individual 10-minute average values often fell below the MDL of the instrument (0.1 ng m^{-3}) giving a value of 0. Hg_p values ranged between 0 and 665 pg m^{-3} and RGM between 0 and 143 pg m^{-3}.

As shown in Table 2-1 and Figure 2-4, a total of 31 independent AMDE events were observed throughout the study period, with the first in the Amundsen Gulf occurring on February 11. This is earlier than reported in more northern latitudes such as Alert due to the earlier inception of polar sunrise, which is necessary for the formation of bromine radicals (Lindberg et al., 2002). The last AMDE

occurred on May 27. The start time, end time, duration, location, minimum, and maximum values for all 31 AMDEs can be found in Table 2-1. The number of AMDEs observed during this study was much higher than previously reported from costal stations where typically 10 or so events were observed during spring and early summer (Hedgecock et al., 2008). This suggests that the dynamic environment in flaw lead areas may contribute to increased depletion events, and thus the potential for increased Hg deposition over the ocean. The presence of many AMDEs, some very short lived, may also suggest that local chemistry is largely responsible rather than depleted air masses moving into our measurement area.

Table 2-1 : Characteristics of the 31 AMDE events observed in the Amundsen Gulf in 2008, Minimum and Maximum values are based on individual 10-minute averages (N/A denotes when data is not available due to instrument malfunction or poor sampling conditions).

AMDE ID	Beginning UTC	End UTC	Duration Hours	Start Location	Min GEM ng m^{-3}	Max Hg_p pg m^{-3}	Max RGM pg m^{-3}
AMDE #1	2/11/2008 4:15	2/12/2008 12:05	31.83	N 71.07 W 124.77	0.81	68	3
AMDE #2	2/16/2008 20:40	2/18/2008 16:40	44.00	N 71.34 W 126.55	0.64	92	16
AMDE #3	2/29/2008 5:05	3/1/2008 10:35	29.50	N 70.91 W 123.80	0.29	86	4
AMDE #4	3/3/08 20:25	3/5/2008 15:45	43.33	N 70.94 W 122.88	0.00	386	14
AMDE #5	3/7/2008 1:55	3/8/2008 17:05	39.17	N 71.09 W 123.54	0.36	127	17
AMDE #6	3/11/2008 10:25	3/20/2008 6:00	211.58	N 71.04 W 123.91	0.00	173	97
AMDE #7	3/20/2008 10:40	3/24/2008 15:40	101.00	N 70.93 W 122.85	0.00	363	75
AMDE #8	3/24/2008 21:45	3/27/2008 1:35	51.83	N 71.08 W 121.81	0.00	548	47
AMDE #9	3/28/2008 2:15	3/28/2008 23:30	21.25	N 71.06 W 121.79	0.99	220	41
AMDE #10	3/30/2008 19:35	4/5/2008 7:35	132.00	N 71.06 W 121.79	0.00	665	85
AMDE #11	4/9/2008 18:50	4/11/2008 16:50	46.00	N 71.31 W 124.58	0.55	195	143
AMDE #12	4/14/2008 22:05	4/16/2008 11:15	37.17	N 71.09 W 123.99	0.21	240	68
AMDE #13	4/18/2008 4:50	4/20/2008 10:40	53.83	N 70.66 W 122.05	0.09	151	58
AMDE #14	4/21/2008 3:20	4/21/2008 14:20	11.00	N 70.73 W 121.83	0.57	41	19
AMDE #15	4/21/2008 21:10	4/22/2008 3:20	6.17	N 70.68 W 121.70	0.58	297	19
AMDE #16	4/22/2008 6:00	N/A	N/A	N 70.64 W 121.74	N/A	N/A	N/A
AMDE #17	4/26/2008 21:10	4/27/2008 15:10	18.00	N 70.59 W 122.44	0.53	23	73
AMDE #18	4/27/2008 18:30	4/28/2008 7:30	13.00	N 70.61 W 122.55	0.84	124	44
AMDE #19	4/28/2008 22:40	4/29/2008 15:40	17.00	N 70.71 W 123.24	0.82	186	32
AMDE #20	4/29/2008 20:20	4/30/2008 19:20	23.00	N 70.75 W 123.65	0.55	158	53

AMDE ID	Beginning UTC	End UTC	Duration Hours	Start Location	Min GEM ng m^{-3}	Max Hg_p pg m^{-3}	Max RGM pg m^{-3}
AMDE #21	4/30/2008 23:20	5/2/2008 8:05	32.75	N 70.79 W 124.00	0.27	79	83
AMDE #22	5/2/2008 13:55	5/2/2008 19:20	5.42	N 70.84 W 124.70	0.95	20	74
AMDE #23	5/3/2008 6:30	5/3/2008 18:10	11.67	N 70.88 W 125.17	1.09	65	27
AMDE #24	5/4/2008 3:40	5/5/2008 3:20	23.67	N 70.96 W 125.67	0.63	113	54
AMDE #25	5/5/2008 5:00	5/5/2008 17:20	12.33	N 71.09 W 126.13	0.62	65	59
AMDE #26	5/6/2008 8:30	5/6/2008 20:00	11.50	N 71.29 W 126.50	0.89	28	75
AMDE #27	5/6/2008 23:10	5/7/2008 10:50	11.67	N 71.02 W 127.06	0.89	18	64
AMDE #28	5/7/2008 15:10	5/8/2008 2:20	11.17	N 70.95 W 127.19	0.65	16	81
AMDE #29	5/8/2008 6:00	5/8/2008 20:50	14.83	N 70.18 W 124.83	0.94	12	53
AMDE #30	5/9/2008 0:30	5/10/2008 4:10	27.67	N/A	0.65	21	61
AMDE #31	5/27/2008 5:35	5/29/2008 17:35	60.00	N74.34 W 127.32 (McClure Strait)	0.41	5	43

Figure 2-4shows the atmospheric Hg speciation for the entire sampling period. Shorter AMDEs took place up until early March (AMDEs 1-5) and lasted on average 37.6 hours. In mid-March and early April longer events were observed with the longest, AMDE 6, lasting over 200 hours. Events occurring after April 20 (AMDEs 14 - 30) occurred more sporadically and presented with shorter durations with an average of only 15.7 hours. AMDE 30 was the last event to be witnessed in the Amundsen Gulf occurring on May 9. As the ice receded in the Gulf, the ship travelled further north to McClure Strait above Banks Island. As the ship approached an ice shelf spanning the entire width of the strait, a final depletion event (AMDE 31) was observed on May 27, 17 days after AMDEs ceased in the Amundsen Gulf.

In mid-April there is a distinct shift from Hg_p dominant Hg(II) species to RGM dominant species. A possible explanation for this is that there was a higher amount of particulates in the atmosphere earlier in the spring, possibly due to the presence of Arctic Haze in March and April. Arctic Haze is a phenomena observed in late winter where periods of low visibility are caused by an accumulation of airborne

pollution from southern latitudes in the Arctic (Hileman, 1983). This haze is associated with higher particle loadings, particularly sulphates which Hg has a high affinity for, which may quickly scavenge the newly formed RGM to form Hg_p. The lifetime of GEM during a depletion event is very short and in some studies has led to increased deposition onto snow surfaces (Lu et al., 2001), whereas in others, no real increases in snow surface Hg levels were found (Ferrari et al., 2005, Lu et al., 2001). Instances where increased Hg deposition on snow is observed suggest that the event is occurring locally. If no increase is observed, it is likely that most Hg(II) has been previously deposited, and the low GEM levels observed are due to a depleted air mass which has been transported into the area of study. Snow measurements were carried out during the entire CFL study by Amanda Chaulk, another graduate student at the University of Manitoba.

The large spike of GEM seen in mid-May (Figure 2-4) is thought to be mainly Hg^0 out gassing from Arctic water which may have become super-saturated due to the thick ice barrier which is removed around this time (see Chapter 3). Photoreduction of Hg(II) species from snow, water, and melt ponds may also contribute to the large spike of GEM seen in response to warming snow temperatures (Section 1.5.1).

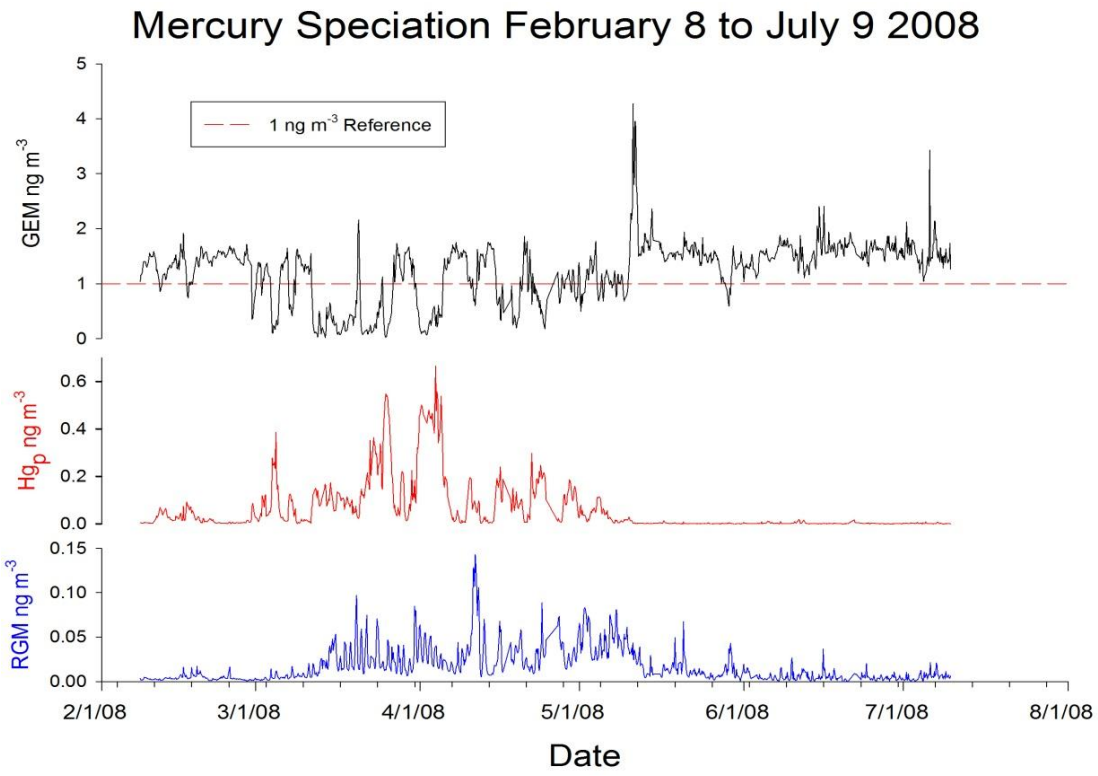

Figure 2-4: GEM (Black), Hgp (Red), and RGM (Blue) in the lower troposphere over the Amundsen Gulf for the study period of February 8 to July 9 2008. The dashed line represents 1 ng m 3, a commonly used threshold for identifying AMDEs.

2.4 Discussion

AMDE events observed can result from both local, regional, and long distance chemistry (Gauchard et al., 2005). Identifying the originating locations of the events is important in determining the parameters that influence their occurrence. Atmospheric Hg species were examined with respect to temperature, wind speed, wind direction, and the surrounding sea ice environment. Difficulty in getting complete wind measurement datasets to match up with AMDE events resulted in only 12 AMDEs being suitable for further analysis: AMDEs 2, 3, 4, 7, 8, 9, 14, 15, 26, 27, 28, and 31. Satellite images of the Amundsen Gulf were requested for the dates of these events to help determine the role of the sea ice; however, after date matching and georeferencing, only events 2 and 4 have a full dataset including images. AMDE

6, the longest event, has 4 satellite images associated with it, but unfortunately wind data over this time is intermittent.

2.4.1 Role of Temperature

Temperature plays a key role in AMDEs as cold temperatures seem to be required for heterogeneous reactions to form active bromine species onto frozen surfaces such as frost flowers, sea salt aerosols, and snow and ice surfaces (Lindberg et al., 2002, Steffen et al., 2005, Simpson et al., 2007, Steffen et al., 2007). All events occurred at atmospheric temperatures below 0°C; however, the actual temperature values (as long as they are below 0) do not seem to affect the occurrence of an event as events were seen at -5°C as well as -30°C. No events were seen at temperatures above zero which is consistent with several other studies (Lindberg et al., 2002, Steffen et al., 2005) and colder temperatures have been correlated with AMDE frequency and intensity (Cole and Steffen, 2010). In the context of climate change, increasing temperatures may decrease the frequency and severity of AMDEs, and thus potentially lead to less deposition of Hg from the atmosphere. Alternatively, it may also lead to more AMDE active flaw lead environments across the Arctic. Further discussion regarding AMDEs in the context of climate change can be found in Chapter 4.

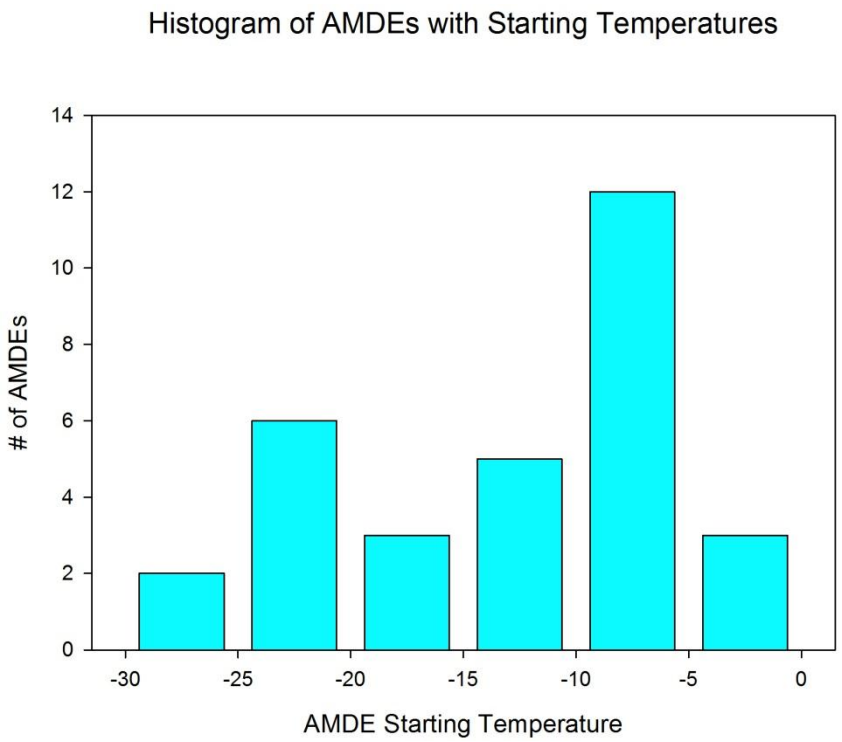

Figure 2-5: Histogram portraying the number of AMDEs with their starting temperatures in groups of 5°C ranging between -30°C and 0°C.

Figure 2-5 shows the distribution of AMDEs with their starting temperatures with the highest number of AMDEs starting at temperatures ranging between -10 and -5°C. This suggests that higher variability in terms of AMDEs occur at warmer temperatures. A scatterplot showing the relationship between event duration and starting temperature (Figure 2-6) suggests that events starting in colder temperatures will have the tendency to last longer than events starting at warmer temperatures. This relationship revealed an R^2 value of 0.25 suggesting that up to 25% of the duration can be explained by the temperature in which the event begins. Temperature will also affect the surrounding sea ice environment, thus the heightened variation at warmer temperatures may also be influenced by the increasingly dynamic sea ice environment at warmer temperatures.

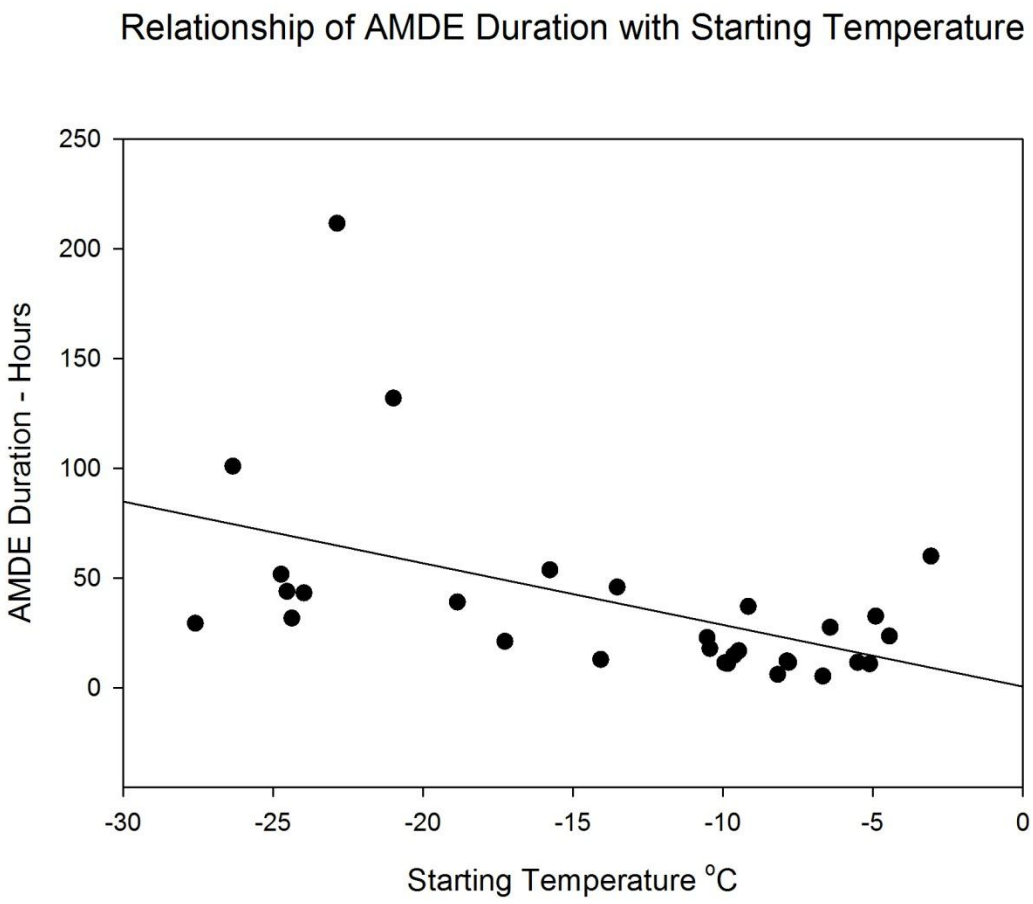

Figure 2-6: Scatterplot showing the relationship of AMDE duration (hours) with associated starting temperatures (°C) $R^2 = 0.25$.

Figure 2-7 shows temperatures and GEM averaged every hour and every 3 hours respectively. From these data it seems evident that most events begin with a sharp decrease in temperature suggesting that a drop in temperature may act as a trigger for AMDEs. A swift drop in temperature may enhance the re-freezing of open leads in the area as well as promote the formation of frost flowers by strengthening the temperature gradient. This process may enhance BrO production on a local scale and thus contribute to the commencement of an AMDE. Figure 2-8 shows a more detailed view of the GEM to temperature relationship for several AMDEs witnessed early in the season. This trend was commonly observed with nearly every event. The

major outgassing event occurring in mid-May may also be the result of increasing temperatures as it occurred just prior to temperatures reaching the 0°C threshold. The peak of outgassing events has been commonly observed around this temperature; however, it is typically observed later in the year at Alert, occurring in June or July (Cole and Steffen, 2010).

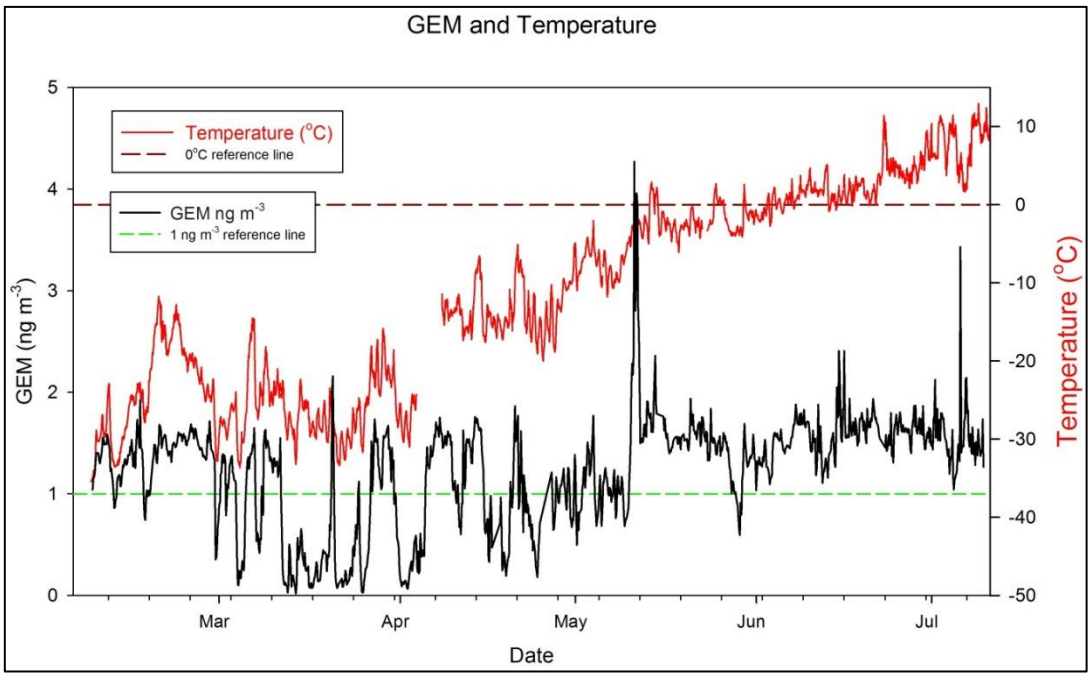

Figure 2-7: GEM (ng m^{-3}) and temperature (°C) in the lower troposphere over the Amundsen Gulf for the entire sampling period in 2008.

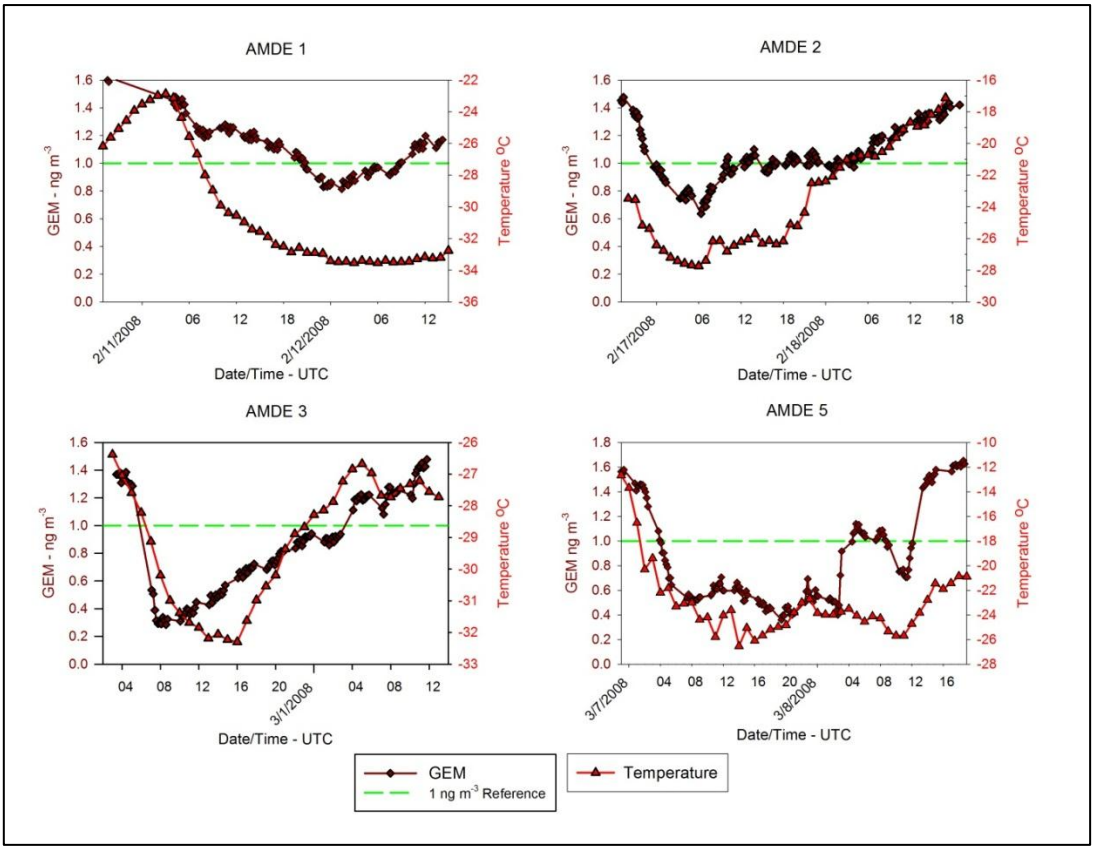

Figure 2-8: The effect of temperature (°C) on GEM concentrations (ng m^{-3}) during AMDEs 1, 2, 3, and 5 over the Amundsen Gulf in 2008.

AMDE 31 (Figure 2-9) is unique as it occurred well after the final event was seen in the Amundsen Gulf. Near the end of May, the ship travelled north above Banks Island into McClure Strait in search of ice. Hours before reaching the ice edge, which stretched between Banks Island and Prince Patrick Island, GEM concentrations began to fall. The depletion strengthened over night while the ship was beset in the ice and then weakened the following day as the ship moved away from the ice edge and was met with a sharp increase in temperature. The sharp increase in temperature to above 0°C noted at the end of the event may be due to the ships movement into open water. A corresponding decrease in wind speed and increase in RGM (not shown) over the event site again suggests that this was a localized occurrence. This

further strengthens our hypothesis that cold temperatures as well as ice surfaces are necessary for depletion events.

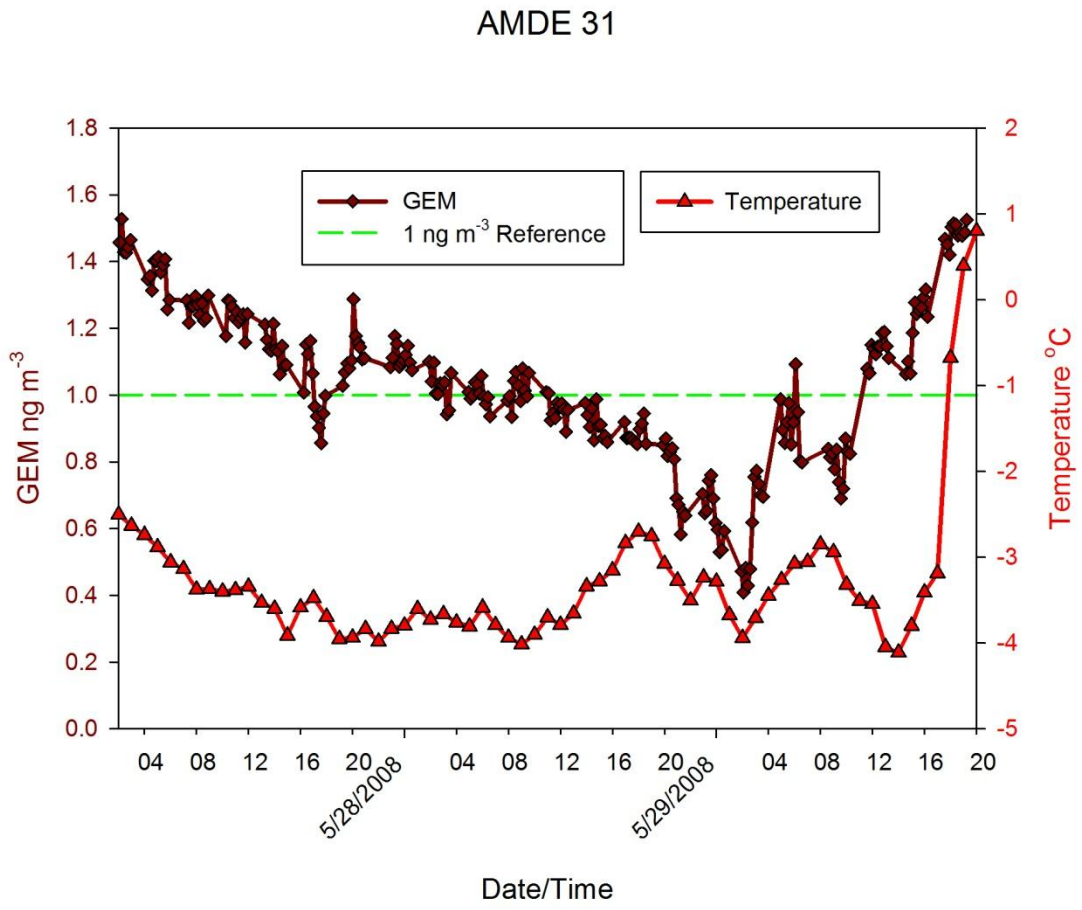

Figure 2-9: The relationship between GEM (ng m^{-3}) and temperature (°C) during AMDE31 over the Amundsen Gulf in 2008.

2.4.2 Role of the Sea Ice Environment

Regions of enhanced BrO are largely present over areas of young sea ice (Simpson et al., 2007). Increased BrO can be seen over some regions of the Arctic from the GOME Satellite as early as mid-February. From the imagery it is evident that the BrO is produced over the frozen ocean, possibly accelerated in certain regions by the presence of frost flowers as discussed in Section 1.4.4. The applicability of the satellite imagery is limited due to its low resolution; however, it can be used to show

the presence of BrO over key areas at a given time. In 2008, the GOME satellite observations revealed that the highest density of BrO concentrations over the Amundsen Gulf occurred from March 13 to 17 (Figure 2-10). This happens to coincide with the longest depletion event that we observed, AMDE 6, which lasted from March 11 - 20. The highest BrO concentrations coinciding with the longest uninterrupted depletion event is evidence suggesting the role of BrO and the marginal ice zone in its formation. Having the ship positioned directly in this zone of active BrO production provided an opportunity to study these events at the source, something that has not been previously done for an entire AMDE season.

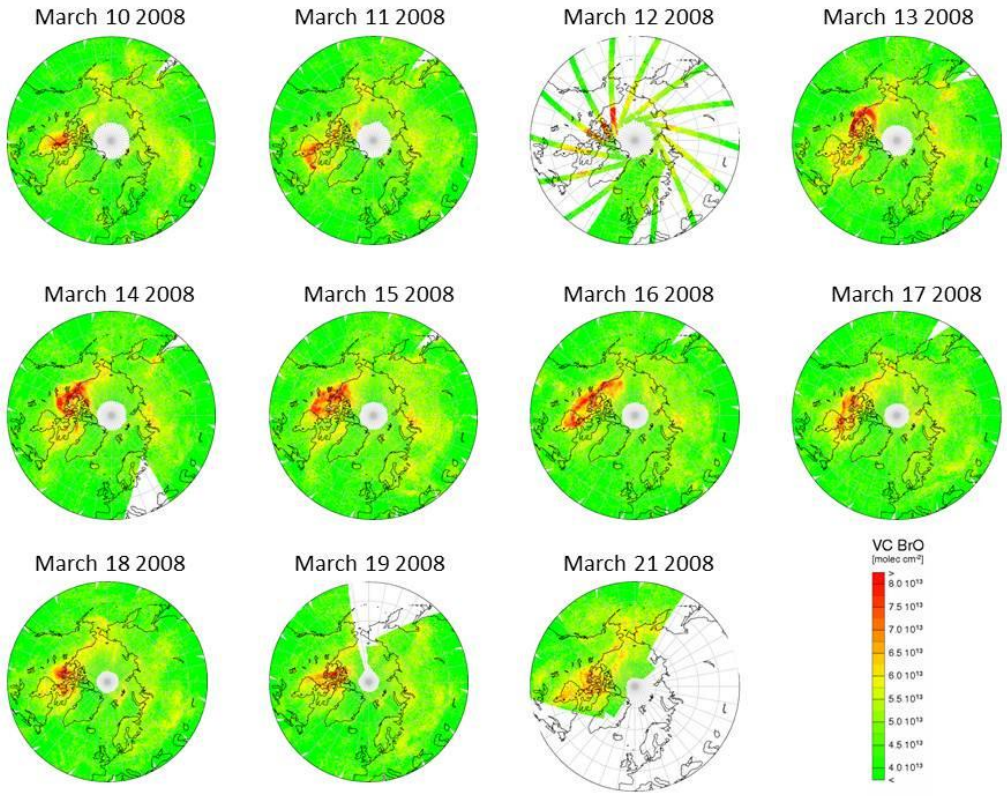

Figure 2-10: GOME satellite images of the Arctic showing concentrations of BrO in the troposphere for the period March 10 - 21 2008 (Courtesy of Andreas Richter, University of Bremen).

The ship's crew was responsible for visually determining the ice cover surrounding the ship on a regular basis, and estimating a percentage ice cover (Figure 2-11). Open leads were visible from the ship starting in mid-February, and an ice cover between 80-100% remained fairly constant until mid-May when the ice cover grew sparser, and the ship began to move into open water. The big jumps between 100% and 0% represent the ship moving from ice to the open water stations which it did regularly towards the end due to the early retreat of ice from the Amundsen Gulf as well as studies conducted between fast ice stations in Darnley and Franklin bay.

The first two AMDEs observed were short lived, and were observed on February 11 and 16. These events coincide well with the first visual presence of open leads beginning on February 17. Areas of open water may have been present beyond the visual range of the ship resulting in the earlier presence of AMDEs; however, in the following months open leads are commonly observed with the presence of AMDEs.

Figure 2-12 portrays the monthly hours of AMDEs showing that March had the highest combined time of depletion events which then tapered off into May as temperatures rose and the ice in the Gulf receded. March also has the coldest average temperature of the study time series of -26°C. Increased lead formation may also have an effect on air temperature as more exposed water will act to increase the temperature of the surrounding air, alternatively, at temperatures this cold, the re-freezing of open leads would commence almost immediately, and with that there is an increased potential of frost flower formation, which may increase the emission of BrO from the surface.

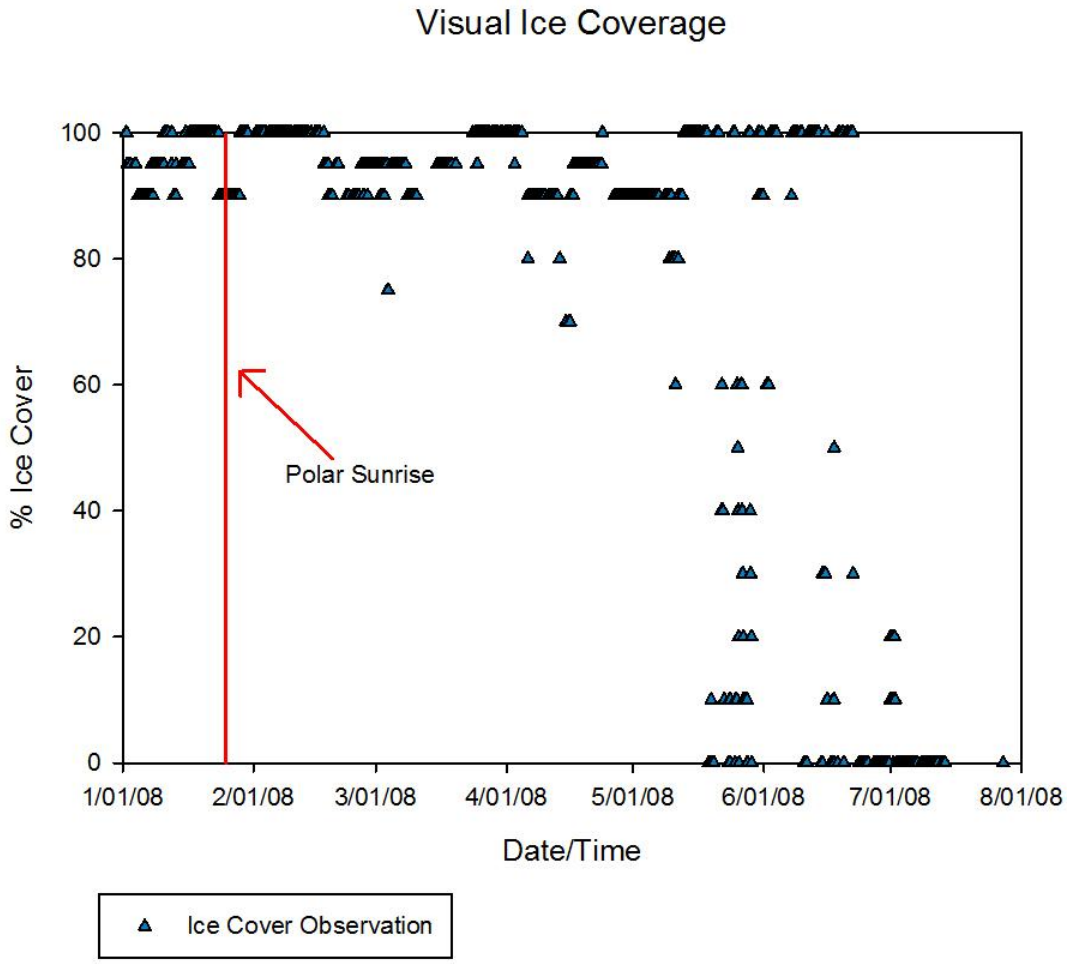

Figure 2-11: Visual ice coverage surrounding the ships position (Approx. 5km radius) as recorded in the ships log during the study period in 2008. Polar sunrise is identified by the red vertical line (February 25, 2008).

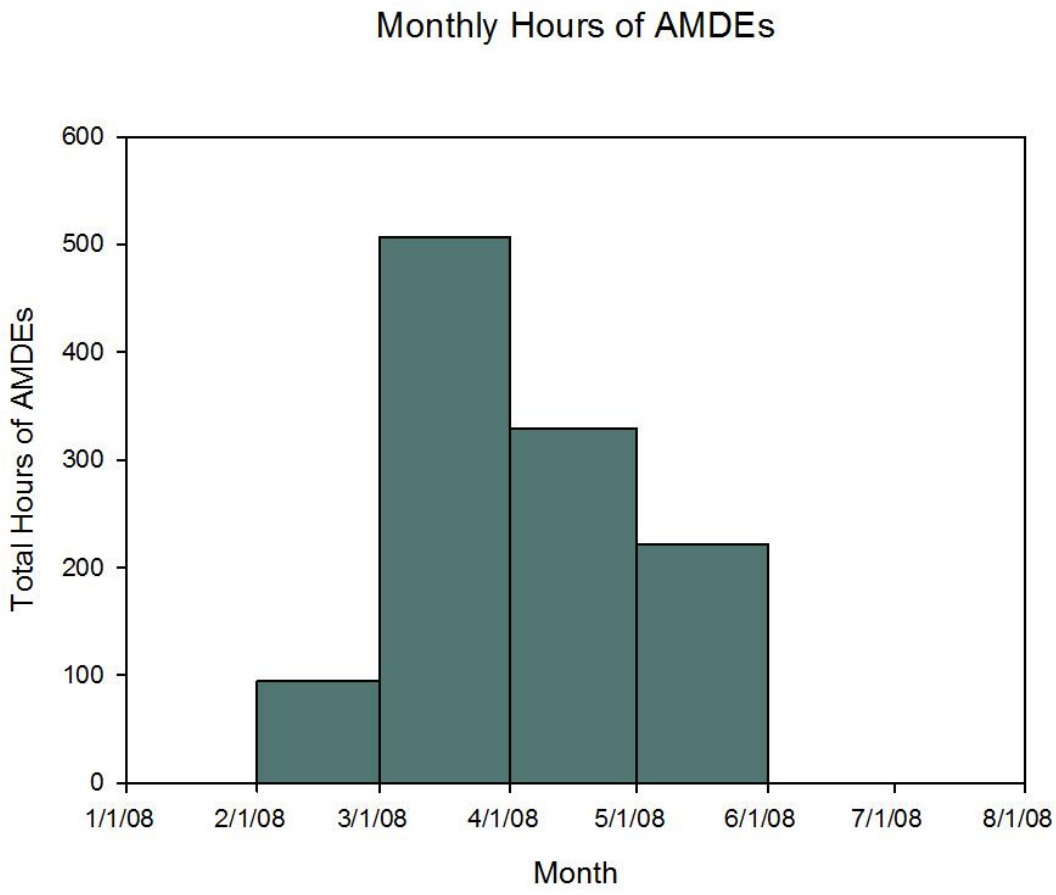

Figure 2-12: Histogram showing the number of hours of depletion during each month during the study period in 2008.

Radarsat images (Figure 2-13 andFigure 2-14) can be used to identify areas of open water (leads or polynyas) as well as areas of young ice where there is the potential for frost flower formation (Alvarez-Aviles et al., 2008). Areas which appear brighter have a higher degree or surface roughness thus are associated with regions of new ice. Images were obtained from the CIS for key periods where meteorological data as well as Hg speciation data were available. They are also useful for determining the role of wind direction as it is possible to visualize what types of ice coverage is present around the ship's location and where the wind is coming from. During AMDE 2 and 6, there are multiple leads present around the ship's position as can be seen from the multiple white cracks in the ice cover (Figure 2-13 andFigure

2-14). For AMDE 6, there appears to be very large areas of potential frost flowers forming from the shores of Banks Island where the ice pack is pulling away, open water is also visible along the shoreline. This very large area of new ice and potential frost flowers may be a large contributing factor in AMDEs 6, 7, and 8 being the longest lasting period of depletion witnessed throughout the study period.

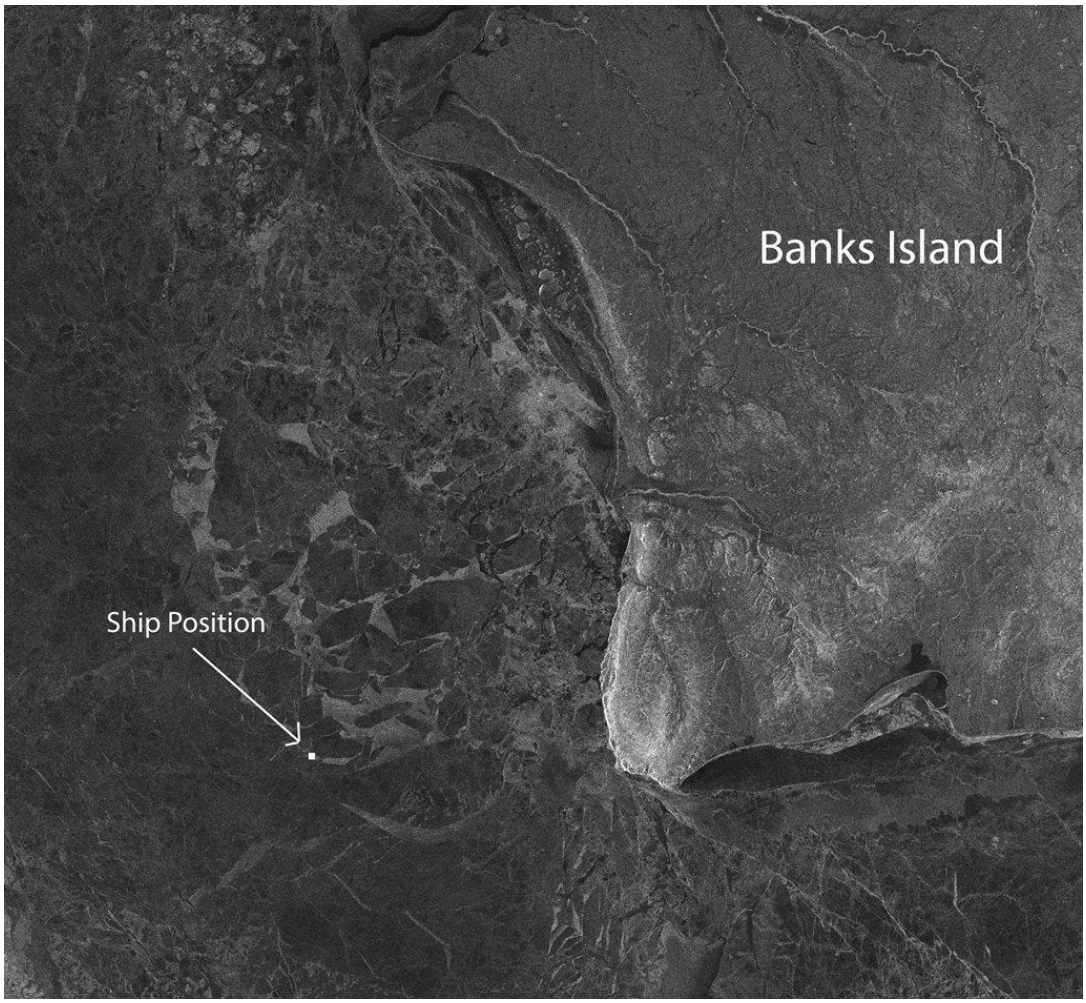

Figure 2-13: Radarsat image of Amundsen Gulf during AMDE2 on February 17, 2008, Areas of new ice appear brighter than areas of older ice, open water will appear black.

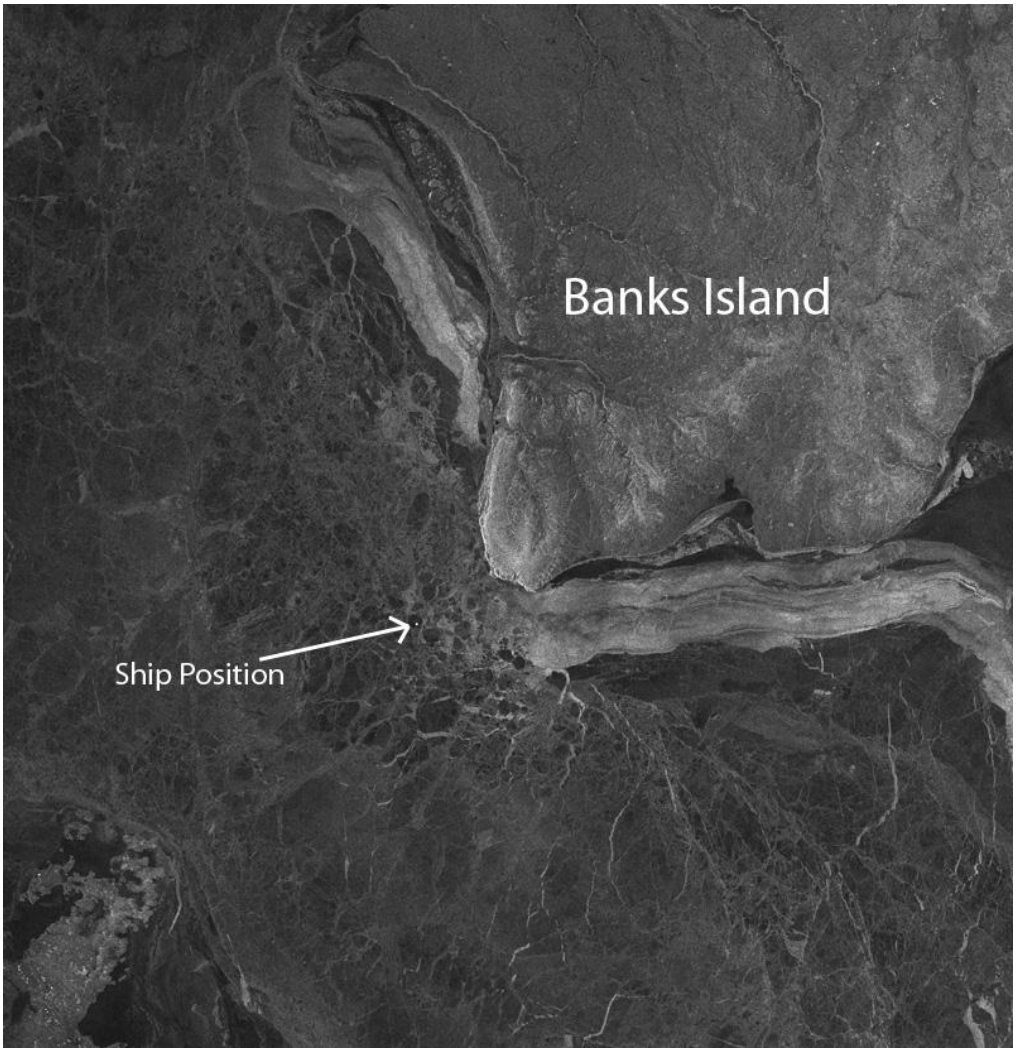

Figure 2-14: Radarsat image of Amundsen Gulf, during AMDE 6 on March 19 2008.

The sea ice may act as a barrier to atmospherically deposited Hg thus reducing the amount entering the aquatic system by trapping it on the surface, and allowing time for the oxidized Hg species to be photoreduced to Hg^0, and re-volatize to the atmosphere. If the sea surface remains frozen during the period of active AMDEs, the amount of Hg(II) entering the aquatic food web may be reduced. The dynamic sea ice conditions of flaw lead systems may increase the risk of Hg contamination since there is the potential for increased Hg(II) deposition to the aquatic system due to the ocean being open to exchange with the atmosphere. Alternatively, the ice cover may also

prevent DGM from being released to the atmosphere (Section 1.6.4 and Chapter 3), thus trapping deposited Hg(II) within the aquatic system.

The major outgassing event witnessed in mid-May (Figure 2-4) also coincides with the period where the ice in the Gulf is receding and the ice concentrations is significantly reduced (Figure 2-11). Temperatures in this case are approaching yet have not yet reached 0°C (Figure 2-7), thus this outgassing event may have been accelerated by the early removal of ice rather than the increase in temperature. Currently the specific origin of these outgassing events is unclear; however, all factors leading to the removal of ice, such as temperatures, wind speed, and wind direction, and the physical properties of the ice, may control when the major outgassing event will occur.

2.4.3 Role of Wind Speed

Calm weather, low wind speeds, and non-turbulent air flow are conditions which have been found to be favourable for AMDEs (Lu et al., 2001). As discussed previously, high wind speeds may increase the rate at which Hg(II) is removed from the event area and possibly deposited elsewhere. Conversely, it may also increase the input of GEM into the area where conditions are favourable for Hg depletion thus accelerating the transformation of GEM to Hg(II), given that there are no other limiting factors at play such as BrO concentration. Simulation studies have found that the rate of decrease in GEM concentrations compare well with those observed during events; however, the simulation values typically decrease below observed concentrations after a given period of time (Hedgecock et al., 2008). This is most likely due to the fact that the simulations do not consider the input of GEM carried in

by winds from other areas. Lower wind speeds over an area where an active AMDE is taking place may lead to increased Hg_p and RGM production due to the inability of the formed Hg(II) to be evacuated from the area. This may lead to increased deposition of Hg_p in areas of active depletion (Figure 2-15). The open ocean is an ideal location for identifying the relationship to wind speed, as it is not affected by local topography.

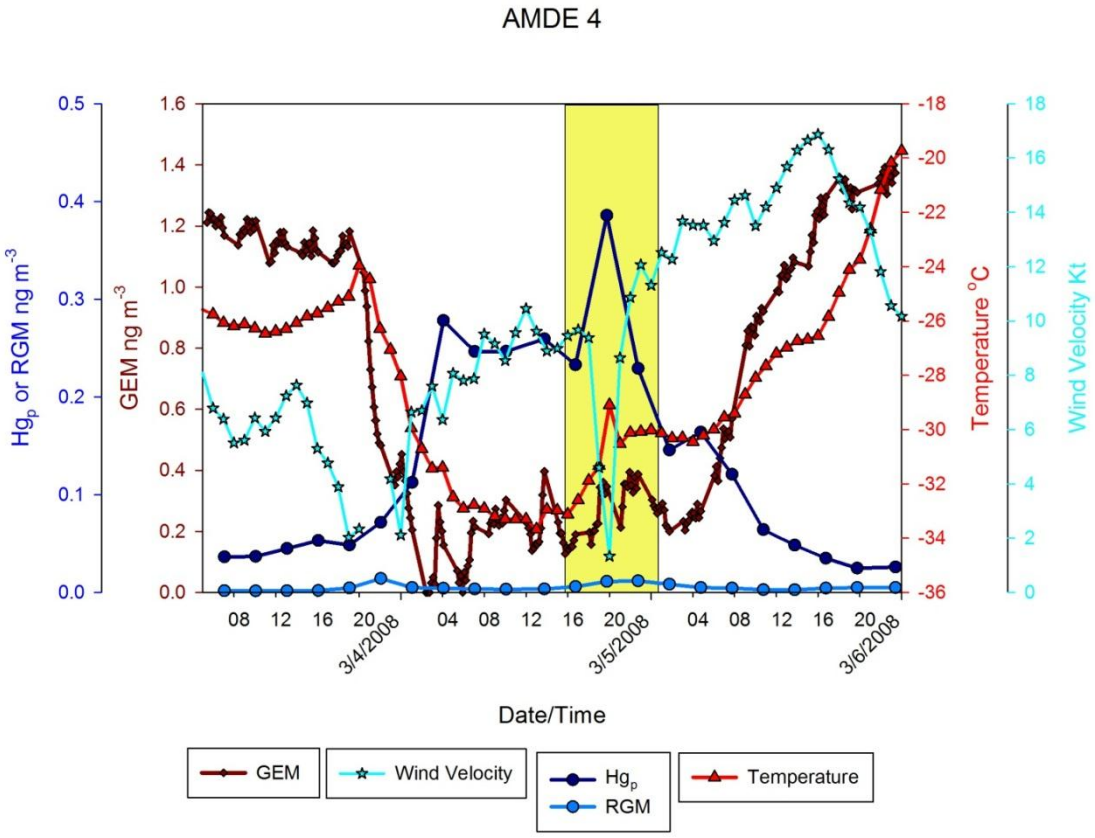

Figure 2-15: AMDE 4 occurring on March 4 – 5, 2008, showing the relationship between Hg_p (ng m^{-3}) and wind speed (kt). The highlighted area shows the period in which wind speed drops, and Hg_p increases.

Figure 2-15 shows an active AMDE situated over the ships location during a period at the beginning of March where wind speed dropped significantly. The simultaneous increase in Hg_p, its intensity, and duration, suggests that it is being

formed directly over the ship's location. The maximum Hg_p concentration measured during this event was 0.4 ng m^{-3} (March 20) and was one of the highest values observed over the entire study period. As the winds started to increase, Hg_p drops off and an increase in temperature marked the end of the depletion event. Small increases in RGM were observed at the start of the event, and also during the period of low wind. This suggests that if the event is occurring directly at the ship position, the RGM is rapidly being scavenged by atmospheric particles forming Hg_p, potentially particles associated with the Arctic Haze as previously mentioned.

The presence of RGM has been suggested as an indicator that an event is due to local chemistry rather than the transport of an already depleted air mass (Gauchard et al., 2005, Lindberg et al., 2002). This example suggests otherwise as there is a small increase in RGM versus a large increase of Hg_p during a period of low wind. The low wind coupled by an increase in Hg(II) suggests that this event is occurring locally, and Hg(II) concentrations are potentially increased in low wind situations. Hg_p formed during an event is not deposited immediately thus would be quickly removed from the area of measurement by winds, or build up in the atmosphere until carried away and deposited to ocean or terrestrial environments. High wind situations may prevent the deposition of Hg_p by keeping particles airborne and limit the variation in measurements due to continuous mixing in the lower troposphere.

Increased wind speeds can destroy frost flower fields which may contribute to a decrease in observed events. This may also be a reason why lower wind speeds have been found to favour AMDEs. 7 out of the 12 events suitable for analysis with wind speeds ended with increasing wind speeds, thus it is possible that these increased

winds are destroying nearby sources of bromine, and thus leading to the cessation of an event.

2.4.4 Role of Wind Direction

Depending on its origin, wind direction may also play a role in observed AMDEs. Air masses above areas with dynamic sea ice properties, such as open leads or frost flowers, will most likely contain higher concentrations of BrO than land based sites, where active depletion can occur. Depleted air masses or active AMDE cells, may then be transported by winds from these regions, to the measurement site. Winds approaching the measurement site from a land covered surface where the possibility of depletion does not exist may contain higher concentrations of GEM. Satellite imagery allows the possibility to visualize the ice conditions surrounding the ship, and assess if the air masses have been previously depleted and transported, or if the AMDE is a result of local chemistry.

Wind direction may be more important for studies conducted from coastal sites and less relevant for studies situated over the ocean in a flaw lead system. In coastal regions, winds originating from areas of new ice and higher frost flower densities have been shown to enhance both Hg and ozone depletion events (Gauchard et al., 2005). Satellite images taken during the study period generally revealed leads and young ice forming 360 degrees around the ship. The satellite images taken during AMDEs 2 and 6 show that new ice, and thus areas of potential frost flowers, occurs in all directions from the ships position (Figure 2-13 and Figure 2-14). This situation was typical throughout the measurement period, thus no discernable trend was observed between wind direction and depletion events during this study. Wind

direction has, however, been shown to play a role at Alert, as the integrated AMDE frequency has been found to be significantly higher with winds from a North or North-easterly direction verses winds from the southwest which represent winds which have traversed land (Cole and Steffen, 2010).

2.4.5 Role of AMDE Duration

The minimum GEM value of an event is strongly related to the duration for which the event took place (Figure 2-16). A total of 5 events reached a minimum GEM value of zero; AMDEs 4,6,7,8, and 10, all of which occurred during the month of March (based on 10-minute averages). The average duration of these events is 108 hours whereas the average duration of all events combined is 38 hours. From the observations, any event lasting longer than 60 hours achieved a minimum GEM value below the limit of detection. Removing the zero events from the regression line as they are already fully depleted reveals an R^2 of 0.42, thus 42% of the minimum GEM values can be explained by the duration of the event. This result suggests that the longer the conditions are present for Hg depletion, the lower the GEM value will be. The depletion duration versus minimum GEM values was found to follow zero order kinetics which means that the rate is not dependent on the concentration of GEM in the atmosphere as long as there are sufficient concentrations of BrO present to sustain the reaction.

Events where GEM values reach zero are more likely to be related to local chemistry because depleted air masses moving into our area would most likely be subjected to some re-volatilization of deposited Hg(II) and mixing, thus some GEM would still likely be present in a depleted air mass sample. This may account for a

large portion of the variability seen as well as variations in available BrO, temperatures, and wind speeds.

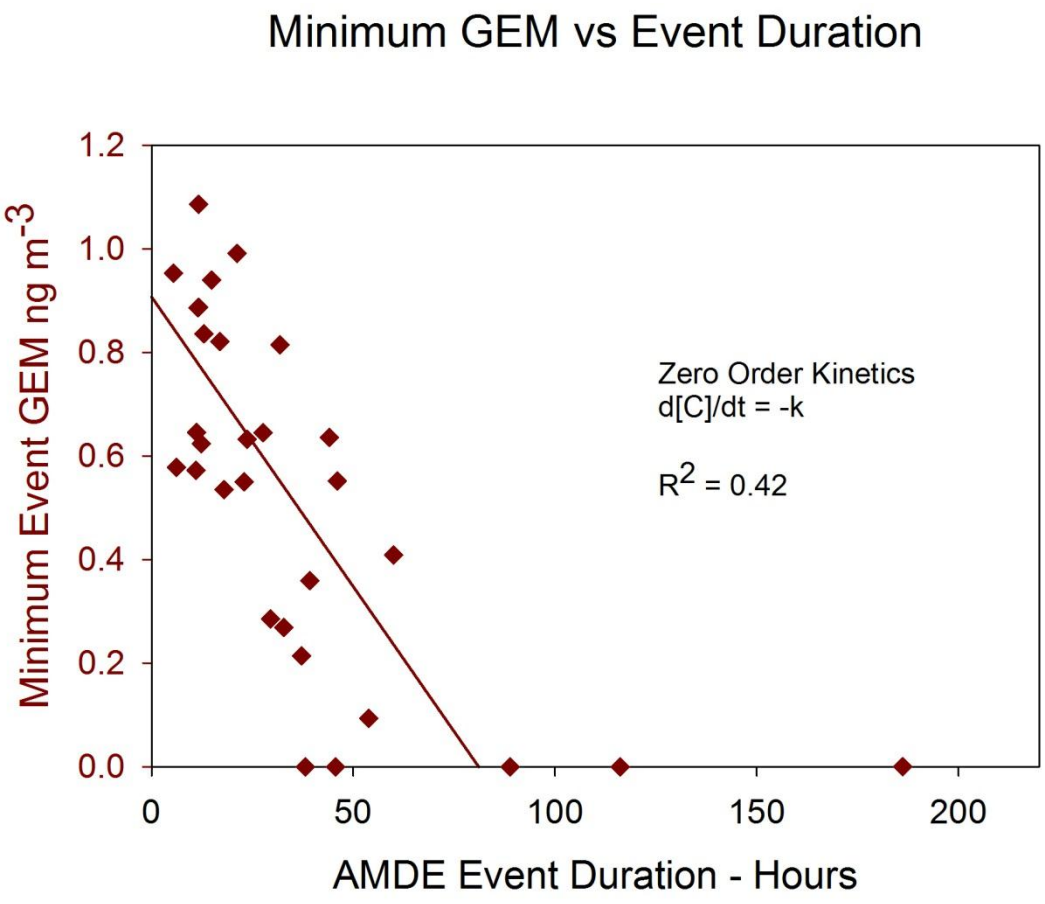

Figure 2-16: The relation between the minimum GEM (ng m^{-3}) and the duration (hours) of the AMDE. Events reaching zero are not included in the regression as they are assumed to be fully depleted. The rate constant is shown to follow zero order kinetics.

2.4.6 A Closer Look

The following is a closer look at several events where full meteorological data were available to accompany the Hg data. Two of the longest events (AMDE 6 and 7) occurred very close together with AMDE 6 lasting 211 hours and AMDE 7 lasting 101 hours. Separating the two events, GEM values rose above 1.0 ng m^{-3} for only 4 hours and 40 minutes. AMDE 8 followed very closely behind (only 4 hours after AMDE 7), and lasted 51 hours. Each event reached a GEM value of 0 ng m^{-3} on more

than one occasion for 10 minute average values. These 3 events combined corresponded to the most significant depletion period witnessed during the 6-month study with a total depletion time of 364 hours, or just over 15 days (Figure 2-17).

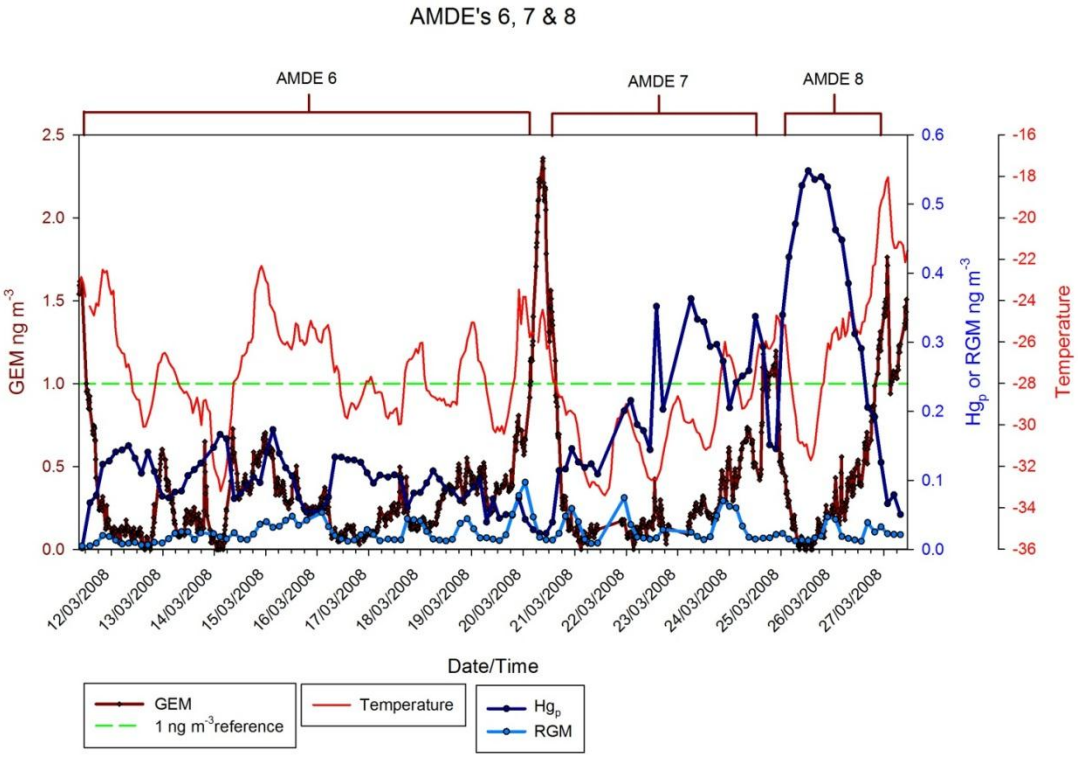

Figure 2-17: AMDEs 6, 7, and 8 from March 12 to March 27, 2008. The combined is the longest period of Hg depletion during the CFL study representing a total of 364 hours of depletion.

As seen with other events, AMDEs 6, 7, and 8 all commence with a drop in temperature. Once started, the temperature fluctuates diurnally, and all 3 events seem to cease during periods where the temperature is increasing. Unlike the other two events, a very sharp and strong increase in Hg_p was observed during AMDE 8 reaching a maximum of 548 pg m^{-3} (which is the second highest value seen from all events during the study). This increase is puzzling as it occurred concurrently with sporadically shifting and increasing wind speeds (not shown). It is possible that this increase is due to the movement of an already Hg-depleted air mass into the region.

There also appears to be a diurnal fluctuation of RGM which is less evident than in Hg_p, This may be due to increased RGM production during the hours when solar radiation is high. The RGM may then adsorb onto airborne particles forming Hg_p which gradually increases in concentration as these events progress. A possible explanation for this is that the increasing wind speeds keep particulates airborne thus resulting in higher Hg_p during the final event.

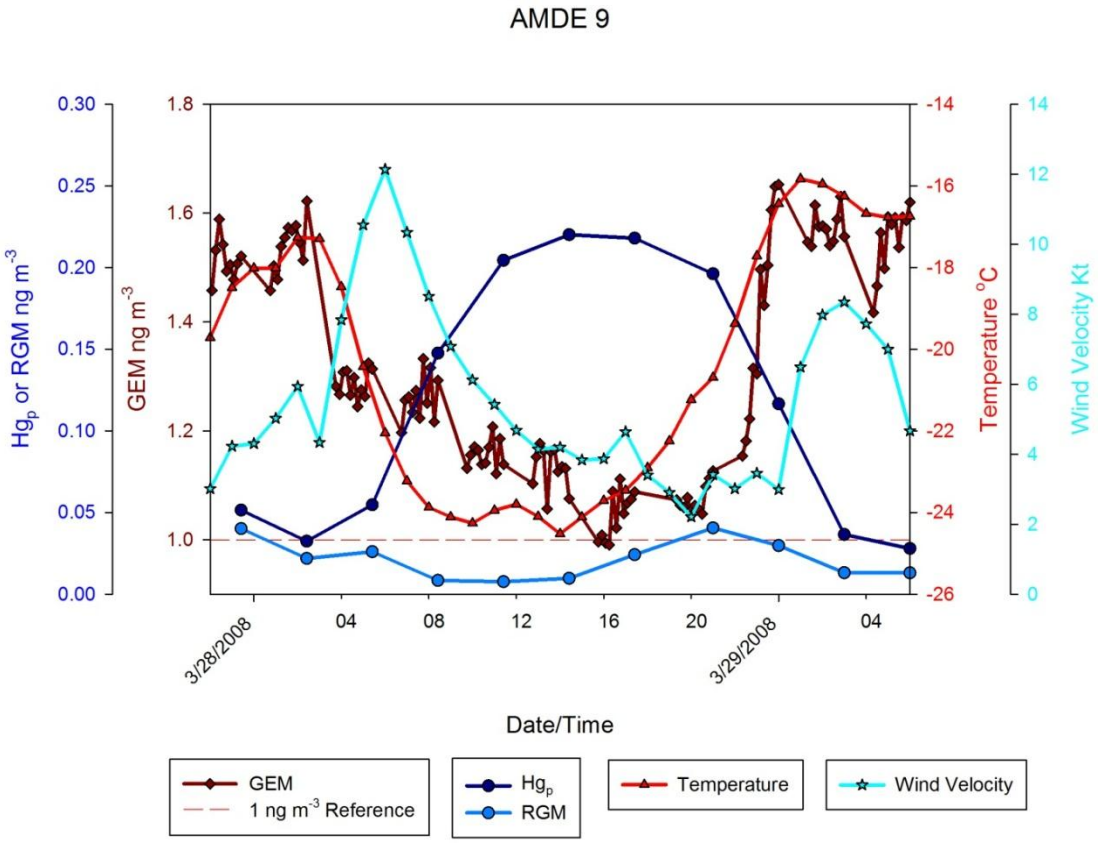

Figure 2-18: AMDE 9 on March 28 2008 showing the relationship of temperature (°C) and wind speed (kt).

AMDE 9 (Figure 2-18) is another good example of the typically observed temperature relationship. The GEM concentration did not pass below 1.0 ng m^{-3} for very long; however, there is a significant increase in Hg_p associated with the GEM depletion and is thus considered to be an event. In this event, the wind was constant

from the north with little variation. It appears that the onset of the event starts with an increase in wind speed which may represent an active AMDE cell moving over the sampling site. The wind then dies down resulting in a significant increase in Hg_p and a slight decrease in RGM. This decrease in RGM coupled with an increase in Hg_p was noted on several occasions (Figure 2-17) which could represent newly produced RGM adsorbing to particulates in the atmosphere; increasing the concentration of Hg_p. This phenomenon may be a good indicator of a local AMDE event as long as there is a significant amount of particulates in the atmosphere available for adhesion. The end of the event is matched well with another increase in wind speed in which GEM rapidly recovers and Hg_p concentrations drop. The end of the event may have been initiated by a non-depleted air mass moving and displacing the current more active air mass. It is suspected that this is an active AMDE cell that has moved over the sampling site.

2.4.7 Comparison with AMDEs at Other Arctic Locations

There have been many campaigns studying AMDEs in the Arctic, sub-Arctic, and Antarctic over the last 15 years. Since this study was conducted in the Canadian Arctic, the data will only be compared with results from studies conducted in the Northern hemisphere. The seasonal trend in Hg speciation and variations described in Chapter 1, Section 1.2 was generally captured with this dataset; however, there were some differences in the data that can most likely be attributed to the study location.

One major discrepancy between this dataset and others is the number of events observed. A total of 31 events were observed during this campaign which is significant considering that many coastal areas of the Arctic experience ~ 10 events

over the depletion season (Hedgecock et al., 2008). A study in Ny-Ålesund, Svalbard (78º 54´N, 11º 53´E), recorded five AMDEs during a one month field experiment from April 10 to May 10, 2003 at 2 separate sampling sites (Gauchard et al., 2005). In the Amundsen Gulf, over the same time period, 20 events were recorded. Coastal sites may receive air masses from locations over the ocean which has undergone mixing during transport. This may result in longer AMDEs being observed at coastal sites, as they would receive an "averaged" result from various regions resulting in longer and smoother events. The more numerous, shorter lived yet closely spaced events witnessed over the Amundsen Gulf suggest that the tropospheric chemistry responsible for AMDEs is likely happening over the ocean, especially in or near flaw lead systems.

Steffen et al. (2005) presented an analysis of ongoing measurements from 3 different sites across the Arctic providing an excellent base for comparison with our data: Alert, Canada (82.5º N; 62.3º W), Amderma, Russia (69.72º N; 61.62º E), and Kuujjuarapik, Canada (55.5º N; 77.7º W). The average number of AMDEs at Alert is 10 per season, 7 at Kuujjuarapik, and 11 at Amderma (Steffen et al., 2005), all significantly less than what was recorded over the Amundsen Gulf. The AMDEs at Amderma and Kuujjuarapik are abrupt and last 1-3 days whereas at Alert they are generally longer lived, the longest being approximately 11 days (Steffen et al., 2005). Over the Amundsen Gulf, the events were generally abrupt and short lived with the average being about 1.5 days. AMDE 6 was the longest event lasting nearly 9 days. Events 6, 7, and 8 were closely linked and only separated by a few hours, with the total depletion period lasting just over 15 days. These results indicate that the

Amundsen Gulf and the Banks Island flaw lead in general is a very active site for AMDEs.

Alert is the site of the longest and most complete dataset where the GEM concentration has been monitored nearly continuously since 1995. Due to the variability of the data, it was broken up into its respective seasons, with the spring season being defined as April to June. From 1995 to 2002, the average springtime median is 1.39 ng m^{-3}, which is slightly higher than the springtime median in the Amundsen Gulf reported here (1.25 ng m^{-3}). This value fits into the range of spring time medians for the given years (Table 2-2). Values for Amundsen Gulf were calculated using 3 hour averages for the period.

Table 2-2: Comparison of spring median, minimum, maximum, and range for GEM at Alert (Steffen et al., 2005) and the Amundsen Gulf (reported in ng m^{-3}).

	1995 Alert	1996 Alert	1997 Alert	1998 Alert	1999 Alert	2000 Alert	2001 Alert	2002 Alert	2008 Amundsen
Spring Median	1.59	1.62	1.26	1.54	1.35	1.10	n/a	1.46	1.25
Spring Minimum	0.13	0.08	0.03	0.07	0.07	0.08	n/a	0.20	0.07
Spring Maximum	2.92	2.84	2.58	3.04	3.23	3.96	n/a	3.62	4.27
Spring Range	2.80	2.76	2.55	2.97	3.16	3.88	n/a	3.42	4.20

The spring maximum and range was greater in the Amundsen Gulf than for all other reported years in Alert (Table 2-2). In fact the GEM maximum and range values reported for the Amundsen Gulf in 2008 are higher than all values reported for winter, spring, summer and fall for years 1995 – 2002 in Alert. The higher values may be due to the study location, in that the Amundsen study is directly over the ocean near the flaw lead which may expose it to more degassing from the water column near the end of spring, whereas the Alert site is coastal, thus Hg degassed

from snow and water surfaces may have had the time to mix and dilute in the atmosphere prior to being transported to the sample site. Since the Amundsen Gulf values are greater than all other reported values for all seasons between 1995 and 2002 (Steffen et al., 2005), it is not suspected that the higher values are due to the later onslaught of AMDEs at the higher latitudes of Alert.

The GEM data from all 3 sites including the Amundsen Gulf were compiled into boxplots to show the monthly dispersion of variability in GEM. Figure 2-19 shows the variation in GEM concentrations by month for all data collected and used in Steffen 2005 for the monthly period between February and July as the same period of data collected in the Amundsen Gulf.

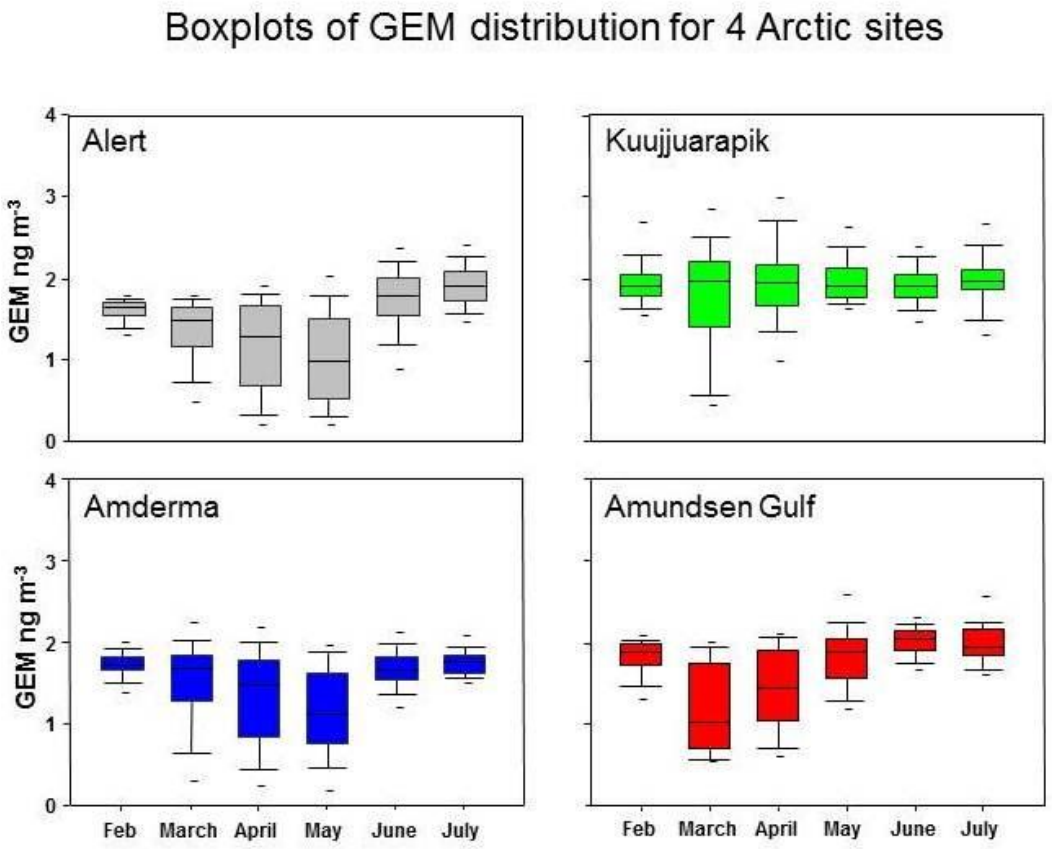

Figure 2-19: Box plots of monthly GEM concentration of all data collected from Alert, Amderma, and Kuujjuarapik (Steffen et al., 2005) as well as the same period in the Amundsen Gulf. The median is represented as the middle line in the box, the box boundaries show the 25th and 75th percentile, the whiskers above and below show the 10th and 90th percentiles, while the dashes indicate the 5th and 95th percentiles.

The highest variability attributed to AMDEs for Alert and Amderma occurred over the months April and May. In the Amundsen Gulf, this period of increased variability occurred one month earlier in March and April. March is the strongest month for variability for Kuujjuarapik; however, the median concentration is no lower at this time which may be a result of local re-emission influences (Steffen et al., 2003b). The variability in the Amundsen Gulf follows more closely with the pattern observed in Alert and Amderma compared to the sub-Arctic Kuujjuarapik site; however, greater variability occurs earlier on in the year over the Amundsen Gulf. The Amundsen Gulf in 2008 presented with lower median concentrations in March

and April than the average of all other sites. The major degassing period in the Amundsen Gulf also occurred in May, which is earlier than the other more northerly sites. The effect that latitude has on temperatures as well as the onset of polar sunrise can largely account for the variation seen in timing between studies.

The lower medians in March and April in the Amundsen Gulf can most likely be attributed to the AMDEs occurring in-situ where they are subjected to less atmospheric mixing prior to measurement as well as earlier onset due to the earlier polar sunrise date. Polar sunrise at our sampling location occurred on January 25, 2008, and shortly after that we witnessed our first depletion event on February 11. Events were witnessed earlier in the Amundsen Gulf than at Alert, which typically begin in mid-March (Schroeder and Munthe, 1998). Events are limited by the availability of BrO for the oxidation reaction; this may explain why March is more active in terms of AMDEs than the other sites as this month is also where we saw our largest bromine explosion (Section 2.4.2).

In the Gulf, the degassing period witnessed in mid-May was very rapid and short lived (Figure 2-4) with elevated concentrations only observed for approximately 22 hours starting on May 10. The maximum concentrations; however, were higher than any reported for all 3 sites in an 8 year period (Table 2-2). The short degassing period may have also been a result of the ships position and movement as over that 22 hour time period of the degassing event, the ship travelled 55 km south-west in the southern part of the Gulf from Cape Parry to Franklin Bay. Due to the ships position, relatively close to the southern shore, we may have failed to capture the true extent of the degassing period which may have been occurring further north over the

Amundsen Gulf. Events at all 3 sites reviewed by Steffen et al. 2005 arrested as soon as temperatures consistently reached 0ºC, which is also what we observed as the cessation of the final event recorded near McClure strait, AMDE 31.

2.5 Conclusion

This study was the first to be conducted over the open ocean from a relatively static position, for the duration of an entire AMDE season (pre-, during, and post-AMDEs). For a 6 month period, GEM, RGM, and Hg_p were continuously measured from the bow of the CCGS Amundsen in the Amundsen Gulf in the high Canadian Arctic. The data revealed a total of 31 depletion events which was much higher than the number of episodes reported to occur at coastal sites. It is thought that the dynamic sea ice conditions present in the gulf provided a consistent source of bromine radicals following polar sunrise, which facilitated the oxidation of GEM in the atmosphere thus increasing the amount of AMDEs recorded. It was also found that the duration in which these conditions are present has a significant impact on the minimum concentrations of GEM observed during the events.

This study provides further evidence of the essential role of tropospheric temperature, and identified that a drop in temperature is important in initiating AMDEs. This relationship was found at the beginning of nearly every recorded event and may be related to the formation of frost flowers in areas of new ice surrounding the ship. Wind speed at times was also found to play a potential role in the events. In this study, wind direction did not seem to play an important role, which may be related to the presence of ice 360 degrees around the ship for most of the sampling period. It is also thought that most of the events witnessed in the Gulf were the result

of in-situ events as opposed to ex-situ events transported from other areas. The dataset presented here is the first of its kind, and certainly provides insight into the behaviour of atmospheric Hg in marginal ice zone regions.

Chapter 3: Dissolved Gaseous Mercury and Air-Sea Exchange in the Amundsen Gulf

This Chapter reports DGM from various locations and conditions in the Amundsen Gulf throughout the CFL system study, and instantaneous air-sea Hg^0 exchange fluxes calculated from suitable samples.

3.1 Hypothesis

Increased Hg deposition surrounding flaw lead areas from AMDEs may lead to increased concentrations of Hg(II) in the water column. Thus, it is expected that increased concentrations of DGM will be observed as Hg(II) is known to rapidly undergo photoreduction back to Hg^0 (Section 1.6.2.1) in the presence of sunlight. This increase of Hg(II) in the system is predicted to result in positive Hg^0 flux values throughout the AMDE season signifying evasion from the ocean surface to the atmosphere. Nearing the end of the AMDE season (mid-May to June) a spike of atmospheric Hg is also noted (Figure 2-4) which is expected to be a result of rapid degassing of deposited Hg; therefore, during this time, higher evasional fluxes of Hg^0 are expected.

3.2 Experimental

3.2.1 Sample Collection

DGM sampling took place between February 26 and June 23, 2008, alongside atmospheric Hg monitoring during the CFL system study from onboard the CCGS Amundsen, as detailed in Chapter 2. DGM samples were collected in specially

designed 1-L Teflon (PTFE) containers which are the same vessels used during analysis (Figure 3-1). PTFE is a suitable material to use since Hg and other metals will not bind to the container walls. Collecting the samples in the same vessels used in the analysis avoids having to transfer the sample to another container, and thus limits the amount of DGM potentially lost during the decanting process. Sample vessels and tubing was first cleaned with 10% HCl and tested to assure that it was free of contamination prior to sample collection. The vessels were prepared within the clean environment of the PILMS laboratory, and then double bagged for transport to the sampling site.

Samples were collected using the "clean hands, dirty hands" sampling method (Fitzgerald, 1999). Depending on the site conditions, the samples were collected with different techniques 1) Direct sampling: Where the water was directly accessible by hand (e.g., via ice edge), the pre-cleaned PTFE vessel was directly submerged into the water to be sampled. The vessel was rinsed three times, and then capped tightly while still under the water to assure that there were no air bubbles, as the presence of air in the sample may allow for some DGM to be lost due to evasion. 2) Sampling via a Niskin bottle: Where water cannot be directly accessed, a portable metal-free Niskin bottle (pre-cleaned and tested for Hg baseline) was lowered to the depth from the side of the ship or through holes cut in the ice. The Niskin bottle was then transported back immediately to the PILMS laboratory and the sample was transferred to the PTFE sample vessel. 3) Sampling via the ship's rosette system: Where applicable, samples were also taken from the ship's rosette bottles at different sampling depths (the minimum depth was 12 m below the surface). The sample was flowed into the bottom of the PTFE vessel through a flexible tube, and was allowed to overflow out

the top for 1 minute to ensure a thorough rinse. 4) Sampling via the seawater sample line inside the PILMS laboratory; The PILMS was equipped with a Teflon seawater sample line which continuously pumps sub-surface seawater underneath the ship directly into the laboratory. At the time of sampling, the sample tap was let run for 5 minutes before being filled into the PTFE sample vessel.

In each case, the samples were analyzed in PILMS as soon after collection as possible (generally within 30 minutes). Care was taken to avoid excessive exposure to UV radiation and temperature changes during transportation back to the lab.

3.2.2 Sample Analysis

The apparatus of the DGM analysis is illustrated in Figure 3-1. All the tubing was made of PFA. At the beginning of the sampling analysis, the completely filled sample vessel was opened and excess sample water was quickly decanted to the 1-L mark and then sealed again with the PFA purging wand and sample lines connected as shown in Figure 3-1. The samples bottle was then purged with zero air produced by a Tekran model 1100 zero air generator for 50 minutes at a flow rate of 0.75 L min^{-1}. The resulting air stream passed through a soda lime trap to remove moisture, and into a Tekran model 2357B for analysis (Section 2.2.2).

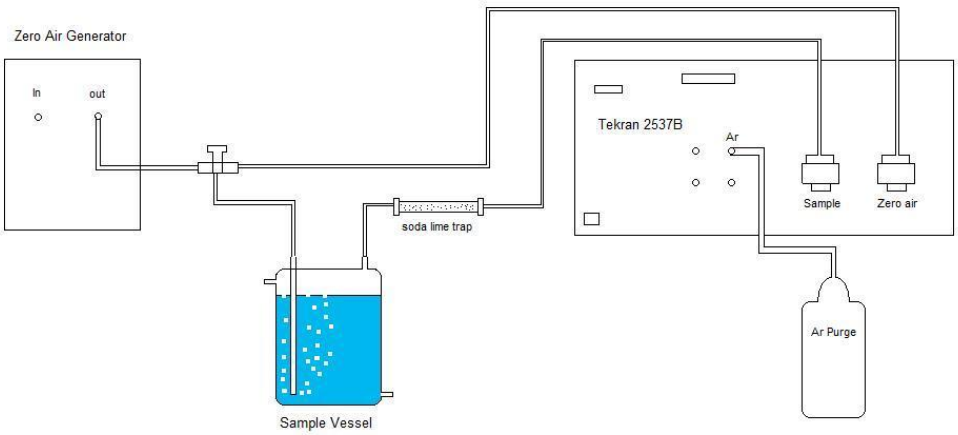

Figure 3-1: Tekran 2537 CVAFS unit DGM analysis setup used onboard the CCGS Amundsen in the PILMS laboratory during the CFL study.

A sampling rate of 0.75 L min^{-1} was chosen as it was close to the natural output of the zero air generator; this helped to maintain atmospheric pressures within the vessel. A sampling time of 50 minutes was found to be optimal, as anything beyond this time period yielded less than 5% of the initial DGM result (Figure 3-2). Some methods call for blank corrections whereas others do not; in this study, sample concentrations were not blank corrected. A detailed account on the operation of the DGM sampling method used, as well as the chosen instrument parameters can be found in Appendix A.

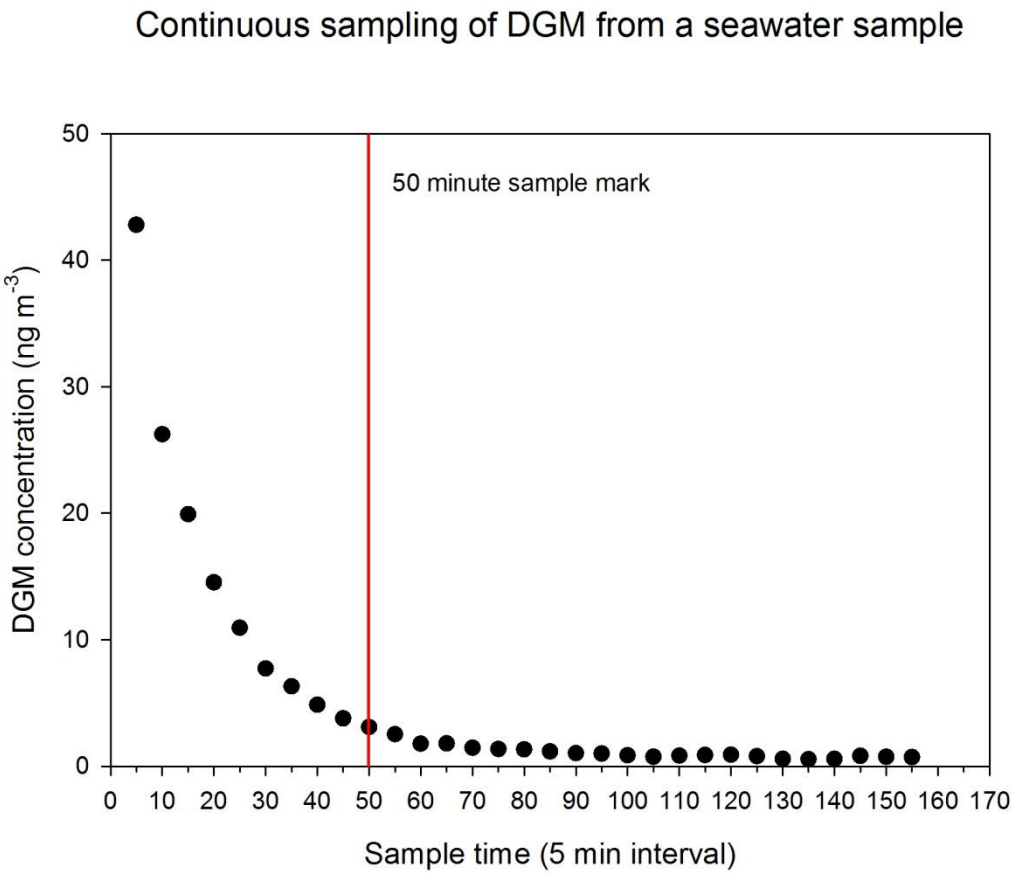

Figure 3-2: Continuous sampling of DGM from a seawater sample at 5 minute intervals in the PILMS laboratory. A 50 minute sample time (vertical line) was chosen as this time interval shows high DGM recovery.

3.2.3 Data Analysis

Meteorological data at the time of sample collection were obtained from the ship borne sensors. Sea surface temperature was collected from the standard AVOS system in the ship's bridge, and wind data from a meteorological tower (Dr. T. Papakyriakou, University of Manitoba) mounted at the bow of the ship, ~14 m above the ocean surface. Averaged data during the hour nearest the sample collection time were used for sea surface temperature as well as wind speed. Details of the sampling site were also recorded including the sample collection method and surrounding ice conditions at the time of sampling.

Data were then QA/QC'd to remove any points suspected to not represent true DGM concentrations. Any DGM data points that were not accompanied with complete ancillary data were not included in the results. Variation was found between analysts; if large discrepancies were noted, all data points from that analyst were removed to limit the possibility of a systematic error.

3.2.4 Flux Calculations

The instantaneous air-water fluxes of Hg^0 were calculated based on the general equations described in Section 1.7. The transfer velocity (k_w) was estimated based on the following equation (Poissant et al. 2000; Wanninkhof, 1985; see also Section 0):

$$k_w = 2.8 \times 10^{-6} \times 0.45 u_{10}^{1.64} (Sc_{Hg}/Sc_{C02})^{-0.5} \quad \textbf{Equation 37}$$

This equation was chosen as it uses a corrected Sc value for CO_2 and is a method that has been widely used in Hg^0 flux calculations. Results with this method also yield values near the centre of the spread of all k_w methods. k_w calculations involving the different wind speed regimes (e.g., Liss and Merlivat., 1986) were avoided as the lack of fetch in the leads generally meant that the sea surface was calm regardless of increasing wind speed. Breaking waves and bubbles were generally not observed during the DGM measurements thus they should not be incorporated into the k_w equations as strongly or an overestimation can occur. A conversion factor of 2.8 x 10^{-6} was used to convert the unit to the standard m s^{-1} unit.

The Henry's Law constant (K_H) was calculated using Equation 13, then corrected for electrolyte solutions using Equation 14 in Section 1.7.1. The density of

the seawater (ρ) used in calculating K_H and Sc was set at a constant value of 1027 kg m^{-3}, which is a good approximation of salinity in the Amundsen Gulf. The Sc number for CO_2 was corrected using Equation 30 and *Sc* for Hg^0 was deduced from Equation 22. The diffusivity (D) constant was calculated from Equation 23; the kinematic viscosity (η) used in calculating D was set to a constant value of 0.001793 Pa s^{-1}, which is the viscosity of freshwater at 0°C (See Appendix B).

Wind speed recorded during the DGM measurements was obtained from the meteorological tower mounted at the bow of the ship, where the anemometers are mounted approximately 14 m above the ocean surface. It was thus necessary to correct the observed wind speed to reflect wind at 10 m for use in the flux calculation. This was conducted using the NOAA COARE algorithm which is a well-used method for normalizing wind speeds for use in flux calculations (Fairall et al., 2003). Flux calculations were also performed using the various methods for determining the k_w values outlined in Section 1.7.3 in order to compare between methods. Flux reported here refers to the flux of Hg^0 only between the sea surface and the atmosphere. Depositional fluxes of Hg_p and RGM (Hg(II)) to the surface were not studied and thus are unknown.

3.3 Results

3.3.1 DGM

The DGM results ranged between 11.6 – 332.0 ng m^{-3} throughout the study period in the Amundsen Gulf, with an average (± standard deviation or s.d.) of 88.3 ± 53.1 ng m^{-3}. A total of 50 spot samples from various conditions were analyzed and separated into their respective groups including: open water (surface), under ice, at

depth > 10 m, and melt water (Table 3-1). Individual DGM concentrations over the entire study period are shown in Figure 3-3.

Table 3-1: Summary of DGM concentration (ng m^{-3}) in the Amundsen Gulf reported from this study.

Group	Average	Standard Deviation	Range	# of Samples
All	88.3	53.1	11.6 – 332.0	50
Under Ice	96.9	64.1	11.6 – 332.0	28
Open Water (Surface)	69.1	29.2	22.6 - 106.5	16
Deeper water (depth > 10 m)	102.8	36.1	77.4 - 164.1	5
Melt Pond	81.8	n/a	n/a	1

DGM samples collected from under the ice have an average (± s.d) of 96.9 ± 64.1 ng m^{-3} (n = 28) and the largest range of all types measured. The under ice samples represent all those collected from under the ice through drilled holes, or those collected from the PILMS seawater line while the ship was surrounded in ice (see Section 3.2.1). The open water sample group represented samples collected from either open leads or the open ocean and comprised of 16 samples with an average of 69.1 ± 29.2 ng m^{-3}. 5 samples were collected using the ship's rosette at depths greater than 10 m which yielded an average of 102.8 ± 36.0 ng m^{-3}. Of these, one sample was taken at a depth of 332 m (bottom) and yielded the highest DGM concentration of the group at 164.1 ng m^{-3}. The increased DGM concentration at depth may be due to the microbial reduction of Hg(II) near the sediment interface (Section 1.6.2.2). The rest were taken at a depth of 12 m, which is the shallowest depth possible while using the rosette in the ships moon pool. Only one sample was performed in melt pond water near a drainage hole which yielded a DGM of 81.8 ng m^{-3}.

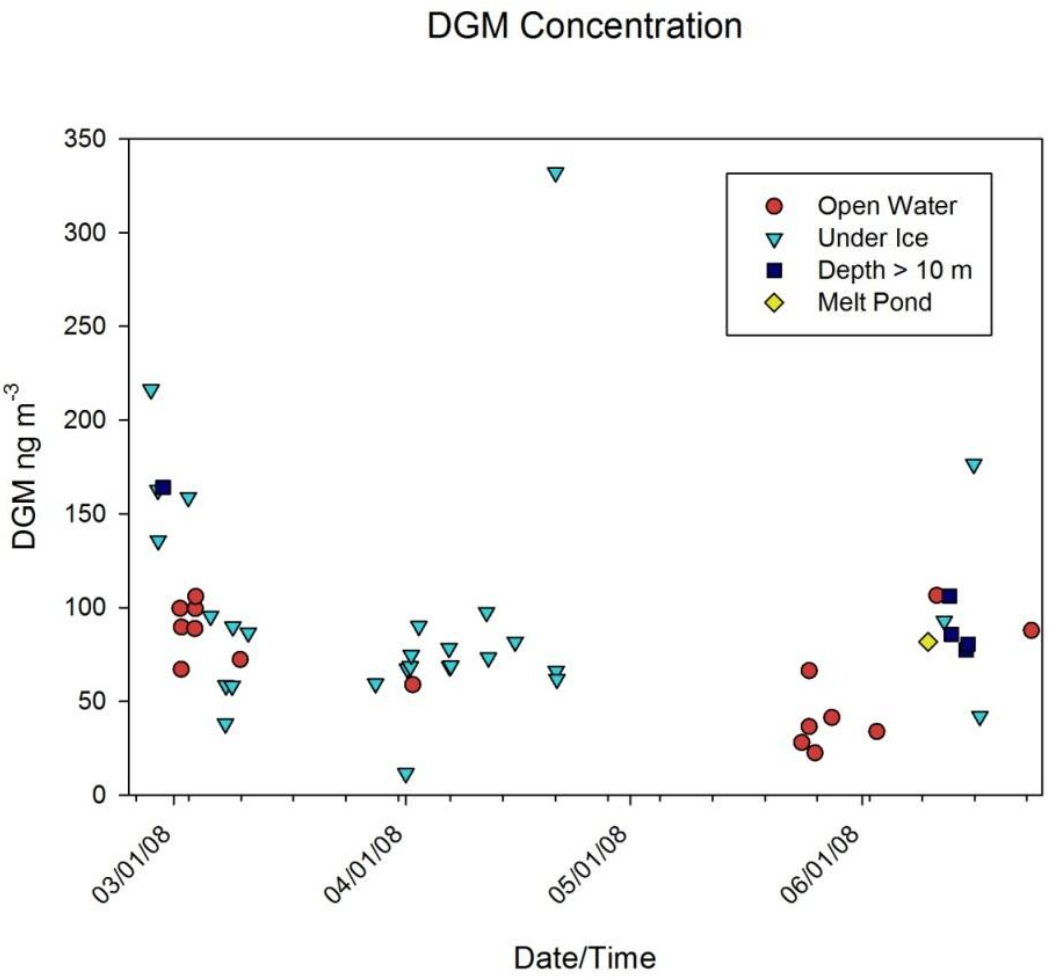

Figure 3-3: Individual DGM samples retrieved from the Amundsen Gulf during the CFL study period in 2008.

A one tailed difference of means test was performed to test the hypothesis that DGM concentrations measured from under ice conditions is greater than those from open water. A variance test was performed which concluded that the variances between ice and open water samples was indeed different. A separate variance estimate was used in the t-test, which revealed that the DGM values retrieved from water samples under the ice are significantly greater than those retrieved from open water ($p = 0.028$).

3.3.2 Hg^0 Flux across the Ocean-Atmosphere Interface

The instantaneous Hg^0 flux across the ocean-atmosphere interface was calculated for surface samples only; samples taken at depth were not included as they would not represent interfacial flux. Only one surface sample was not included in the flux calculations due to the unavailability of the GEM concentration at that time. Results are shown in Table 3-2 and Figure 3-4. Under Ice flux values were also calculated, however, they should be taken as theoretical or potential values as the ice is potentially acting as a barrier to the gas exchange. Once the ice is removed, the calculated flux value may become the actual Hg^0 flux value for a period of time until DGM concentrations at the surface decrease and equilibrium is reached.

Table 3-2: Instantaneous ocean-atmosphere flux (ng m^{-2} d^{-1}) of Hg^0 in the Amundsen Gulf reported during this study.

Group	Average	Standard Deviation	Range	# of Samples
All	178.5	291.9	0.8 – 1778.2	44
Under Ice	215.5	358.5	3.8 – 1778.2	27
Open water	116.0	95.2	0.8 – 344.7	16
Melt pond	74.6	n/a	n/a	1

The Hg^0 flux from all surface samples yields an average of 178.5 ± 291.9 ng m^{-2} d^{-1} with a range of 0.8 to 1778.2 ng m^{-2} d^{-1}. The flux measured from a total of 27 samples under ice measured 215.5 ± 358.5 ng m^{-2} d^{-1}, and the flux measured from 16 open water samples yielded 116.0 ± 95.2 ng m^{-2} d^{-1}. The instantaneous flux rate from the single melt pond water sample was 74.6 ng m^{-2} d^{-1}.

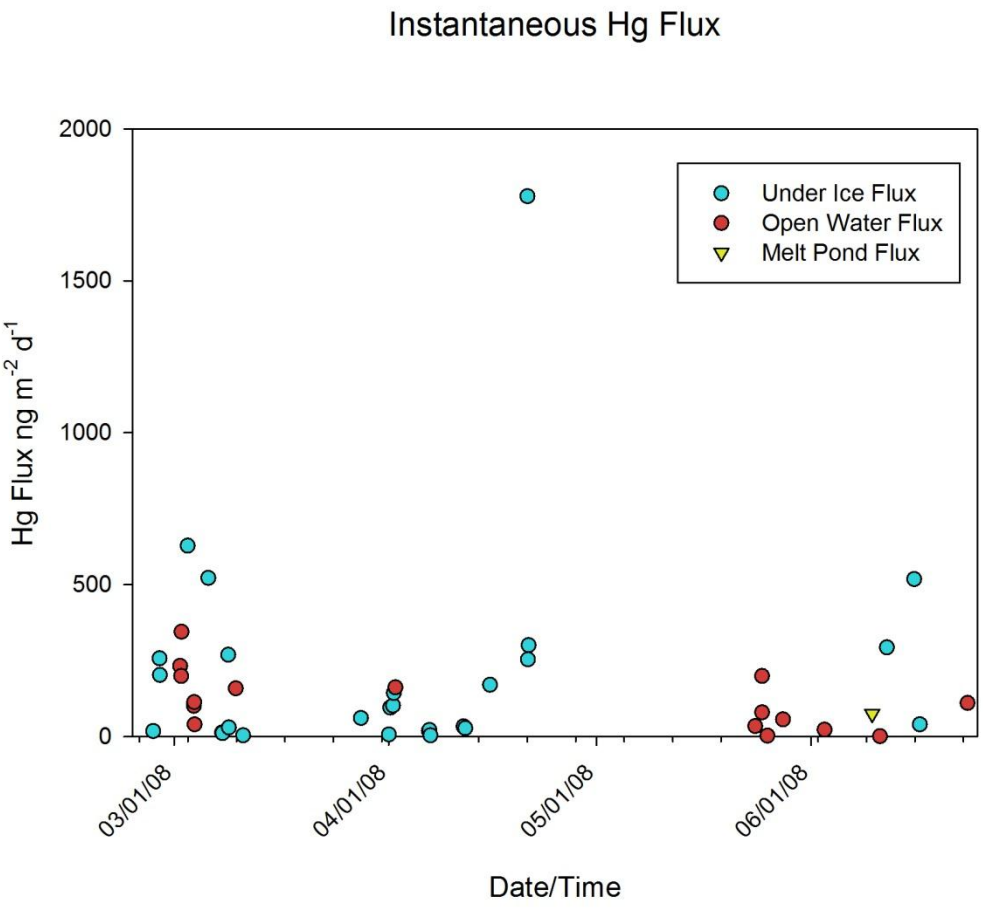

Figure 3-4: Instantaneous ocean-atmosphere Hg^0 flux calculated for the Amundsen Gulf during CFL study period in 2008.

3.4 Discussion

3.4.1 DGM

The DGM concentrations reported in this study agree in general with similar studies in the Arctic Ocean (Andersson et al., 2008b, St. Louis et al., 2007). The higher DGM concentrations under the ice most likely can be attributed to the trapping of DGM produced in the water under the ice, as DGM in open water can readily partition to the atmosphere. Similar findings were also reported by Andersson et al., 2008b (Table 3-3), where an increase from approximately 15 to 70 ng m^{-3} was observed as the ship moved from open waters into ice covered conditions. Increased

DGM concentrations of approximately 100 ng m^{-3} have been measured near the Mackenzie River plume, and open water in the Canadian archipelago was found to be slightly higher, around 40 ng m^{-3},when compared to open water on the west side of Greenland. St. Louis et al. (2007) also reported very high concentrations of DGM below ice near Ellesmere Island, with an average of 129 ± 30 ng m^{-3}.

Contrary to these results, winter DGM concentrations in boreal lakes were found to have lower concentrations under ice than during the summer (Poulain et al., 2004). This may be due; however, to a thick layer of snow on the surface limiting light penetration into the water column and thus limiting the photochemical production of DGM. Ice in the Amundsen Gulf was typically snow free throughout the winter and spring, thus significant light penetration through the ice was possible. This may have allowed for the build-up of DGM under the ice and lead to the increased concentrations found. Boreal lakes may completely freeze over during the winter which would prevent deposited Hg(II) from entering the system. In the Amundsen Gulf, atmospheric deposition to the aquatic environment is possible due to the actions of AMDEs and the presence of open leads. This deposition combined with enhanced sunlight (increasing daylight hours) may contribute to the enhanced DGM observed.

Table 3-3: DGM concentrations reported in Oceans and Lakes (either range or average) from various studies in the northern hemisphere compared to this study.

Site(s)	DGM ng m^{-3}	Reference
Marine and Coastal		
Amundsen Gulf	88.3 ± 53.1	This study
Arctic Ocean	44.1 ± 22.1	Andersson et al., 2008b
Ellesmere Island	129 ± 36	St. Louis et al., 2007
Ny-Alesund (79°N)	12 - 70	Sommar et al., 2007
North Atlantic	11 - 35	Temme et al., 2005
North Atlantic	4.0 - 140.4	Mason et al., 1998
Baltic Sea	10 - 32	Kuss and Schneider, 2007
Western Mediterranean	134.4	Cossa et al., 1997
Tokyo Bay	52 ± 26	Narukawa et al., 2006
Freshwater		
10 Arctic Alaskan lakes	8 – 86	Tseng et al., 2004
Arctic Lakes	40.1 - 120.4	Amyot et al., 1997b
Temperate Regions	20 - 60	
Tropical Regions	10 - 20	
Amituk lake, NWT	31.5 - 40.7	
ELA lake 658	80.2 - 240.7	Poulain et al., 2004
Lac St. Louis, QC	27.6 ± 0.1	O'Driscoll et al., 2008
Big Dam West Lake, NS	76 ± 31.1	O'Driscoll et al., 2003
Puzzle Lake, NS	27 ± 21.8	O'Driscoll et al., 2003
Upper St. Laurence River	0 - 60.4	O'Driscoll et al., 2007

The average DGM concentration we measured in the Amundsen Gulf is about 2 times that reported along a transect of the Arctic Ocean (Andersson et al., 2008b). Higher relative concentrations in the Amundsen Gulf may be explained by increased Hg loadings from riverine inputs, and/or increased DOC input which has been found to facilitate DGM production (Costa and Liss, 1999, O'Driscoll et al., 2006, Garcia et al., 2006). The increased levels may also be due to either the time of year in which the sampling took place, or potentially to increased Hg loadings to the surface from active AMDEs situated over the Gulf. The dynamic ice shifting in the Gulf may also lead to increased Hg deposition directly to the water column, and thus lead to increased DGM concentrations as the Hg(II) is photoreduced back to Hg^0. Increased DGM concentrations in Arctic regions during the winter months may also be

enhanced due to lower temperatures, which, in turn, can increase the diffusional resistance between air and water, and subsequently reduce the transfer rates (Mackay et al., 1995).

DGM concentrations may vary between seawater and freshwater samples as it has been shown that Hg(II) oxidation can be stimulated by chloride ions (Yamamoto, 1996), thus direct comparison is not possible. Table 3-3; however, does show that data from this study is within the range of DGM concentrations recorded in other studies, both fresh water and marine. The average total inorganic and organic Hg(II) concentration in the Amundsen Gulf seawater throughout the study period was approximately 300 ng m^{-3}. The contribution of organic Hg components is usually small when compared to inorganic Hg(II), thus for this purpose it can be neglected. Typically DGM concentrations are an order of magnitude lower than the Hg(II) concentration (Morel et al., 1998), and for most samples this remained true in this study. Several under ice samples, however, had similar concentrations of DGM and Hg(II), which can largely be attributed to the supersaturation condition created by the ice cap.

DGM concentrations were also compared to wind speed as it has been found that higher wind speeds can lead to decreased DGM concentrations by increasing Hg evasion from the surface of the Mediterranean Sea (Fantozzi et al., 2007). In our case, however, no trend was observed for open water samples. This may be due to the fact that during sampling time, most of the water was covered with ice, and thus the effect of wind is not as strong as noted in open water areas.

Slight decreasing trends in DGM concentrations over time and sea surface temperature were observed; however, the data was highly variable and not statistically significant with R^2 values around 0.02. A decreasing trend is expected as a function of gas solubility and temperature; however, the high variation is most likely a factor of varying meteorological conditions. There was also an increase in open water sampling near the end of May and June due to changing ice conditions which may also influence the trend. Due to these factors as well as the non-continuous sampling routine, it is not possible to speculate too far into DGM concentrations with time of year in this case. Diurnal patterns in DGM were also not witnessed in this study as most samples were taken during daylight hours, and thus no comparison can be made. Future study with higher temporal resolution is required to determine daily and seasonal trends in DGM concentrations in the Gulf.

3.4.2 Atmospheric Hg^0 Flux

Andersson et al. (2008b) calculated a hypothetical average Hg^0 flux value of 57.8 ng m^{-2} d^{-1} using the following parameters: TGM = 1.7 ng m^{-3}, wind speed = 6 m s^{-1}, and water temperature = -1°C. The model used in flux calculations for this paper yielded a result of 69.0 ng m^{-2} d^{-1} for the same hypothetical situation; a difference of only 16%. This error is considered reasonable for our purposes as average salinity and viscosity was used in all calculations, and this model uses actual GEM concentrations instead of TGM, which would lead to reduced flux values in the calculations. DGM concentrations in this study were also not blank corrected, which may lead to slightly higher reported values over some other studies.

All flux results calculated in this study were found to be positive signifying Hg^0 evasion from the ocean to the atmosphere. This is not surprising given the amount of Hg potentially being introduced to the surface from the active AMDEs found to be occurring over the sampling site. As previously mentioned the relative amount of Hg(II) deposited to the surface is unknown; however, it is evident that there is an increased amount of DGM at the surface, and thus Hg^0 flux from the sea to air is expected

The flux calculations assume that the water is open to the surface, and that an increase in wave action leads to an increase in DGM evasion. The Amundsen Gulf was, however, mostly covered in ice with only small pockets of leads open during the time of sampling. Due to the lack of fetch, the results may be overestimated as the actual wave action would not be as significant as predicted in the model.

Andersson et al. (2008b) calculated an overall Hg^0 flux range across the Arctic Ocean and Canadian archipelago of -38.5 to 2358.9 ng m^{-2} d^{-1} with the highest concentrations occurring on the Alaskan coast. The range observed with samples collected in the Amundsen Gulf was 0.8 to 1778.2 ng m^{-2} d^{-1}, thus within the same order of magnitude for this area. The highest DGM sample recorded (Figure 3-3) in the Gulf was 332 ng m^{-3}, much higher than the second highest concentration of 216 ng m^{-3}, and significantly higher than the rest of the samples. Both of these two high DGM samples were taken from under ice conditions, and both samples were retrieved from the ship's sampling line. One explanation to the high value is that it was taken later in the season (April 21, versus Feb 26 for the second highest), which is the period after the most intense AMDEs in the gulf, and the ice conditions were

becoming more dynamic. There is also the potential contamination in PILMS' built-in seawater sampling line; however it was not apparent in other samples taken around the same time.

Overall, flux values of Hg^0 in the Gulf were higher than most studies in other areas (Table 3-4), however, only slightly higher for Arctic marine studies. The higher flux (and DGM) values recorded may be due, in part, to the source of water in the Gulf. As mentioned earlier, the Amundsen Gulf receives water from the Pacific and Chukchi Sea (RU), which circulates up past Alaska along the northern coast and into the Gulf. Along the way there is the potential for significant riverine input, most notably the Mackenzie, where increased Hg inputs have been measured during the spring (Leitch et al., 2007). This input may introduce more Hg(II) substrate into the water, as well as potentially increase DOC or humic substances.

Table 3-4: Air-water flux of Hg^0 reported from various studies (range or average) in the northern hemisphere compared to this study.

Site(s)	Average Flux ng $m^{-2}d^{-1}$	Reference
Marine and Coastal		
Amundsen Gulf	178 ± 292	This study
Arctic Ocean	-38 to 2359	Andersson et al., 20008b
Ellesmere Island	130 ± 30	St.Louis et al., 2007
Ny-Alesund (79°N)	2.4 to 168	Sommar et al., 2007
Baltic Sea	-6 to 150	Kuss and Schneider, 2007
Long Island Sound, CT	72.8	Rolfhus and Fitzgerald, 2004
Tokyo Bay	140 ± 120	Narukawa et al., 2006
Freshwater		
10 Arctic Alaskan lakes	28 ± 10 (12 – 40)	Tseng et al., 2004
Amituk Lake, NWT	1.92	Amyot et al., 1994
Merretta Lake, NWT	11.6	
Wisconsin Lakes	4.8 - 54.9	
Ontario Lakes	1.0 - 30.8	
Upper St. Laurence River	4.8 to 26.4	O'Driscoll et al., 2007

No correlation was found between the concentration of GEM in the atmosphere and the calculated flux values. In theory, when the concentration of GEM in the atmosphere is low, higher flux would be expected as DGM in the water would more readily partition to the atmosphere due to a higher concentration gradient. This lack of correlation may be another result of the large role that the meteorological and sea ice conditions play on gas exchange. No significant trend was observed either between GEM concentrations in the atmosphere versus concentrations of DGM in the water. Despite the slight decreasing trend in DGM over the study period, there is no discernable positive or negative trend in the flux calculations.

The lowest flux result (0.8 ng m^{-3}) was taken from open water; far from any present ice with the zodiac and Niskin, whereas the highest flux result was taken in ice conditions from the sea water sample line in the PILMS laboratory (1778.2 ng m^{-3}). The sample with the lowest DGM concentration did not yield the lowest flux result; as the lowest flux value was associated with a DGM concentration of 106.5 ng m^{-3}. The lowest flux result was associated with a wind speed of 0.6 m s^{-1}, and the lowest DGM sample was associated with a wind speed of 6.17 m s^{-1} which resulted in a higher estimated flux value for that sample. Water temperatures between the highest and lowest flux values is similar, thus the major difference was wind speeds at the time of sampling as well as the ice conditions. The highest flux value was a result of both a high DGM concentration of 332 ng m^{-3} (the highest) and a very high wind speed (12.8 m s^{-1}) which resulted in a very high evasional flux. Due to the higher wind speeds it is unlikely that this rate would be sustained for a long period of time.

3.4.3 Comparison between Transfer Velocity Calculation Methods

The above Hg^0 flux results were calculated based on the Poissant et al. (2000) method for calculating k_w. To compare how sensitive the flux values are to different methods for k_w calculations, flux values were calculated for the entire dataset using various k_w methods described in Section 1.7.3. The results are shown in Table 3-5.

Table 3-5: Hg^0 fluxes calculated based on several different methods for estimating the transfer velocity (k_w). Results reported during this study use the Poissant et al., 2000 method.

k_w method	Average ng m^{-2} d^{-1}	Standard Deviation ng m^{-2} d^{-1}	Range ng m^{-2} d^{-1}
Poissant et al., 2000	178.4	291.8	0.8 – 1778.2
Liss and Merlivat, 1986	117.1	215.8	-221.4 – 1062.6
Wanninkhof 1992	263.1	471.7	0.3 – 2874.23
Loux, 2004	74.8	72.6	3.5 – 457.5
Nightingale et al., 2000	224.3	381.7	2.0 – 2352.5

Table 3-5 reveals that depending on how the k_w is estimated, the flux results could be very different as he average flux based on the different methods ranges from 74.8 to 263.1 ng $m^{-2}d^{-1}$. In the literature it was stated that the Nightingale et al. (2000) method was found to fall between the Wanninkhof (1992), and Liss & Merlivat (1986) estimations, which is also the case here. Compared to the Poissant et al. (2000) method (Table 3-5), Liss & Merlivat (1986) predicted a lower flux over all at both ends of the range. Wanninkhof (1992) had the largest range, as well as the highest average flux value. Loux (2004) had a higher value in the low range, however a very low prediction for the upper range resulting in the lowest overall average. Nightingale et al. (2000) had a high low range prediction, as well as a higher upper range prediction with the average falling slightly above the overall mean for all methods. From these results, it is evident that the method used by Poissant et al. (2000) was a good middle approximation over the other 4 methods. In fact, the

average of all methods yields 171.5 ng m^{-2} d^{-1}, which is very close to the average calculated based on the Poissant et al. (2000) method.

3.5 Conclusion

The DGM concentrations in the Gulf averaged 88.27 ± 53.1 ng m^{-3} with a range of values between 11.6 – 332.0 ng m^{-3} is reported. There is statistically significant evidence to suggest that seawater samples retrieved from under the ice contain higher amounts of DGM than those retrieved from open water, or within open leads. DGM values reported here suggest that the Amundsen Gulf may experience elevated concentrations of DGM in the winter and spring, which may be a result of active AMDEs in the area, as well as the dynamic sea ice environment. The higher values are consistent with other studies conducted in the area (Andersson et al., 2008b), and more study is required to determine if it is due to the nature of the CFL system, or due to the inputs from rivers or upwelling areas.

Hg^0 flux values across the ocean-atmosphere interface calculated based on the stagnant film model and the k_w method from Poissant et al. (2000) revealed an average flux of 178.4 ng ± 291.8 ng $m^{-2}d^{-1}$ with a range of 0.8 to 1778.2 ng $m^{-2}d^{-1}$. No significant increasing or decreasing trend in the flux was observed over the study period. The flux values in the Amundsen Gulf are higher than those reported for a transect in the Arctic Ocean (Andersson et al., 2008b) which is likely due to the supersaturation of the Gulf water with DGM relative to the atmosphere; potentially due to the actions of AMDEs and the ice acting as a barrier to evasion. This resulted in a positive net flux from the water to the atmosphere throughout the entire study period.

Chapter 4: Conclusions and Future Directions

4.1 Conclusions

The objectives of this study were to determine the potential influence of the sea ice environment on AMDEs, DGM, and the ocean-atmosphere flux of Hg^0. Circumpolar flaw lead areas, such as the Amundsen Gulf, provide a unique area to study these influences, as the sea ice environment is constantly changing. Atmospheric Hg components (GEM, Hg_p, and RGM) were measured continuously for a period between mid-January to mid-July, 2008, and alongside these measurements were spot samples for DGM which were sampled under a variety of conditions. DGM, GEM, and meteorological conditions were used to calculate the theoretical Hg^0 flux rates between the ocean and atmosphere.

The Amundsen Gulf was found to be a very active site for AMDEs. A total of 31 events were captured throughout the study period, which is much higher than expected at coastal sites. It is thought that the dynamic ice conditions in the Gulf may have provided an environment in which Hg^0 could be readily oxidized to its reactive form due to the augmented activation of bromine radicals. The continual exposure and freezing of seawater in the Gulf also promotes the growth of frost flowers, which have been hypothesized to be a significant source of reactive bromine to the atmosphere. The GOME satellite images confirmed that increased concentrations of BrO were present over the study site during periods of active AMDEs.

Temperature was also found to play a large role in the initiation, cessation, and duration of events. It was found that most events typically started with a sharp decrease in temperature; the reason behind this is unclear, but may be linked to re-freezing of ice in the area. No events were seen at temperatures above 0°C, and some events were terminated at the same time as temperatures achieved that threshold. The duration of events was also found to be prolonged at colder temperatures, whereas at warmer temperatures, the events were more frequent, and shorter lived.

Enhanced DGM concentrations (88.3 ng m^{-3}) were found in the Amundsen Gulf when compared to reported results from other more temperate areas (See Table 3-3). Concentrations were also enhanced, approximately 2 times, over a reported average value for DGM during an Arctic transect (Andersson et al., 2008b). It is thought that the higher values observed in the Amundsen Gulf are due to either increased Hg(II) available for reduction (which may potentially be due to AMDE deposition to the surface), or the inability of abiotically produced DGM under the ice to evade to the atmosphere. DGM concentrations under ice were found to be significantly higher than in open water, which suggests that the ice cover is indeed acting as a barrier to atmospheric exchange.

The average Hg^0 flux value calculated for the duration of the study was 178.5 ng m^{-2} d^{-1} with values ranging between 0.8 to 1778.2 ng m^{-2} d^{-1}. There was no significant trend observed throughout the duration of the study, which may be due to the dependence of flux rates on meteorological conditions. Positive flux rates were recorded for all DGM samples taken which signifies evasion from the ocean surface

to the atmosphere. This is potentially due to increased Hg(II) deposition to the surface, however the rate of deposition attributed to AMDEs is unknown.

This study provides the first atmospheric Hg and DGM measurements situated over the ocean for an entire AMDE season (pre-AMDEs to post-AMDEs), and portrays the importance of the sea ice environment in Hg cycling in the Arctic; however, there are still many questions that need to be answered. The following section will outline key knowledge and technological gaps that currently exist, as well as highlight improvements which can be made to future studies.

4.2 Areas of Potential Improvement in This Study

There are several improvements that can be made to future similar ship borne studies. First, there is a need for more consistent meteorological data. Incomplete meteorological data were often noted when attempting to compare it to the Hg data which lead to difficulties in analyzing all AMDEs and identifying trends. This was mainly due to the placement of the meteorological instruments, and contamination from normal ship operation, especially in terms of wind speed and direction. The meteorological tower on the front of the ship was more accurate than the standard ship sensors; however, much of the data had to be removed depending on which direction the ship was facing as the wind measurements get corrupted as it moves around the ship structures. This resulted in the wind data being intermittent, and that made it difficult in assessing the influences of these parameters. There were ice borne measurements of meteorological data when the ship was positioned at a site for an extended period of time. In the future, it would be useful to look at these data in relation to the Hg data to help determine trends, as it would be more accurate and not

affected by the ship. Furthermore, in this study atmospheric pressure was not considered. This would be helpful in future work with this dataset to determine when new air masses move into an area which may help determine the origin of the AMDEs. Future studies over or near flaw lead areas should pay careful attention to acquiring a valid consistent meteorological dataset for the study period to help solidify some of the relationships seen.

Another major data gap in this study is reliable ice coverage data. The satellite images provide a good estimate for certain AMDEs; however, the time series for the images used in this study were too far between for any significant results to be drawn. Calculating sea ice concentrations (ice to open water ratio) as well as young ice to old ice ratios from a given radius around the ship would be important for determining the effects of the flaw lead system on AMDEs. The visual ice coverage is simply an estimate and is subject to the interpretation of the observer.

This study was very useful in underlining some of the difficulties in sampling DGM in situ from a ship based setting. One of the main issues was obtaining a steady reliable sample to be used in analysis. As part of the CFL project design, a Teflon sample line was installed with the intent to provide a clean seawater sample to the labs onboard including PILMS. Once this system was in use in the Arctic it encountered many problems which resulted in it not being useful for our purpose. Some of the problems included clogging with ice, which in turn burned out the pump motor rendering the system inoperable. When the system was running, it was often contaminated with rust from the ship's hull which could potentially skew Hg results and made filtering samples impossible. Since DGM concentration is susceptible to

temperature changes, the 5-10 degree split in sea surface temperatures vs. lab temperatures may also lead to lower than actual results. Finally as time went on, a build-up of red algae was found in the sample line.

Due to these problems, sampling from the seawater sample line was stopped and only spot samples were collected on an opportunistic basis. Spot sampling is not ideal as it is more time consuming, and often requires cooperation with ship operations as samples must be collected from the rosette, on the ice, or from the side of the ship. Spot sampling also decreases the sample resolution that is possible, making it hard to determine diurnal or other temporal patterns.

Because of the complications with sampling, many different methods had to be employed in order to obtain samples (i.e., Niskin, rosette, or submerging vessel). Each method may introduce their own specific error due to the different sample handling methods required. For example, sampling from the Niskin required that the sample be collected in the field and returned to the lab full where it would then be decanted to the sample vessel. This was required as transferring the sample to the vessel in field was often impossible due to the rapid freezing of the Niskin spigot. The Niskin also requires very tedious cleaning which is time consuming, and the longer the sample remains in the Niskin, the higher risk of contamination. Sampling from the rosette is also not ideal as the rosette bottles are often used by several other science groups, and this may lead to contamination as the bottles may not be clean at the time of sampling. Sampling from the rosette also only allows for a minimum depth of 12 m, thus it is not suited for surface sampling. The ideal way for spot sample collection is to submerge the vessel directly in the sample; however, this was

often not possible as water temperatures were too cold to submerge your hands long enough for proper filling. If sampling from a hole in the ice, this method may not be accurate as the surface water may have already had the chance to equilibrate with the atmosphere leading to lower than actual under ice results. The ice was often over 2 m thick, thus in order to get under it, it is necessary to use the Niskin. It would be ideal if the same sampling method could be used throughout the project to avoid variation occurring from the sampling method, this should be considered in future studies.

Future studies should place more attention upon improved collection between the open water and under ice conditions. The best way to obtain under water ice samples would be to have a diver collect a sample in the sample vessel from directly below the ice at a significant distance from any open water. This type of study would greatly help remove some of the variables associated with the under ice sampling used during this study and further identify how great an increase is seen under ice versus open water with higher accuracy.

Improvements to the DGM collection and analysis in this study could also be done by using dark sample collection vessels. The vessels used in this study were Teflon, thus they were opaque, however would still allow for the penetration of light into the samples. This may enhance DGM concentration as discussed in Section 1.6.2.1. By using a dark or covered bottle, this variable could be eliminated. The PILMS laboratory is also well lit with high wattage bulbs; performing DGM analysis in the dark or low light would help preserve the samples, and limit variances due to light (Lindberg et al., 2000). The importance of meteorological data was pointed out

above when discussing AMDEs and the same importance applies to DGM measurements, especially if they are to be used with flux calculations.

The sea surface temperatures during this study were collected from the ships AVOS system, however, it would be more accurate to take temperature manually at the same time of sampling directly at the site, this would help to improve the accuracy of flux calculations. It would also be useful to look photosynthetically active radiation (PAR) measurements as well to help determine how much of the variance can be explained by the incoming solar radiation. PAR was measured as part of the CFL study, thus future work with these data should incorporated these measurements. It would also be important to measure the amount of light penetration through the ice to determine the rate at which DGM may be abiotically produced.

For calculating Hg^0 flux values in this study, the kinematic viscosity (η) used in calculating the diffusivity was set to a constant value of 0.001793 Pa s^{-1}, which is the viscosity of freshwater at 0°C (See Appendix B). A method for determining viscosity for seawater at a specific salinity at temperatures below 0°C could not be found, thus future work with this dataset, as well as future studies situated in the Arctic, should incorporate a method for determining the actual viscosity of the sample in order to remove as much of the error as possible in calculating flux. Having actual measurements of parameters such as these will act to reduce the large margin of error currently associated with this type of calculations.

Another potential source of error was introduced due to the longevity of the study. Since the study covered a time period over 6 months, it was necessary for different scientists to collect and perform the DGM analysis. At times, a high degree

of variation was seen between the DGM analysts which resulted in a smaller dataset; as large sections of data had to be removed. This may be due to slight differences in the analysts sample handling, or potentially a step being missed, however it brings into question the reproducibility and reliability of the results. This factor alone highlights the importance for a standard DGM procedure to be created and used.

4.3 Future Directions

Placing a priority on future directions in polar Hg research is difficult due to the interdisciplinary nature of Hg dynamics in these regions. It is well known that climates in Polar Regions are quickly and drastically changing, thus future directions should place a priority on how Hg cycling will be altered with respect to climate change.

Since the discovery of AMDEs in the mid-1990s, Hg cycling in Arctic environments has received a lot of attention from the scientific community, and many studies have been conducted increasing our understanding. Even though it has been an intensely studied topic for over 15 years, there is still much to discover and many knowledge gaps remain. The central data gap is well known and remains to be the determination of the actual amount of Hg deposited to the marine environment that is attributed to AMDEs. As outlined in Chapter 1, AMDE-deposited Hg may either be released to the water column where it may potentially become incorporated into the food chain, and alternatively it may be photoreduced back to the atmosphere as Hg^0. The contribution of AMDEs to Hg loadings to the Arctic Ocean, however, is yet to be accurately quantified. A review by Steffen et al. (2007) identifies the largest gap as our understanding of the chemical processes that drive deposition and re-emission of

Hg in polar environments. This pressing question will, and should continue to be, the central focus in ongoing research into AMDEs in the future.

While continuous monitoring at the coastal Alert station (Environment Canada) has been in place for more than a decade and has provided ground-breaking data into the occurrence of AMDEs, efforts should be taken to study AMDEs from the ocean sites. Due to the very high AMDE activity witnessed over the Amundsen Gulf, more data from this region and elsewhere would be valuable in confirming the higher AMDE activities over the ocean as well as confirming differences from coastal site measurements. Potential future studies should also focus on differences between AMDEs over flaw lead areas versus AMDEs over ice covered areas of the ocean to better assess the role of open water and the dynamic sea ice environment.

Methodologically there is still much room for improvement in atmospheric Hg measurements. There are two major methodological gaps in which future development is required. Firstly there is currently no method for calibrating Hg_p and RGM concentrations in the atmosphere, thus the recovery of the 1130/1135 system is unknown. This information would help fill a valuable data gap in the mass balancing of Hg in the atmosphere, thus it is important that this issue be addressed and a method for quantifying these components is developed. Secondly it is essential to identify the exact species of RGM and Hg_p produced during AMDEs; this will confirm the exact chemical oxidation pathway taken. This would help determine which environmental factors may have the highest influence on the occurrence of AMDEs, which may help determine the potential impacts of expected climate change trends. As discussed in Chapter 1, laboratory and kinetic studies have confirmed that active bromine species

are the most likely suspect (Raofie and Ariya, 2004, Raofie and Ariya, 2003); however in situ measurements of atmospheric Hg(II) species resulting from AMDEs have yet to be conducted. Understanding the chemical processes taken is essential for models to accurately predict the influence of AMDEs, as well as to determine the potential pathway that AMDE deposited Hg species may take once introduced to the cryosphere or hydrosphere.

Some questions raised during this study include the rate in which RGM formed during events adheres to particles in the atmosphere. If particle loading is high, such as during polar sunrise and Arctic Haze, this rate may be extremely fast. Some studies have suggested that the presence of high levels of RGM in the atmosphere indicates that the event is occurring locally, whereas previously depleted air masses are higher in Hg_p (Gauchard et al., 2005, Lindberg et al., 2002). Knowing the rate at which RGM can adhere to particles would be essential for confirming this assessment. If this rate is fast and particle loadings in the atmosphere are sufficient, this may be an incorrect assumption and alternate methods are required in determining the origin of the AMDE. This assumption also does not agree well with the data presented in Chapter 2; as high Hg_p concentrations were often associated with events thought to be occurring locally. This information may also be helpful in understanding the shift from Hg_p to RGM dominant Hg(II) later in the season, which may simply be due to a decrease in particulates in the atmosphere available for adhesion.

Future studies may also want to look into where in the atmosphere the products of AMDEs are being produced. Due to the suggested role of sea ice

surfaces, does the reaction take place directly on the surface of the ice, or does it occur freely throughout the troposphere as long as the required chemical species are present? Simultaneous Hg speciation studies at ground level over ice and upward into the atmosphere may help address this issue and further strengthen the role of sea ice in AMDEs.

This study revealed DGM concentrations that were significantly higher than in more southern temperate regions. Although this has been noted before, it is important to identify the actual cause(s), being it the sea ice cap, increased Hg(II) substrate, higher DOC concentrations or simply lower temperatures. It would also be useful to study DGM in other flaw lead areas similar to that of the Amundsen Gulf to assess if there is a trend in increased DGM concentrations with these areas. If true, that may confirm that the open water created by these leads is actually allowing for increased deposition of Hg(II) to the aquatic surface by AMDEs. This conclusion would be valuable information in assessing the potential ecosystem impact.

As reviewed in Section 1.6.2, it is necessary to determine which factor(s) are primarily responsible for DGM production in the Arctic. It is hypothesised that Abiotic production is the main route; however the role of microbial influences has not been fully established. Different factors may play larger or smaller roles depending on the time of year, as the Arctic experiences large climate variances with the seasons. More study is required to determine the formation pathways, and how they are affected by the seasons.

As outlined in Section 1.6.5, there is also a need for a standardized DGM measurement method in order to compare against other studies and determine any

trends as well as remove variances from different operators during longer studies. Currently there is no method for determining the analytical recovery of DGM since it is not possible to obtain a certified reference sample. Future directions should include the development of a standard method or analysis as well as way of determining if DGM concentration results represent actual values in the field.

There are many methods available for calculating air-sea fluxes; however, the method which is best suited for conditions found in the Arctic is unknown. Future studies should focus on better predicting actual Hg^0 fluxes in the north using both flux chamber and laboratory studies to assess whether or not prediction models are accurate. If not, a new model should be developed in order to account for the differences. Most models are created for temperatures around 20°C and have not been developed for conditions often found in the Arctic. This may be due to the assumption that when air temperatures are in the -20°C range, open water is generally frozen thus air-sea exchange is not possible; in flaw lead areas; however, this is not the case. Models should also be developed specifically for flaw lead areas, where wind may not play as large of a role in gas exchange due to the lack of fetch in newly formed leads. Determining flux through alternate methods for measuring sea surface roughness may be better suited for conditions observed in CFL areas.

It was found in this study that there is a large variation in flux results based on the method used in calculating the k_w (Section 3.4.3). Future studies should focus on the suitability of these methods of estimation and determine which is best for conditions encountered in the Arctic. No studies have been conducted into how the ice surface will affect the k_w rate, and thus exchange between the water and

atmosphere. This type of study would help establish the degree to which the sea ice surface can act as a barrier to gas exchange. It may also be important to better establish how readily gasses such as Hg^0 can diffuse through ice surfaces of different thicknesses.

4.4 Influence of Climate Change

Changes in the Arctic climate will no doubt play a role in AMDE chemistry and occurrence. Climate change in the Arctic will lead to warmer temperatures as well as changes in the extent of sea ice cover and behaviour. With increasing temperatures, it is possible that the sea ice environment will become more dynamic, leading to the direct deposition of Hg to the aquatic system. Areas with reoccurring flaw leads will most likely exhibit changes sooner than other areas and thus it will be necessary for them to remain active areas of study. The influence of the open ocean in the Arctic with relation to climate change will need to be assessed, specifically how the deposition of Hg to the oceans will be affected, as well as the ability of that material to be incorporated into the food chain.

The role of sea ice has been well established as a necessary component in AMDE initiation as it provides a source of reactive halogens to the atmosphere (Section 1.4.3). If this component is slowly eroded with increasing temperatures, it is likely that we will see a decrease in the extent of AMDEs, and thus less impact from them in terms of atmospheric deposition. The effect of shifting sea ice on Hg scavenging by snow and ice as well as halogen emission from open water is unknown and thus future studies in flaw lead areas are necessary to address this gap. Another parameter linked to the sea ice environment and temperature is frost flower formation.

The production of frost flowers is dependent on a large temperature gradient between the surface and the atmosphere (See Section 1.4.4), thus an increase in temperatures may also lead to a decrease in potential frost flower areas, as well as the time period in which they are seen. Contradictory to this, increased temperatures will lead to a shift from multiyear ice to seasonal ice. Since frost flowers are created only on freshly frozen surfaces, it is also possible that for a portion of the year, frost flower activity will be heightened leading to larger bromine explosions and thus more intense AMDEs. More study is required into the role that changing sea ice conditions will have on both frost flower production and AMDEs.

Climate change will also have an effect on the seasons and melt times in the Arctic, thus changes in AMDE timing are likely to be seen. With warmer temperatures in a given area, it is likely that the AMDE season will be shorter, and the amount of time between Hg deposition and mobilization during the spring will shrink (Steffen et al., 2007). This may be due to temperatures reaching the 0°C temperature threshold earlier in the year, and the removal of ice cover leading to advanced emission events. With a shorter AMDE season, it is possible that their effects will be reduced with warming temperatures. Their impact, however, may be increased as Hg deposition of water soluble Hg(II) may be increasingly deposited to aquatic surfaces over frozen surfaces, which may lead to increased Hg contamination in Arctic waters. The ratio between AMDE reduction to AMDE impact should be further explored in future studies.

Another important unknown associated with climate change is the effects on MeHg production as increasing temperatures may also increase the rate in which

methylation of Hg occurs (Steffen et al., 2007). This factor has been recognised and a call for further study of the methylation process in the Arctic with respect to climate change has been suggested (Macdonald and Loseto, 2010). MeHg has the ability to significantly impact human and mammal populations and should be studied in combination with Hg cycling and in order to fully understand the potential of future ecosystem impact.

The rate of DGM formation may be impacted significantly with increasing temperatures in the north. It is possible that the biological role in DGM formation will increase significantly as warmer temperatures will lead to increased productivity as well as bacterial activity (Section 1.6.2.2). As the ice cover recedes, it will allow for increased sunlight penetration into the water which will stimulate increased DGM production over ice covered areas. Increased temperatures may also promote increased Hg input from rivers into the Arctic Ocean as the permafrost melts and drains into the rivers. The increased input may be offset by the increased forms of evasion and more study is required to determine the actual effects.

The rate of DGM evasion from the ocean to the atmosphere is dependent primarily on temperature, volatile Hg species concentrations, and wind speeds (Wanninkhof, 1992, Liss, 1983). Climate change in the Arctic thus has the ability to significantly impact the rate at which DGM is transferred to the atmosphere by potentially impacting all of these parameters. The increase in air temperature may stimulate thermal emission/re-emission of the Hg from the ocean or snow surface by increasing the rate of evasion (Lindberg et al., 2001), and increased Hg(II) inputs as well as wind speeds may also accompany future changes. Typically an increase in

GEM concentration is seen in the summer following AMDEs (Steffen et al., 2005). It is hypothesized that this is due to increased evasion from both water and snow surfaces accompanying increased air temperatures and ice removal rates (See Sections 2.4.1 and 2.4.2). With climate change this peak in GEM may occur sooner, and last longer which could potentially lead to a trend of increasing atmospheric GEM in the Arctic during the summer.

Hg flux has also been found to vary significantly with PAR. The degree of penetration of light through the various ice conditions observed during this study is not known, nor was it recorded for open water samples. Since abiotic production is thought to be the primary contributor to DGM production in the Arctic (Section 1.6.4), it is possible that thinning ice covers accompanying climate change will allow for increased light penetration though the ice. This may result in increased DGM production, as well as evasion once the ice cover is removed. Future studies into DGM and Hg^0 Flux in the Arctic should include these variables in the data interpretation.

The effect of climate change on DGM is potentially easier to predict due to its significant dependence on temperature, thus future studies should focus on quantifying if there will be significant increases in Hg input to the Arctic Ocean, and whether or not the removal processes can offset this contamination.

Future study approaches to Hg in the Arctic should take a multidisciplinary approach and include components from the study of sea ice, microbiology, cryobiology, oceanography, climatology, ecology, toxicology, atmospheric chemistry, and laboratory investigations to provide a better understanding in Arctic

Hg cycling, and potential future trends and areas of concern in relation to global climate change.

References:

ALBERTS, J. J., SCHINDLER, J. E., MILLER, R. W. & NUTTER, D. E., JR. 1974. Elemental mercury evolution mediated by humic acid. *Science,* 184**,** 895-897.

ALLARD, B. & ARSENIE, I. 1991. Abiotic reduction of mercury by humic substances in aquatic systems - an important process for the mercury cycle. *Water Air and Soil Pollution,* 56**,** 457-464.

ALVAREZ-AVILES, L., SIMPSON, W. R., DOUGLAS, T. A., STURM, M., PEROVICH, D. & DOMINE, F. 2008. Frost flower chemical composition during growth and its implications for aerosol production and bromine activation. *Journal of Geophysical Research-Atmospheres,* 113.

AMATO, P., HENNEBELLE, R., MAGAND, O., SANCELME, M., DELORT, A. M., BARBANTE, C., BOUTRON, C. & FERRARI, C. 2007. Bacterial characterization of the snow cover at Spitzberg, Svalbard. *FEMS microbiology Ecology,* 59**,** 255-264.

AMYOT, M., GILL, G. A. & MOREL, F. M. M. 1997a. Production and loss of dissolved gaseous mercury in coastal seawater. *Environmental Science & Technology,* 31**,** 3606-3611.

AMYOT, M., MCQUEEN, D. J., MIERLE, G. & LEAN, D. R. S. 1994. Sunlight-induced formation of dissolved gaseous mercury in lake waters. *Environmental Science & Technology,* 28**,** 2366-2371.

AMYOT, M., MIERLE, G., LEAN, D. & MC QUEEN, D. J. 1997b. Effect of solar radiation on the formation of dissolved gaseous mercury in temperate lakes. *Geochimica et Cosmochimica Acta,* 61**,** 975-987.

AMYOT, M., SOUTHWORTH, G., LINDBERG, S. E., HINTELMANN, H., LALONDE, J. D., OGRINC, N., POULAIN, A. J. & SANDILANDS, K. A. 2004. Formation and evasion of dissolved gaseous mercury in large enclosures amended with 200 $HgCl_2$. *Atmospheric Environment,* 38**,** 4279-4289.

ANDERSSON, M., GÅRDFELDT, K. & WÄNGBERG, I. 2008a. A description of an automatic continuous equilibrium system for the measurement of dissolved gaseous mercury. *Analytical and Bioanalytical Chemistry,* 391**,** 2277-2282.

ANDERSSON, M. E., SOMMAR, J., GÅRDFELDT, K. & LINDQVIST, O. 2008b. Enhanced concentrations of dissolved gaseous mercury in the surface waters of the Arctic Ocean. *Marine Chemistry,* 110**,** 190-194.

ANDREAS, E. L., GUEST, P. S., PERSSON, P. O. G., FAIRALL, C. W., HORST, T. W., MORITZ, R. E. & SEMMER, S. R. 2002. Near-surface water vapor over polar sea ice is always near ice saturation. *Journal of Geophysical Research-Oceans,* 107.

ARIYA, P. A., DASTOOR, A. P., AMYOT, M., SCHROEDER, W. H., BARRIE, L., ANLAUF, K., RAOFIE, F., RYZHKOV, A., DAVIGNON, D., LALONDE, J. & STEFFEN, A. 2004. The Arctic: a sink for mercury. *Tellus B,* 56**,** 397-403.

ARIYA, P. A., NEPOTCHATYKH, O., IGNATOVA, O. & AMYOT, M. 2002. Microbiological degradation of atmospheric organic compounds. *Geophysical Research Letters,* 29.

ARNOLD, D., AYOTTE, P., BONDY, G., CHAN, L., DEWAILLY, E., FURGAL, C., GILL, U., KALHOK, S., KUHNLEIN, H., LORING, E., MUCKLE, G., MYLES, E., RECEVEUR, O., STOKKER, Y. & TRACY, B. 2003. Canadian Arctic Contaminants Assessment Report II: Human Health. *Indian Affairs and Northern Development, Ottawa***,** 127.

ASPMO, K., GAUCHARD, P.-A., STEFFEN, A., TEMME, C., BERG, T., BAHLMANN, E., BANIC, C., DOMMERGUE, A., EBINGHAUS, R., FERRARI, C., PIRRONE, N., SPROVIERI, F. & WIBETOE, G. 2005. Measurements of atmospheric mercury species during an international study of mercury depletion events at Ny-Alesund, Svalbard, spring 2003. How reproducible are our present methods? *Atmospheric Environment,* 39**,** 7607-7619.

BANIC, C., BLANCHARD, P., DASTOOR, A., HUNG, H., STEFFEN, A., TORDON, R., POISSANT, L. & WIENS, B. 2005. Atmospheric distribution and long-range transport of mercury. *Short Course Series - Mineralogical Association of Canada,* 34**,** 157.

BANIC, C. M., BEAUCHAMP, S. T., TORDON, R. J., SCHROEDER, W. H., STEFFEN, A., ANLAUF, K. G. & WONG, H. K. T. 2003. Vertical distribution of gaseous elemental mercury in Canada. *Journal of Geophysical Research, [Atmospheres],* 108**,** ACH 6/1-ACH 6/14.

BARKAY, T. 2001. Molecular and biochemical investigation of the potential for microbial mercury volatilization in the Idrijca River-Fulg of Trieste ecosystem. *Materials and Geoenvironment,* 48**,** 109-115.
BARKAY, T., LIEBERT, C. & GILLMAN, M. 1989. Environmental significance of the potential for mer(Tn21)-mediated reduction of Hg^{2+} to Hg^{0} in natural waters. *Applied and Environmental Microbiology,* 55**,** 1196-1202.
BARKAY, T. & POULAIN, A. J. 2007. Mercury (micro)biogeochemistry in polar environments. *FEMS microbiology Ecology,* 59**,** 232.
BARKAY, T., TURNER, R. R., VANDENBROOK, A. & LIEBERT, C. 1991. The relationships of Hg(II) volatilization from a freshwater pond to the abundance of mer genes in the gene pool of the indigenous microbial community. *Microbial Ecology,* 21**,** 151-161.
BERG, T., BARTNICKI, J., MUNTHE, J., LATTILA, H., HREHORUK, J. & MAZUR, A. 2001. Atmospheric mercury species in the European Arctic: Measurements and modelling. *Atmospheric Environment,* 35**,** 2569-2582.
BERG, T., SEKKESAETER, S., STEINNES, E., VALDAL, A.-K. & WIBETOE, G. 2003. Springtime depletion of mercury in the European Arctic as observed at Svalbard. *The Science of The Total Environment,* 304**,** 43-51.
BOTTENHEIM, J. W. & CHAN, E. 2006. A trajectory study into the origin of spring time Arctic boundary layer ozone depletion. *Journal of Geophysical Research-Atmospheres,* 111.
BOTTENHEIM, J. W., GALLANT, A. G. & BRICE, K. A. 1986. Measurements of NOY species and ozone at 82 N latitude. *Geophysical Research Letters,* 13**,** 113-16.
BROOKS, S. B., SAIZ-LOPEZ, A., SKOV, H., LINDBERG, S. E., PLANE, J. M. C. & GOODSITE, M. E. 2006. The mass balance of mercury in the springtime arctic environment. *Geophysical Research Letters,* 33.
CARPI, A. & LINDBERG, S. E. 1998. Application of a teflon(TM) dynamic flux chamber for quantifying soil mercury flux: Tests and results over background soil. *Atmospheric Environment,* 32**,** 873-882.
CHENG, M.-D. & SCHROEDER, W. H. 2000. Potential atmospheric transport pathways for mercury measured in the Canadian high Arctic. *Journal of Atmospheric Chemistry,* 35**,** 101-107.
CHOI, A. L. & GRANDJEAN, P. 2008. Methylmercury exposure and health effects in humans. *Environmental Chemistry,* 5**,** 112-120.
CLARKSON, T. W. & MAGOS, L. 2006. The toxicology of mercury and its chemical compounds. *Critical Reviews in Toxicology,* 36**,** 609-662.
CLEVER, H. L., JOHNSON, S. A. & M.E., D. 1985. The solubility of mercury and some sparingly soluble mercury salts in water and aqueous electrolyte solutions. *Journal of Physical and Chemical Reference Data,* 14**,** 631 - 680.
COANTIC, M. 1986. A model of gas transfer across air-water interfaces with capillary waves. *Journal of Geophysical Research, [Oceans],* 91**,** 3925-43.
COBBETT, F. D., STEFFEN, A., LAWSON, G. & VAN HEYST, B. J. 2007. GEM fluxes and atmospheric mercury concentrations (GEM, RGM and Hg_p) in the Canadian Arctic at Alert, Nunavut, Canada (February-June 2005). *Atmospheric Environment,* 41**,** 6527-6543.
COLE, A. S. & STEFFEN, A. 2010. Trends in long-term gaseous mercury observations in the Arctic and effects of temperature and other atmospheric conditions. *Atmospheric Chemistry and Physics,* 10**,** 4661-4672.
COLE, J. J. & CARACO, N. F. 1998. Atmospheric exchange of carbon dioxide in a low-wind oligotrophic lake measured by the addition of SF_6. *Limnology and Oceanography,* 43**,** 647-656.
CONSTANT, P., POISSANT, L., VILLEMUR, R., YUMVIHOZE, E. & LEAN, D. 2007. Fate of inorganic mercury and methyl mercury within the snow cover in the low arctic tundra on the shore of Hudson Bay (Quebec, Canada). *Journal of Geophysical Research-Atmospheres,* 112.
COSSA, D., MARTIN,J.M., TAKAYANAGI, K. & SANJUAN, J. 1997. The distribution and cycling of mercury species in the western Mediterranean. Deep-Sea Research Part II-Topical Studies in Oceanography, 44, 721-740.
COSTA, M. & LISS, P. 2000. Photoreduction and evolution of mercury from seawater. *The Science of The Total Environment,* 261**,** 125-135.
COSTA, M. & LISS, P. S. 1999. Photoreduction of mercury in sea water and its possible implications for Hg-0 air-sea fluxes. *Marine Chemistry,* 68**,** 87-95.

DEACON, E. L. 1977. Gas transfer to and across an air-water interface. *Tellus,* 29**,** 363 - 374.
DOMMERGUE, A., FERRARI, C., GAUCHARD, P. A., BOUTRON, C. F., POISSANT, L., PILOTE, M., JITARU, P. & ADAMS, F. 2003. The fate of mercury species in a sup-arctic snow-pack during snowmelt. *Geophysical Research Letters,* 30.
DOUGLAS, T. A. & STURM, M. 2004. Arctic haze, mercury and the chemical composition of snow across northwestern Alaska. *Atmospheric Environment,* 38**,** 805-820.
DOUGLAS, T. A., STURM, M., SIMPSON, W. R., BLUM, J. D., ALVAREZ-AVILES, L., KEELER, G. J., PEROVICH, D. K., BISWAS, A. & JOHNSON, K. 2008. Influence of snow and ice crystal formation and accumulation on mercury deposition to the Arctic. *Environmental Science & Technology,* 42**,** 1542-1551.
DOUGLAS, T. A., STURM, M., SIMPSON, W. R., BROOKS, S., LINDBERG, S. E. & PEROVICH, D. K. 2005. Elevated mercury measured in snow and frost flowers near arctic sea ice leads. *Geophysical Research Letters,* 32.
EBINGHAUS, R., KOCK, H. H., TEMME, C., EINAX, J. W., LOWE, A. G., RICHTER, A., BURROWS, J. P. & SCHROEDER, W. H. 2002. Antarctic springtime depletion of atmospheric mercury. *Environmental Science & Technology,* 36**,** 1238-1244.
FAIRALL, C. W., BRADLEY, E. F., HARE, J. E., GRACHEV, A. A. & EDSON, J. B. 2003. Bulk parameterization of air-sea fluxes: Updates and verification for the COARE algorithm. *Journal of Climate,* 16**,** 571-591.
FANTOZZI, L., FERRARA, R., FRONTINI, F. P. & DINI, F. 2007. Factors influencing the daily behaviour of dissolved gaseous mercury concentration in the Mediterranean Sea. *Marine Chemistry,* 107**,** 4-12.
FANTOZZI, L., FERRARA, R., FRONTINI, F. P. & DINI, F. 2009. Dissolved gaseous mercury production in the dark: Evidence for the fundamental role of bacteria in different types of Mediterranean water bodies. *Science of The Total Environment*, 407**,** 917-924.
FERRARI, C. P., GAUCHARD, P.-A., ASPMO, K., DOMMERGUE, A., MAGAND, O., BAHLMANN, E., NAGORSKI, S., TEMME, C., EBINGHAUS, R., STEFFEN, A., BANIC, C., BERG, T., PLANCHON, F., BARBANTE, C., CESCON, P. & BOUTRON, C. F. 2005. Snow-to-air exchanges of mercury in an Arctic seasonal snow pack in Ny-Alesund, Svalbard. *Atmospheric Environment,* 39**,** 7633-7645.
FERRARI, C. P., PADOVA, C., FAÏN, X., GAUCHARD, P.-A., DOMMERGUE, A., ASPMO, K., BERG, T., CAIRNS, W., BARBANTE, C., CESCON, P., KALESCHKE, L., RICHTER, A., WITTROCK, F. & BOUTRON, C. 2008. Atmospheric mercury depletion event study in Ny-Alesund (Svalbard) in spring 2005. Deposition and transformation of Hg in surface snow during springtime. *Science of The Total Environment,* 397**,** 167-177.
FITZGERALD, W. F. 1999. Clean hands, dirty hands: Clair patterson and the aquatic biogeochemistry of mercury. *In C. I. Davidson, Clean hands, Clair Patterson's crusade against environmental lead contamination, Nova Science***,** 119 - 137.
FITZGERALD, W. F., ENGSTROM, D. R., LAMBORG, C. H., TSENG, C.-M., BALCOM, P. H. & HAMMERSCHMIDT, C. R. 2004. Modern and historic atmospheric mercury fluxes in Northern Alaska: Global sources and Arctic depletion. *Environmental Science & Technology,* 39**,** 557-568.
FITZGERALD, W. F., MASON, R. P. & VANDAL, G. M. 1991. Atmospheric cycling and air-water exchange of mercury over midcontinental lacustrine regions. *Water Air and Soil Pollution,* 56**,** 745-767.
FOSTER, K. L., PLASTRIDGE, R. A., BOTTENHEIM, J. W., SHEPSON, P. B., FINLAYSON-PITTS, B. J. & SPICER, C. W. 2001. The role of Br_2 and BrCl in surface ozone destruction at polar sunrise. *Science,* 291**,** 471-474.
FREW, N. M. 1997. The role of organic films in air-sea gas exchange. *The Sea Surface and Global Change. Cambridge: Cambridge University Press***,** 121-172.
GARBARINO, J. R., SNYDER-CONN, E., LEIKER, T. J. & HOFFMAN, G. L. 2002. Contaminants in Arctic snow collected over Northwest Alaskan sea ice. *Water, Air, & Soil Pollution,* 139**,** 183-214.
GARCIA, E., LAROULANDIE, J., SAINT-SIMON, X. R. & AMYOT, M. 2006. Temporal and spatial distribution and production of dissolved gaseous mercury in the Bay St. Francois wetland, in the St. Lawrence River, Quebec, Canada. *Geochimica et Cosmochimica Acta,* 70**,** 2665-2678.

GARCIA, E., POULAIN, A. J., AMYOT, M. & ARIYA, P. A. 2005. Diel variations in photoinduced oxidation of Hg-0 in freshwater. *Chemosphere,* 59**,** 977-981.
GÅRDFELDT, K., HORVAT, M., SOMMAR, J., KOTNIK, J., FAJON, V., WÄNGBERG, I. & LINDQVIST, O. 2002. Comparison of procedures for measurements of dissolved gaseous mercury in seawater performed on a Mediterranean cruise. *Analytical and Bioanalytical Chemistry,* 374**,** 1002-1008.
GAUCHARD, P.-A., ASPMO, K., TEMME, C., STEFFEN, A., FERRARI, C., BERG, T., STROM, J., KALESCHKE, L., DOMMERGUE, A., BAHLMANN, E., MAGAND, O., PLANCHON, F., EBINGHAUS, R., BANIC, C., NAGORSKI, S., BAUSSAND, P. & BOUTRON, C. 2005. Study of the origin of atmospheric mercury depletion events recorded in Ny-Alesund, Svalbard, spring 2003. *Atmospheric Environment,* 39**,** 7620-7632.
GOODSITE, M. E., PLANE, J. M. C. & SKOV, H. 2004. A theoretical study of the oxidation of Hg^0 to $HgBr_2$ in the troposphere. *Environmental Science & Technology,* 38**,** 1772-1776.
GRANDJEAN, P., WEIHE, P., WHITE, R. F., DEBES, F., ARAKI, S., YOKOYAMA, K., MURATA, K., SØRENSEN, N., DAHL, R. & JØRGENSEN, P. J. 1997. Cognitive Deficit in 7-Year-Old Children with Prenatal Exposure to Methylmercury. *Neurotoxicology and Teratology,* 19**,** 417-428.
HAMMERSCHMIDT, C. R., LAMBORG, C. H. & FITZGERALD, W. F. 2007. Aqueous phase methylation as a potential source of methylmercury in wet deposition. *Atmospheric Environment,* 41**,** 1663-1668.
HASSELMAN, K. E. A. 1975. Measurements of wind wave growtth and swell decay during the joint north sea wave project (JONSWAP). *Erganzugsh. Dtsch. Hydrogr. Z.,* 12.
HEDGECOCK, I. M., PIRRONE, N. & SPOVIERI, F. 2008. Chasing quicksilver northward: mercury chemistry in the Arctic troposphere. *Environmental Chemistry,* 5**,** 1-4.
HILEMAN, B. 1983. Arctic haze. *Environmental Science & Technology,* 17**,** A232-A236.
HOLMES, P., JAMES, K. A. F. & LEVY, L. S. 2009. Is low-level environmental mercury exposure of concern to human health? *Science of The Total Environment,* 408**,** 171-182.
IMPEY, G. A., MIHELE, C. M., ANLAUF, K. G., BARRIE, L. A., HASTIE, D. R. & SHEPSON, P. B. 1999. Measurements of photolyzable halogen compounds and bromine radicals during the Polar Sunrise Experiment 1997. *Journal of Atmospheric Chemistry,* 34**,** 21-37.
IMPEY, G. A., SHEPSON, P. B., HASTIE, D. R. & BARRIE, L. A. 1997. Measurement technique for the determination of photolyzable chlorine and bromine in the atmosphere. *Journal of Geophysical Research-Atmospheres,* 102**,** 15999-16004.
JAHNE, B., LIBNER, P., FISCHER, R., BILLEN, T. & PLATE, E. J. 1989. Investigating the transfer process across the free aqueous viscous boundary layer by the controlled flux method. *Tellus,* 41**,** 117-195.
JAHNE, B., O., M. K., BOSINGER, R., DUTIZI, A., HUBER, W. & LIBNER, P. 1987. On parameters influencing air-water gas exchange. *Journal of Geophysical Research,* 92**,** 1937 - 1949.
JOHANSEN, P., MUIR, D., ASMUND, G. & RIGET, F. 2004. Human exposure to contaminants in the traditional Greenland diet. *Science of The Total Environment,* 331**,** 189-206.
JONES, A. E., ANDERSON, P. S., WOLFF, E. W., TURNER, J., RANKIN, A. M. & COLWELL, S. R. 2006. A role for newly forming sea ice in springtime polar tropospheric ozone loss? Observational evidence from Halley station, Antarctica. *Journal of Geophysical Research-Atmospheres,* 111.
JONES, G. J., B.P., P. & MOREL, F. M. M. 1987. Trace metal reduction by phtoplankton: The role of plasmalemma redox enzymes[1,2]. *Journal of Phycology,* 23**,** 237-244.
KALESCHKE, L., RICHTER, A., BURROWS, J., AFE, O., HEYGSTER, G., NOTHOLT, J., RANKIN, A. M., ROSCOE, H. K., HOLLWEDEL, J., WAGNER, T. & JACOBI, H. W. 2004a. Frost flowers on sea ice as a source of sea salt and their influence on tropospheric halogen chemistry. *Geophysical Research Letters,* 31.
KALESCHKE, L., RICHTER, A. & BURROWS, J. P. 2004b. Frost flowers on sea ice as a source of sea salt and their influence on tropospheric halogen chemistry. *Geophysical Research Letters,* 31.
KELLY, D. J. A., BUDD, K. & LEFEBVRE, D. D. 2007. Biotransformation of mercury in pH-stat cultures of eukaryotic freshwater algae. *Archives of Microbiology,* 187**,** 45-53.
KIM, J. & FITZGERALD, W. 1988. Gaseous mercury profiles in the tropical Pacific Ocean. *Geophysical Research Letters,* 15**,** 40-43.

KIRK, J. L., ST. LOUIS, V. L. & SHARP, M. J. 2006. Rapid reduction and reemission of mercury deposited into snowpacks during atmospheric mercury depletion events at Churchill, Manitoba, Canada. *Environmental Science & Technology,* 40**,** 7590-7596.

KOCK, H. H., BIEBER, E., EBINGHAUS, R., SPAIN, T. G. & THEES, B. 2005. Comparison of long-term trends and seasonal variations of atmospheric mercury concentrations at the two European coastal monitoring stations Mace Head, Ireland, and Zingst, Germany. *Atmospheric Environment,* 39**,** 7549-7556.

KRABBENHOFT, D. P., HURLEY, J. P., OLSON, M. L. & CLECKNER, L. B. 1998. Diel variability of mercury phase and species distributions in the Florida Everglades. *Biogeochemistry,* 40**,** 311-325.

KUSS, J. & SCHNEIDER, B. 2007. Variability of the gaseous elemental mercury sea-air flux of the Baltic Sea. *Environmental Science & Technology,* 41**,** 8018-8023.

LALONDE, J. D., AMYOT, M., ORVOINE, J., MOREL, F. M. M., AUCLAIR, J. C. & ARIYA, P. A. 2004. Photoinduced oxidation of Hg^0(aq) in the waters from the St. Lawrence estuary. *Environmental Science & Technology,* 38**,** 508-514.

LALONDE, J. D., POULAIN, A. J. & AMYOT, M. 2002. The role of mercury redox reactions in snow on snow-to-air mercury transfer. *Environmental Science & Technology,* 36**,** 174-178.

LAMBORG, C. H., ROLFHUS, K. R., FITZGERALD, W. F. & KIM, G. 1999. The atmospheric cycling and air-sea exchange of mercury species in the South and equatorial Atlantic Ocean. *Deep-Sea Research Part II-Topical Studies in Oceanography,* 46**,** 957-977.

LANDIS, M. S., STEVENS, R. K., SCHAEDLICH, F. & PRESTBO, E. M. 2002. Development and characterization of an annular denuder methodology for the measurement of divalent inorganic reactive gaseous mercury in ambient air. *Environmental Science & Technology,* 36**,** 3000-3009.

LANZILLOTTA, E., CECCARINI, C., FERRARA, R., DINI, F., FRONTINI, F. P. & BANCHETTI, R. 2004. Importance of the biogenic organic matter in photo-formation of dissolved gaseous mercury in a culture of the marine diatom Chaetoceros sp. *Science of The Total Environment,* 318**,** 211-221.

LANZILLOTTA, E. & FERRARA, R. 2001. Daily trend of dissolved gaseous mercury concentration in coastal seawater of the Mediterranean basin. *Chemosphere,* 45**,** 935-940.

LAURIER, F. J. G., MASON, R. P., WHALIN, L. & KATO, S. 2003. Reactive gaseous mercury formation in the North Pacific Ocean's marine boundary layer: A potential role of halogen chemistry. *Journal of Geophysical Research-Atmospheres,* 108.

LEGAGNEUX, L., CABANES, A. & DOMINE, F. 2002. Measurement of the specific surface area of 176 snow samples using methane adsorption at 77 K. *Journal of Geophysical Research-Atmospheres,* 107.

LEITCH, D. R., CARRIE, J., LEAN, D., MACDONALD, R. W., STERN, G. A. & WANG, F. 2007. The delivery of mercury to the Beaufort Sea of the Arctic Ocean by the Mackenzie River. *Science of The Total Environment,* 373**,** 178-195.

LI, C. S., CORNETT, J., WILLIE, S. & LAM, J. 2009. Mercury in Arctic air: The long-term trend. *Science of The Total Environment,* 407**,** 2756-2759.

LINDBERG, S., BULLOCK, R., EBINGHAUS, R., ENGSTROM, D., FENG, X., FITZGERALD, W., PIRRONE, N., PRESTBO, E. & SEIGNEUR, C. 2007. A synthesis of progress and uncertainties in attributing the sources of mercury in deposition. *AMBIO: A Journal of the Human Environment,* 36**,** 19-33.

LINDBERG, S. E., BROOKS, S., LIN, C. J., SCOTT, K., MEYERS, T., CHAMBERS, L., LANDIS, M. & STEVENS, R. 2001. Formation of reactive gaseous mercury in the Arctic: Evidence of oxidation of Hg° to gas-phase Hg-II compounds after Arctic sunrise. *Water, Air, and Soil Pollution: Focus,* 1**,** 295-302.

LINDBERG, S. E., BROOKS, S., LIN, C. J., SCOTT, K. J., LANDIS, M. S., STEVENS, R. K., GOODSITE, M. & RICHTER, A. 2002. Dynamic oxidation of gaseous mercury in the Arctic troposphere at polar sunrise. *Environmental Science & Technology,* 36**,** 1245-1256.

LINDBERG, S. E., VETTE, A. F., MILES, C. & SCHAEDLICH, F. 2000. Mercury speciation in natural waters: Measurement of dissolved gaseous mercury with a field analyzer. *Biogeochemistry,* 48**,** 237-259.

LISS, P. S. 1983. Gas transfer: Experiments and geochemical implications. *NATO ASI Series. Series C, Mathematical and Physical Sciences,* 108**,** 241.

LISS, P. S., CHUCK, A. L., TURNER, S. M. & WATSON, A. J. 2004. Air-sea gas exchange in Anarctic Waters. *Anartic Science,* 16**,** 517-529.

LISS, P. S. & MERLIVAT, L. 1986. Air-sea gas exchange rates: Introduction and synthesis. *NATO ASI Series. Series C, Mathematical and Physical Sciences,* 185**,** 113.

LOCKHART, W. L., STERN, G. A., LOW, G., HENDZEL, M., BOILA, G., ROACH, P., EVANS, M. S., BILLECK, B. N., DELARONDE, J., FRIESEN, S., KIDD, K., ATKINS, S., MUIR, D. C. G., STODDART, M., STEPHENS, G., STEPHENSON, S., HARBICHT, S., SNOWSHOE, N., GREY, B., THOMPSON, S. & DEGRAFF, N. 2005a. A history of total mercury in edible muscle of fish from lakes in northern Canada. *Science of The Total Environment,* 351-352**,** 427-463.

LOCKHART, W. L., STERN, G. A., WAGEMANN, R., HUNT, R. V., METNER, D. A., DELARONDE, J., DUNN, B., STEWART, R. E. A., HYATT, C. K., HARWOOD, L. & MOUNT, K. 2005b. Concentrations of mercury in tissues of beluga whales (Delphinapterus leucas) from several communities in the Canadian Arctic from 1981 to 2002. *Science of The Total Environment,* 351-352**,** 391-412.

LOSETO, L. L., LEAN, D. R. S. & SICILIANO, S. D. 2004a. Snowmelt sources of methylmercury to high arctic ecosystems. *Environmental Science & Technology,* 38**,** 3004-3010.

LOSETO, L. L., SICILIANO, S. D. & LEAN, D. R. S. 2004b. Methylmercury production in High Arctic wetlands. *Environmental Toxicology and Chemistry,* 23**,** 17-23.

LOUX, N. T. 2004. A critical assessment of elemental mercury air/water exchange parameters. *Chemical Speciation and Bioavailability,* 16**,** 127-138.

LOUX, N. T. 2006. A critical assessment of elemental mercury air/water exchange parameters. *Chemical speciation and bioavailability,* 16**,** 127.

LU, J. Y., SCHROEDER, W. H., BARRIE, L. A., STEFFEN, A., WELCH, H., MARTIN, K., LOCKHART, L., HUNT, R. V., BOILA, G. & RICHTER, A. 2001. Magnification of atmospheric mercury deposition to polar regions in springtime: the link to tropospheric ozone depletion chemistry. *Geophysical Research Letters,* 28**,** 3219-3222.

MACDONALD, R. W., HARNER, T. & FYFE, J. 2005. Recent climate change in the Arctic and its impact on contaminant pathways and interpretation of temporal trend data. *Science of The Total Environment,* 342**,** 5-86.

MACDONALD, R. W. & LOSETO, L., L. 2010. Are Arctic Ocean ecosystems exceptionally vulnerable to global emissions of mercury? A call for emphasised research on methylation and the consequences of climate change. *Environmental Chemistry,* 7**,** 133 - 138.

MACKAY, D., WANIA, F. & SCHROEDER, W. H. 1995. Prospects for modeling the behavior and fate of mercury, globally and in aquatic systems. *Water, Air, & Soil Pollution,* 80**,** 941-950.

MARTIN, S., YANLING, Y. & DRUCKER, R. 1996. The temperature dependence of frost flower growth on laboratory sea ice and the effect of the flowers on infrared observations of the surface. *Journal of Geophysical Research: Oceans,* 101**,** 111-12, 125.

MASON, R. P., FITZGERALD, W. F. & MOREL, F. M. M. 1994. The biogeochemical cycling of elemental mercury. anthropogenic influences. *Geochimica et Cosmochimica Acta,* 58**,** 3191-3198.

MASON, R. P., LAWSON, N. M. & SHEU, G. R. 2001. Mercury in the Atlantic Ocean: factors controlling air-sea exchange of mercury and its distribution in the upper waters. *Deep Sea Research Part II: Topical Studies in Oceanography,* 48**,** 2829-2853.

MASON, R. P., MOREL, F. M. M. & HEMOND, H. F. 1995. The role of microorganisms in elemental mercury formation in natural waters. *Water, Air, & Soil Pollution,* 80**,** 775-787.

MASON, R.P., ROLFHUS, K. R. & FITZGERALD, W.F. 1998. Mercury in the North Atlantic. Marine Chemistry, 61, 37-53.

MASON, R. P. & SHEU, G. R. 2002. Role of the ocean in the global mercury cycle. *Global Biogeochemical Cycles,* 16.

MCCONNELL, J. C., HENDERSON, G. S., BARRIE, L., BOTTENHEIM, J., NIKI, H., LANGFORD, C. H. & TEMPLETON, E. M. J. 1992. Photochemical bromine production implicated in Arctic boundary-layer ozone depletion. *Nature,* 355**,** 150-152.

MERLIVAT, L. & MEMERY, L. 1983. Gas exchange across an air-water interface: experimental results and modelling of bubble contribution to transfer. *Journal of Geophysical Research,* 88**,** 707 - 724.

MOREL, F. M. M., KRAEPIEL, A. M. L. & AMYOT, M. 1998. The chemical cycle and bioaccumulation of mercury. *Annual Review of Ecology and Systematics,* 29**,** 543-566.
NARUKAWA, M., MASAHIRO, S., MARUMOTO, K. & ASAKURA, K. 2006. Air-sea exchange of mercury in Tokyo bay. *Journal of Oceanography,* 62**,** 249-257.
NGHIEM, S. V., MARTIN, S., PEROVICH, D. K., KWOK, R., DRUCKER, R. & GOW, A. J. 1997. A laboratory study of the effect of frost flowers on C band radar backscatter from sea ice. *Journal of Geophysical Research-Oceans,* 102**,** 3357-3370.
NRIAGU, J. O. & PACYNA, J. M. 1988. Quantitative assessment of worldwide contamination of air, water and soils by trace metals. *Nature,* 333**,** 134-139.
O'DRISCOLL, N. J., BEAUCHAMP, S., SICILIANO, S. D., RENCZ, A. N. & LEAN, D. R. S. 2003. Continuous analysis of dissolved gaseous mercury (DGM) and mercury flux in two freshwater lakes in Kejimkujik Park, Nova Scotia; Evaluating mercury flux models with quantitative data. *Environmental Science & Technology,* 37**,** 2226-2235.
O'DRISCOLL, N. J., POISSANT, L., CANARIO, J., RIDAL, J. & LEAN, D. R. S. 2007. Continuous analysis of dissolved gaseous mercury and mercury volatilization in the upper St. Laurence River: Exploring temporal relationships and UV attenuation. Environmental Science & Technology, 41, 5342-5348.
O'DRISCOLL, N. J., POISSANT, L., CANARIO, J., RIDAL, J. & LEAN, D. R. S. 2008. Dissolved gaseous mercury concentrations and mercury volatilization in a frozen freshwater fluvial lake. Environmental Science & Technology, 42, 5125-5130.
O'DRISCOLL, N. J., SICILIANO, S. D., LEAN, D. R. S. & AMYOT, M. 2006. Gross photoreduction kinetics of mercury in temperate freshwater lakes and rivers: Application to a general model of DGM dynamics. *Environmental Science & Technology,* 40**,** 837-843.
OLSEN, A., WANNINKHOF, R., TRINANES, J. A. & JOHANNESSEN, T. 2005. The effect of wind speed products and wind speed-gas exchange relationships on interannual variability of the air-sea CO_2 gas transfer velocity. *Tellus Series B-Chemical and Physical Meteorology,* 57**,** 95-106.
OLTMANS, S. J. 1981. Surface ozone measurements in clean air. *Journal of Geophysical Research, C: Oceans and Atmospheres,* 86**,** 1174-80.
OLTMANS, S. J. & KOMHYR, W. D. 1986. Surface ozone distributions and variations from 1973-1984 measurements at the NOAA geophysical monitoring for climatic change baseline observatories. *Journal of Geophysical Research, [Atmospheres],* 91**,** 5229-36.
OUTRIDGE, P. M., MACDONALD, R. W., WANG, F., STERN, G. A. & DASTOOR, A. 2008. A mass balance inventory of mercury in the Arctic Ocean. *Environmental Chemistry,* 5**,** 1-23.
PACYNA, E. G. & PACYNA, J. M. 2002. Global emission of mercury from anthropogenic sources in 1995. *Water, Air, & Soil Pollution,* 137**,** 149-165.
PACYNA, E. G., PACYNA, J. M., STEENHUISEN, F. & WILSON, S. 2006. Global anthropogenic mercury emission inventory for 2000. *Atmospheric Environment,* 40**,** 4048-4063.
PARK, J.-S., OH, S., SHIN, M.-Y., KIM, M.-K., YI, S.-M. & ZOH, K.-D. 2008. Seasonal variation in dissolved gaseous mercury and total mercury concentrations in Juam Reservoir, Korea. *Environmental Pollution,* 154**,** 12-20.
PEROVICH, D. K. & RICHTERMENGE, J. A. 1994. Surface characteristics of lead ice. *Journal of Geophysical Research-Oceans,* 99**,** 16341-16350.
POISSANT, L., AMYOT, M., PILOTE, M. & LEAN, D. 2000. Mercury water-air cxchange over the Upper St. Lawrence River and Lake Ontario. *Environmental Science & Technology,* 34**,** 3069-3078.
POULAIN, A. J., AMYOT, M., FINDLAY, D., TELOR, S., BARKAY, T. & HINTELMANN, H. 2004. Biological and photochemical production of dissolved gaseous mercury in a boreal lake. *Limnology and Oceanography,* 49**,** 2265-2275.
POULAIN, A. J., ORIHEL, D. M., AMYOT, M., PATERSON, M. J., HINTELMANN, H. & SOUTHWORTH, G. R. 2006. Relationship between the loading rate of inorganic mercury to aquatic ecosystems and dissolved gaseous mercury production and evasion. *Chemosphere,* 65**,** 2199-2207.
QURESHI, A., O'DRISCOLL, N. J., MACLEOD, M., NEUHOLD, Y. M. & HUNGERBUHLER, K. 2010. Photoreactions of mercury in surface ocean water: Gross reaction kinetics and possible pathways. *Environmental Science & Technology,* 44**,** 644-649.

RANKIN, A. M. & WOLFF, E. W. 2002. Frost Flowers: Implications for tropospheric chemistry and ice core interpretation. *Journal of Geophysical Research,* 107.
RANKIN, A. M. & WOLFF, E. W. 2003. A year-long record of size-segregated aerosol composition at Halley, Antarctica. *Journal of Geophysical Research-Atmospheres,* 108.
RANKIN, A. M., WOLFF, E. W. & MARTIN, S. 2002. Frost Flowers: Implications for tropospheric chemistry and ice core interpretation. *Journal of Geophysical Research,* 107.
RAOFIE, F. & ARIYA, P. A. 2003. Kinetics and products study of the reaction of BrO radicals with gaseous mercury. *Journal De Physique Iv,* 107**,** 1119-1121.
RAOFIE, F. & ARIYA, P. A. 2004. Product study of the gas-phase BrO-initiated oxidation of Hg^0: Evidence for stable Hg^{1+} compounds. *Environmental Science & Technology,* 38**,** 4319-4326.
RIDLEY, B. A., ATLAS, E. L., MONTZKA, D. D., BROWELL, E. V., CANTRELL, C. A., BLAKE, D. R., BLAKE, N. J., CINQUINI, L., COFFEY, M. T., EMMONS, L. K., COHEN, R. C., DEYOUNG, R. J., DIBB, J. E., EISELE, F. L., FLOCKE, F. M., FRIED, A., GRAHEK, F. E., GRANT, W. B., HAIR, J. W., HANNIGAN, J. W., HEIKES, B. J., LEFER, B. L., MAULDIN, R. L., MOODY, J. L., SHETTER, R. E., SNOW, J. A., TALBOT, R. W., THORNTON, J. A., WALEGA, J. G., WEINHEIMER, A. J., WERT, B. P. & WIMMERS, A. J. 2003. Ozone depletion events observed in the high latitude surface layer during the TOPSE aircraft program. *Journal of Geophysical Research-Atmospheres,* 108.
ROLFHUS, K. R. & FITZGERALD, W. F. 2004. Mechanisms and temporal variability of dissolved gaseous mercury production in coastal seawater. *Marine Chemistry,* 90**,** 125-136.
SALONEN, J. T. P. M. D. P. M., SEPPANEN, K. M., NYYSSONEN, K. M., KORPELA, H. M. D. P., KAUHANEN, J. M. D. P., KANTOLA, M. M., SALONEN, R. M. D. P. & TUOMILEHTO, J. M. D. P. 1995. Response: Intake of Mercury From Fish, Lipid Peroxidation, and the Risk of Myocardial Infarction and Coronary, Cardiovascular, and Any Death in Eastern Finnish Men. Letter. *Circulation,* 91**,** 645.
SANDER, R., KEENE, W. C., PSZENNY, A. A. P., ARIMOTO, R., AYERS, G. P., BABOUKAS, E., CAINEY, J. M., CRUTZEN, P. J., DUCE, R. A., HONNINGER, G., HUEBERT, B. J., MAENHAUT, W., MIHALOPOULOUS, N., TUREKIAN, V. C. & VAN DINGENEN, R. 2003. Inorganic bromine in the marine boundary layer: a critical review. *Atmospheric Chemistry and Physics,* 3**,** 1301-1366.
SANDHEINRICH, M. B. & MILLER, K. M. 2006. Effects of dietary methylmercury on reproductive behavior of fathead minnows. *Environmental Toxicology and Chemistry,* 25**,** 3053-3057.
SANEMASA, I., HARAGUCHI, K. & NAGAI, H. 1981. Effects of salts on the solubility of elemental mercury in water. *Bulletin of the Chemical Society of Japan,* 54.
SCHROEDER, W. H., ANLAUF, K. G., BARRIE, L. A., LU, J. Y., STEFFEN, A., SCHNEEBERGER, D. R. & BERG, T. 1998. Arctic springtime depletion of mercury. *Nature,* 394**,** 331-332.
SCHROEDER, W. H. & MUNTHE, J. 1998. Atmospheric mercury - An overview. *Atmospheric Environment,* 32**,** 809-822.
SCHWARZENBACH, R. P., M., G. P. & D.M., I. 1993. *Environmental Organic Chemistry***,** 228.
SICILIANO, S. D., O'DRISCOL, N. J. & LEAN, D. R. S. 2002. Microbial reduction and oxidation of mercury in freshwater lakes. *Environmental Science & Technology,* 36**,** 3064-3068.
SIMPSON, W. R., ALVAREZ-AVILLES, L., DOUGLAS, T. A. & STURM, M. 2005. Halogens in the coastal snow pack near Barrow, Alaska: Evidence of active bromine air-snow chemistry during springtime. *Geophysical Research Letters,* 32.
SIMPSON, W. R., VON GLASOW, R., RIEDEL, K., ANDERSON, P., ARIYA, P., BOTTENHEIM, J., BURROWS, J., CARPENTER, L. J., FRIEß, U., GOODSITE, M. E., HEARD, D., HUTTERLI, M., JACOBI, H. W., KALESCHKE, L., NEFF, B., PLANE, J., PLATT, U., RICHTER, A., ROSCOE, H., SANDER, R., SHEPSON, P., SODEAU, J., STEFFEN, A., WAGNER, T. & WOLFF, E. 2007. Halogens and their role in polar boundary-layer ozone depletion. *Atmospheric Chemistry and Physics,* 7**,** 4375-4418.
SKOV, H., CHRISTENSEN, J. H., GOODSITE, M. E., HEIDAM, N. Z., JENSEN, B., WAHLIN, P. & GEERNAERT, G. 2004. Fate of elemental mercury in the Arctic during atmospheric mercury depletion episodes and the load of atmospheric mercury to the Arctic. *Environmental Science & Technology,* 38**,** 2373-2382.

SLEMR, F., BRUNKE, E. G., EBINGHAUS, R., TEMME, C., MUNTHE, J., WANBERG, I., SCHROEDER, W. H., STEFFEN, A. & BERG, T. 2003. Worldwide trend of atmospheric mercury since 1977. *Geophysical Research Letters,* 30.

SOMMAR, J., WANGBERG, I., BERG, T., GARDFELDT, K., MUNTHE, J., RICHTER, A., URBA, A., WITTROCK, F. & SCHROEDER, W. H. 2007. Circumpolar transport and air-surface exchange or atmospheric mercury at Ny-Alesund (79 ^{o}N), Svalbard, Spring 2002. *Atmospheric Chemistry and Physics,* 7**,** 151-166.

SPROVIERI, F., PIRRONE, N., LANDIS, M. S. & STEVENS, R. K. 2005. Oxidation of gaseous elemental mercury to gaseous divalent mercury during 2003 polar sunrise at Ny-Alesund. *Environmental Science & Technology,* 39**,** 9156-9165.

ST. LOUIS, V., HINTELMANN, H., GRAYDON, J. A., KIRK, J. L., BARKER, J., DIMOCK, B., SHARP, M. J. & LEHNHERR, I. 2007. Methylated mercury species in Canadian high Arctic marine surface waters and snowpacks. *Environmental Science & Technology,* 41**,** 6433-6441.

ST. LOUIS, V. L., SHARP, M. J., STEFFEN, A., MAY, A., BARKER, J., KIRK, J. L., KELLY, D. J. A., ARNOTT, S. E., KEATLEY, B. & SMOL, J. P. 2005. Some sources and sinks of monomethyl and inorganic mercury on ellesmere island in the Canadian high Arctic. *Environmental Science & Technology,* 39**,** 2686-2701.

STEFFAN, R. J., KORTHALS, E. T. & WINFREY, M. R. 1988. Effects of acidification on mercury methylation, demethylation, and volatilization in sediments from an acid-susceptible lake. *Applied and Environmental Microbiology,* 54**,** 2003-2009.

STEFFEN, A., SCHROEDER, W., BOTTENHEIM, J., NARAYAN, J. & FUENTES, J. D. 2002. Atmospheric mercury concentrations: measurements and profiles near snow and ice surfaces in the Canadian Arctic during Alert 2000. *Atmospheric Environment,* 36**,** 2653-2661.

STEFFEN, A., SCHROEDER, W., MACDONALD, R., POISSANT, L. & KONOPLEV, A. 2005. Mercury in the Arctic atmosphere: An analysis of eight years of measurements of GEM at Alert (Canada) and a comparison with observations at Amderma (Russia) and Kuujjuarapik (Canada). *Science of The Total Environment,* 342**,** 185-198.

STEFFEN, A., SCHROEDER, W. H., EDWARDS, G. & BANIC, C. 2003a. Mercury throughout polar sunrise 2002. *Journal De Physique Iv,* 107**,** 1267-1270.

STEFFEN, A., SCHROEDER, W. H., MACDONALD, R. W., POISSANT, L. & KONOPLEV, A. 2003b. Mercury in the arctic atmosphere. *Indian and Northern Affairs Canada, Ottawa***,** 124 - 142.

STEFFEN, A. T. D., M. AMYOT, P. ARIYA, K. ASPMO, T. BERG,, J. BOTTENHEIM, S. B., F. COBBETT, A. DASTOOR, A. DOMMERGUE,, R. EBINGHAUS, C. F., K. GARDFELDT, M. E. GOODSITE, D. LEAN, & A. POULAIN, C. S., H. SKOV, J. SOMMAR, AND C. TEMME 2007. A synthesis of atmospheric mercury depletion event chemistry linking atmosphere, snow and water. *Atmospheric Chemistry and Physics,* 8**,** 1445-1482.

STRODE, S. A., JAEGLE, L., SELIN, N. E., JACOB, D. J., PARK, R. J., YANTOSCA, R. M., MASON, R. P. & SLEMR, F. 2007. Air-sea exchange in the global mercury cycle. *Global Biogeochemical Cycles,* 21.

SUMNER, A. L. & SHEPSON, P. B. 1999. Snowpack production of formaldehyde and its effect on the Arctic troposphere. *Nature,* 398**,** 230-233.

TACKETT, P. J., CAVENDER, A. E., KEIL, A. D., SHEPSON, P. B., BOTTENHEIM, J. W., MORIN, S., DEARY, J., STEFFEN, A. & DOERGE, C. 2007. A study of the vertical scale of halogen chemistry in the Arctic troposphere during Polar Sunrise at Barrow, Alaska. *Journal of Geophysical Research-Atmospheres,* 112.

TARASICK, D. W. & BOTTENHEIM, J. W. 2002. Surface ozone depletion episodes in the Arctic and Antarctic from historical ozonesonde records. *Atmospheric Chemistry and Physics,* 2**,** 197-205.

TEMME, C., BAUKAU, J., SCHNEIDER, B., ASPMO, K., FAIN, X., FERRARI, C., GAUCHARD, P.A. & EBINGHAUS, R. 2005. Air/water exchange of mercury in the North Atlantic Ocean during Arctic summer. International Conference on Heavy Metals.

TEMME, C., EINAX, J. W., EBINGHAUS, R. & SCHROEDER, W. H. 2003. Measurements of atmospheric mercury species at a coastal site in the Antarctic and over the South Atlantic Ocean during polar summer. *Environmental Science & Technology,* 37**,** 22-31.

TSENG, C.M., LAMBORG, C., FITZGERALD, W.F. & ENGSTROM, D.R. 2004. Cycling of dissolved elemental mercury in Arctic Alaskan lakes. Geochimica et Cosmoshimica Acta, 68, 1173-1184.

TURNER, R. R., VANDERBROOK, A. J., BARKAY, T. & ELWOOD, J. 1989. W.Proceedings of the international converence on heavy metals in the environment. *Geneva; CEP Consultants Ltd.: Edinburgh*, 353.

UPSTILL-GODDARD, R. C., WATSON, A. J., LISS, P. S. & LIDDICOAT, M. I. 1990. Gas transfer velocities in lakes measured with sulfur hexafluoride. *Tellus Series B Chemical and Physical Meteorology,* 42**,** 364-377.

VAN ROOZENDAEL, M., WAGNER, T., RICHTER, A., PUNDT, I., ARLANDER, D. W., BURROWS, J. P., CHIPPERFIELD, M., FAYT, C., JOHNSTON, P. V., LAMBERT, J. C., KREHER, K., PFEILSTICKER, K., PLATT, U., POMMEREAU, J. P., SINNHUBER, B. M., TØRNKVIST, K. K. & WITTROCK, F. 2002. Intercomparison of BrO measurements from ERS-2 GOME, ground-based and balloon platforms. *Advances in Space Research,* 29**,** 1661-1666.

VANDAL, G., MASON, R. & FITZGERALD, W. 1991. Cycling of volatile mercury in temperate lakes. *Water, Air, & Soil Pollution,* 56**,** 791-803.

WAGEMANN, R., LOCKHART, W. L., WELCH, H. & INNES, S. 1995. Arctic marine mammals as integrators and indicators of mercury in the Arctic. *Water, Air, & Soil Pollution,* 80**,** 683-693.

WANGBERG, I., SOMMAR, J., BERG, T., GARDFELDT, K. & MUNTHE, J. 2003. Interpretation of mercury depletion events observed at Ny-Alesund, Svalbard during spring 2002. *Journal De Physique IV,* 107**,** 1353-1356.

WANNINKHOF, R. 1992. Relationship between wind-speed and gas-exchange over the ocean. *Journal of Geophysical Research-Oceans,* 97**,** 7373-7382.

WANNINKHOF, R., LEDWELL, J. & CRUSIUS, J. 1991. Gas transfer velocities on lakes measured with sulfur-hexafluoride. *Air-Water Mass Transfer***,** 441-459.

WANNINKHOF, R., LEDWELL, J. R. & BROECKER, W. S. 1985. Gas exchange-wind speed relation measured with sulfur hexafluoride on a lake. *Science,* 227**,** 1224-1226.

WANNINKHOF, R., LEDWELL, J. R., BROECKER, W. S. & HAMILTON, M. 1987. Gas-exchange on Mono Lake and Crowley Lake, California. *Journal of Geophysical Research-Oceans,* 92**,** 14567-14580.

WANNINKHOF, R., MULHOLLAND, P. J. & ELWOOD, J. W. 1990. Gas-exchange rates for a 1st-order stream determined with deliberate and natrual tracers. *Water Resources Research,* 26**,** 1621-1630.

WANNINKHOF, R. H. & BLIVEN, L. F. 1991. Relationship between gas-exchange, wind-speed, and radar backscatter in a large wind-wave tank. *Journal of Geophysical Research-Oceans,* 96**,** 2785-2796.

WEIS, J. S. 2009. Reproductive, Developmental, and Neurobehavioral Effects of Methylmercury in Fishes. *Journal of Environmental Science and Health, Part C: Environmental Carcinogenesis and Ecotoxicology Reviews,* 27**,** 212 - 225.

WETTLAUFER, J. S. & WORSTER, M. G. 1995. Dynamics of premelted films: Frost heave in a capillary. *Physical Review E,* 51**,** 4679.

WHALIN, L., KIM, E. H. & MASON, R. 2007. Factors influencing the oxidation, reduction, methylation and demethylation of mercury species in coastal waters. *Marine Chemistry,* 107**,** 278-294.

WHITMAN, W. G. 1923. The two-film theory of gas adsorption. *Chemical and Metallurgical Engineering,* 29.

XIAO, Z. F., MUNTHE, J., SCHROEDER, W. H. & LINDQVIST, O. 1991. Vertical fluxes of volatile mercury over forest soil and lake surfaces in Sweden. *Tellus, Series B: Chemical and Physical Meteorology,* 43B**,** 267-269.

XIAO, Z. F., STRÖMBERG, D. & LINDQVIST, O. 1995. Influence of humic substances on photolysis of divalent mercury in aqueous solution. *Water, Air, & Soil Pollution,* 80**,** 789-798.

YAMAMOTO, M. 1996. Stimulation of elemental mercury oxidation in the presence of chloride ion in aquatic environments. *Chemosphere,* 32**,** 1217-1224.

ZENG, T., WANG, Y. H., CHANCE, K., BROWELL, E. V., RIDLEY, B. A. & ATLAS, E. L. 2003. Widespread persistent near-surface ozone depletion at northern high latitudes in spring. *Geophysical Research Letters,* 30.

ZHANG, H. & LINDBERG, S. E. 2001. Sunlight and iron(III)-induced photochemical production of dissolved gaseous mercury in freshwater. *Environmental Science & Technology,* 35**,** 928-935.
ZHANG, T. & HSU-KIM, H. 2010. Photolytic degradation of methylmercury enhanced by binding to natural organic ligands. *Nature Geoscience,* 3**,** 473-476.

Appendix A. Standard Operating Procedure Used for DGM Measurement during the CFL project in 2008

This method details the measurement of DGM in freshly collected water samples by purging the Hg^0 out using zero air, followed by the analysis of Hg^0 by cold vapour atomic fluorescence spectroscopy on a Tekran 2537B.

Before starting, locate the following parts:

- Zero Air Generator (Tekran)
- 2537B Instrument (Tekran; SN324)
- DGM Bottles: 1-L PTFE bottles. One for Milli-Q water (MQ) blank only, and one for samples.
- Purging wand: Teflon tubing with fritz at one end.

Start-up

The instrument should be left in a running mode with zero air on all the time, monitoring continuously the GEM in the room air. If this is the case, go to the cleaning and calibration section.

If not:

i. Turn on the Tekran 2537B instrument and set the Zero Air generator toggle to the ON position.

ii. Open TekCap SN324 on the computer to start the data capturing program.

iii. Leave the end of the sample inlet tubing (marked with blue tape) open to the room air. Alternatively, connect the zero air line to the sample line and allow system to sample zero-air. Confirm that there is no contamination in the tubing.

iv. Let the system warm up for ~30 min.

Cleaning and Calibration

i. If the system is left on all the time, the full calibration (including cleaning) is automatically set up for every 24 hours. Scroll up the computer display and check whether the peak areas of CLN are zero, and the spans are all correct. If yes, the system is ready to use. Go to Blank Analysis.

ii. Otherwise, do a clean first. On the 2537B panel, press the "Esc" to go to the MAIN menu and use the arrow buttons to select CALIBRATE, then CALIB, then CLEAN, then BOTH to clean both cartridges. Make sure the Zero Air Generator is turned on, and that zero is actually zero for calibration (the green light for zero on front panel of 2537B should be on during cleaning).

iii. Perform a full calibration: Use the "Esc" and arrow buttons to select CALBRATE, then FULL to perform an automatic calibration. Verify that results are consistent with the previous calibration.

Blank Analysis

i. Use the "Esc" and arrow buttons to Select METHOD, then METHOD 1. Verify the following set-up:

Data Table 1: Tekran 2537 operating parameters table

Timing-1-			
Sample	3000 sec	**FlushHi**	60 sec
Calib	300 sec	**Meas-Dly**	1 sec
Zero-Sub	No	**BL-Time**	10 sec

Other			
Car-Meas	80.0 ml/min	**SmplRate**	0.75 l/min
Car-Idle	5.0 ml/min	**Warm A**	1%
Car-Flush	100 ml/min	**Warm B**	1%

Timing-2-			
Intg-Dly	10 sec	**Pk-Time**	35 sec
HtrADur	33 sec	**Cool-Dn**	80 sec
HtrBDur	33 sec	**Round**	50 min

Perm-SRC			
AutoCal	yes	**CalibInt**	25 h
Cal-Conc			
PermTime	120 sec		

ii. Select RUN, then INDIVIDUAL, then choose either CARTRIDGE A or CARTRIDGE B (do not select CONTINUOUS).

iii. The system will start from a cleaning cycle first. Press the arrow button and the LCD panel will show the RUN:TIME display. This will take around 4 min in which you can prepare your MQ blank.

iv. Find the 1-L Teflon DGM vessel labeled "MQ Blank", rinse it with MQ three times, and fill it up with MQ water (use a hose to minimize air bubbles) until water spills out from the other outlet on the top. Pour some water out so that the bottle is filled to the rim (~ 1 1L; do not over fill), cap the two outlets on the top with the Teflon end caps. Place the bottle at left side of the 2537B unit and secured with the bungee cord.

v. Attach the Teflon purging wand to the union connector on the zero-air line that has a T-valve on (marked with yellow tape). Tighten the connection. Turn on the T-valve.

vi. When the RUN:TIME status shows 30 sec to go under COOL-Dn, open the end caps on the DGM-MQ bottle, insert the purging wand (the end without fritz), via a union connector, into one of the outlets and push it slightly into the head space of the vessel (careful, not into the water!) for ~ 10 sec to displace the lab air from the head space. Insert the end of the sample air supply line, via a union connector, into the other outlet on top of the DGM-MQ vessel, push it until it stops at the blue tape, and tighten the connector. Now push the purging wand all the way down into the water until it stops at the yellow tape. You should see bubbles coming out from the fritz. Tighten the connector. This whole process should be completed before the COOL Dn cycle is complete. Watch out the purging wand inside of the vessel to see whether there is constant bubbling.

DGM system setup in the PILMS Laboratory on board the CCGS Amundsen in 2008. Photo by Jeffrey Latonas.

vii. The blank will purge for 3000 seconds, and then be automatically analyzed. The reading should be less than 0.3 ng m^{-3} (which corresponds to a DGM concentration of < 10 ng m^{-3}). If not, rerun another MQ blank.

Sample Analysis

i. Run a CLEAN on both cartridges

ii. Run the freshly collected sample in the same way as the MQ blank on the same cartridge.

iii. When done, remove the DGM-Sample bottle, and measure the volume of the water using the 2-L graduated cylinder in the airlock to be used in the DGM calculations.

Data Entry

i. Type the results of both the MQ and the sample into the Excel file DGMdata.xlsx and calculate the DGM. For the MQ, you may use 1 L as the volume.

ii. Record the temperature of the water at time of sampling

iii. Record station information, wind speed, direction, etc., as per the worksheet.

Shut-down

i. "Idle" mode: If you are planning to run the DGM analysis in the near future, leave the system in a continuously running mode. To do this, change the sample time to 300 sec, and run in the continuous mode with the sample line open to the air, or connected to the zero air generator. Make sure the zero air generator is in the ON position in case an autocal is initiated. The room air of PILMS has been extremely good and is usually below the instrument MDL of 0.1ng m^{-3}

Appendix B. Data Tables

Data Table 2: Dynamic viscosity (Pa s^{-1}) of fresh water with temperature

T ^{0}C	0	1	2	3	4	5	6	7	8	9
-20	4.2420E-03	4.2022E-03	3.8190E-03	3.6300E-03	3.4550E-03	3.2930E-03	3.1410E-03	3.0000E-03	2.8680E-03	2.7450E-03
-10	2.6290E-03	2.5210E-03	2.4190E-03	2.3240E-03	2.2340E-03	2.1490E-03	2.0700E-03	1.9940E-03	1.9230E-03	1.8560E-03
0	1.7930E-03	1.7320E-03	1.6750E-03	1.6210E-03	1.5690E-03	1.5200E-03	1.4740E-03	1.4290E-03	1.3870E-03	1.3460E-03
10	7.3080E-03	1.2710E-03	1.2360E-03	1.2020E-03	1.1700E-03	1.1390E-03	1.1100E-03	1.0810E-03	1.0540E-03	1.0280E-03
20	1.0026E-03	9.7850E-04	9.5530E-04	9.3300E-04	9.1150E-04	8.9070E-04	8.7080E-04	8.5150E-04	8.3300E-04	8.1500E-04
30	7.9780E-04	7.8100E-04	7.6490E-04	7.4930E-04	7.3420E-04	7.1960E-04	7.0540E-04	6.9180E-04	6.7850E-04	6.6560E-04
40	6.5320E-04	6.4110E-04	6.2940E-04	6.1800E-04	6.0700E-04	5.9630E-04	5.8590E-04	5.7580E-04	5.6600E-04	5.5640E-04
50	5.4710E-04	5.3810E-04	5.2930E-04	5.2080E-04	5.1240E-04	5.0430E-04	4.9640E-04	4.8870E-04	4.8120E-04	4.7400E-04
60	4.6680E-04	4.5990E-04	4.5310E-04	4.4620E-04	4.4010E-04	4.3380E-04	4.2760E-04	4.2160E-04	4.1580E-04	4.1000E-04
70	4.0450E-04	3.9900E-04	3.9370E-04	3.8840E-04	3.8340E-04	3.7840E-04	3.7350E-04	3.6870E-04	3.6400E-04	3.5950E-04
80	3.5500E-04	3.5060E-04	3.4630E-04	3.4210E-04	3.3800E-04	3.3400E-04	3.3000E-04	3.2620E-04	3.2240E-04	3.1870E-04
90	3.1500E-04	3.1150E-04	3.0800E-04	3.0460E-04	3.0120E-04	2.9790E-04	2.9460E-04	2.9150E-04	2.8840E-04	2.8530E-04
100	2.8230E-04	2.7930E-04	2.7640E-04	2.7360E-04	2.7080E-04	2.6810E-04	2.6540E-04	2.6270E-04	2.6010E-04	2.5760E-04
110	2.5510E-04	2.5260E-04	2.5020E-04	2.4780E-04	2.4540E-04	2.4310E-04	2.4090E-04	2.3860E-04	2.3640E-04	2.3430E-04
120	2.3220E-04	2.3010E-04	2.2800E-04	2.2600E-04	2.2400E-04	2.2210E-04	2.2010E-04	2.1820E-04	2.1640E-04	2.1450E-04
130	2.1270E-04	2.1090E-04	2.0920E-04	2.0740E-04	2.0580E-04	2.0410E-04	2.0240E-04	2.0080E-04	1.9920E-04	1.9760E-04
140	1.9600E-04	1.9450E-04	1.9300E-04	1.9150E-04	1.9000E-04	1.8860E-04	1.8710E-04	1.8570E-04	1.8430E-04	1.8290E-04
150	1.8160E-04									

Data Table 3: Standard density of water free of dissolved salts and gasses (IUPAC), * the leading figure decreases by 1

T °C	0	0.1	0.2	0.3	0.4	0.5	0.6	0.7	0.8	0.9
0	999.8426	8493	8558	8622	8683	8743	8801	8857	8912	8964
1	999.9015	9065	9112	9158	9202	9244	9284	9323	9360	9395
2	999.9429	9461	9491	9519	9546	9571	9595	9616	9636	9655
3	999.9672	9687	9700	9712	9722	9730	9738	9743	9747	9749
4	999.9750	9748	9746	9742	9736	9728	9719	9709	9696	9683
5	999.9668	9651	9632	9612	9591	9568	9544	9518	9490	9461
6	999.9430	9398	9365	9330	9293	9255	9216	9175	9132	9088
7	999.9043	8996	8948	8898	8847	8794	8740	8684	8627	8569
8	999.8509	8448	8385	8321	8256	8189	8121	8051	7980	7908
9	999.7834	7759	7682	7604	7525	7444	7362	7279	7194	7108
10	999.7021	6932	6842	6751	6658	6564	6468	6372	6274	6174
11	999.6074	5972	5869	5764	5658	5551	5443	5333	5222	5110
12	999.4996	4882	4766	4648	4530	4410	4289	4167	4043	3918
13	999.3792	3665	3536	3407	3276	3143	3010	2875	2740	2602
14	999.2464	2325	2184	2040	1899	1755	1609	1463	1315	1166
15	999.1016	0864	0712	0558	0403	0247	0090	9932*	9772*	9612*
16	998.9450	9287	9123	8957	8791	8623	8455	8285	8114	7942
17	998.7769	7595	7419	7243	7065	6886	6706	6525	6343	6160
18	998.5976	5790	5604	5416	5228	5038	4847	4655	4462	4268
19	998.4073	3877	3680	3481	3282	3081	2880	2677	2474	2269
20	998.2063	1856	1649	1440	1230	1019	0807	0594	0380	0164
21	997.9948	9731	9513	9294	9073	8852	8630	8406	8182	7957
22	997.7730	7503	7275	7045	6815	6584	6351	6118	5883	5648
23	997.5412	5174	4936	4697	4456	4215	3973	3730	3485	3240
24	997.2994	2747	2499	2250	2000	1749	1497	1244	0990	0735
25	997.0480	0223	9965*	9707*	9447*	9186*	8925*	8663*	8399*	8135*
26	996.7870	7604	7337	7069	6800	6530	6259	5987	5714	5441
27	996.5166	4891	4615	4337	4059	3780	3500	3219	2938	2655
28	996.2371	2087	1801	1515	1228	0940	0651	0361	0070	9778*
29	995.9486	9192	8898	8603	8306	8009	7712	7413	7113	6813
30	995.6511	6209	5906	5602	5297	4991	4685	4377	4069	3760
31	995.3450	3139	2827	2514	2201	1887	1572	1255	0939	0621
32	995.0302	9983*	9963*	9342*	9020*	8697*	8373*	8049*	7724*	7397*
33	994.7071	6743	6414	6085	5755	5423	5092	4759	4425	4091
34	994.3756	3420	3083	2745	2407	2068	1728	1387	1045	0703
35	994.0395	0015	9671*	9325*	8978*	8631*	8283*	7934*	7585*	7234*
36	993.6883	6531	6178	5825	5470	5115	4759	4403	4045	3687
37	993.3328	2968	2607	2246	1884	1521	1157	0793	0428	0062
38	992.9695	9328	8960	8591	8821	7850	7479	7107	6735	6361
39	992.5987	5612	5236	4860	4483	4105	3726	3347	2966	2586
40	992.2204									